RICE UNIVERSITY

Near-Infrared Silica-Based Gold Nanoshells as Potential Rapid Diagnostic Imaging Agents for Breast Cancer Tumor Detection

by

Lissett Ramirez Bickford

A THESIS SUBMITTED
IN PARTIAL FULFILLMENT OF THE
REQUIREMENTS FOR THE DEGREE

Doctor of Philosophy

APPROVED, THESIS COMMITTEE:

Rebekah A. Drezek, Professor
Bioengineering, Electrical & Computer Eng.
Chair of Thesis Committee

Tomasz S. Tkaczyk, Assistant Professor
Bioengineering, Electrical & Computer Eng.

Jason H. Hafner, Associate Professor
Physics and Astronomy, Chemistry

HOUSTON, TEXAS
JANUARY 2011

ABSTRACT

Near-Infrared Silica-Based Gold Nanoshells as Potential Rapid Diagnostic Imaging Agents for Breast Cancer Tumor Detection

by

Lissett Ramirez Bickford

Although much research has focused on using near-infrared silica-based gold nanoshells for dual-imaging and therapeutic applications *in vivo*, these particles may also prove useful as rapid diagnostic imaging agents for *ex vivo* applications, such as intraoperative tumor margin detection. In this thesis, gold nanoshells were successfully designed to target breast cancer cells through antibodies against the extracellular Human Epidermal growth factor Receptor 2 (HER2), whose overexpression is associated with more aggressive forms of breast cancer. By comparing HER2-positive breast cancer cells to normal (nonneoplastic) breast cells, the nanoshells effectively labeled HER2-overexpression within 5 minutes of incubation time. These nanoshells also enhanced contrast of the same cancer cells using two-photon microscopy, which enabled subsequent validation of preferential labeling using a distinctive co-culture experiment.

To ultimately translate these findings to the clinic, nanoshells of similar design were studied for their effectiveness at enhancing contrast of malignancy in breast tissue sections and intact human breast tissue. Through detailed experimental conditions, these nanoshells increased contrast of cancer cells in sectioned HER2-overexpressing breast tissue within 5 minutes of incubation time using reflectance confocal microscopy, a unique imaging capability not previously reported. Finally, these targeted nanoshells

were used to effectively visualize HER2 receptor expression in intact human breast tissue specimens within the same 5 minute incubation time point. Through two-photon imaging, it was shown that these nanoparticles preferentially labeled tissue surface receptors, with minimal penetration depth. Importantly, the enhanced surface labeling was observed macroscopically through a standard stereomicroscope and confirmed microscopically through reflectance confocal microscopy and immunohistochemistry. These results suggest that anti-HER2-nanoshells used in tandem with a near-infrared reflectance confocal microscope and a standard stereomicroscope may potentially be used to discern HER2-overexpressing cancerous tissue from normal tissue in near real time and offer a rapid supplement to current diagnostic techniques.

ACKNOWLEDGEMENTS

Funding for this project has been supported by the Department of Defense National Defense Science and Engineering (NDSEG) Fellowship, a Department of Defense Congressionally Directed Breast Cancer Research Program Era of Hope Scholar Award to Rebekah Drezek, the Center for Biological and Environmental Nanotechnology (EEC-0118007 and EEC-0647452), and the John and Ann Doerr Fund for Computational Biomedicine.

I would like to thank Dr. Rebekah Drezek for her guidance in completing this research and Dr. Tse-Kuan Yu for providing me with clinical experiences at M.D. Anderson Cancer Center so that I can better understand and appreciate the need for rapid diagnostics. I would also like to thank Dr. Tomasz Tkaczyk and Dr. Jason Hafner for serving as my committee members. Last, but not least, I thank the following people for their help and contributions: Joseph Chang, Jiantang Sun, Ying Hu, Kun Fu, Vengadesan Nammalvar, and Nadhi Thekkek.

DEDICATION

To my husband and mother – the strongest pillars of support in my life.

TABLE OF CONTENTS

LIST OF FIGURES

Page

LIST OF TABLES

Page

CHAPTER 1

THESIS OVERVIEW

Due to their advantageous and flexible optical properties, silica-based gold nanoshells, which have a dielectric silica core and a gold outer shell, were studied for their imaging potential as rapid contrast agents for the HER2/neu biomarker. This assessment began with a look at their rapid labeling ability in *in vitro* cell studies, followed by *ex vivo* tissue sections and, lastly, intact (non-sectioned) tissue specimens. Crucial to confirming experimental results and understanding mechanisms of nanoshell-targeting, the effectiveness of using gold nanoshells as contrast agents for two-photon microscopy was also analyzed and the utility of this more recent discovery was demonstrated through *in vitro* cell studies and *ex vivo* tissue studies.

Beginning in Chapter 2, the potential use of silica-based gold nanoshells as rapid imaging agents for breast cancer tumor margin detection is considered. Although it is expected that the ability to use these nanoparticles for near-real time diagnostics will unlock many possibilities, their potential for assisting surgeons in delineating tumor margins intraoperatively is more closely evaluated. Currently, tumor margins are determined outside of the operating suite and several days or weeks may elapse before a result is presented to the patient. By employing gold nanoshells as rapid diagnostic imaging agents, surgeons and pathologists may be able to arrive at conclusive information without further delay or the need for repeat procedures.

Next, in Chapter 3, current methods employed for tumor margin detection are explained.[1] These methods include those in practice at both tertiary care centers and at

community-based hospitals. Although there are procedures in place to assist surgeons with adequate removal of cancerous tissue, key limitations with each method are identified. Specifically, the time needed to arrive at a final consensus on whether or not all cancerous tissue has been removed from a patient at the time of surgery is acknowledged. By examining the limits of current procedures, the stage is set for appreciating the need for a more immediate supplement to these current techniques.

In order to visualize malignancy based on molecular markers of disease, it is desirable to combine the beneficial properties of contrast agents with specific imaging tools. Although several gold-based contrast agents have been studied in tandem with a variety of imaging systems for visualization of microscopic disease[2-18], in Chapter 4, our attention focuses on scattering-based imaging systems. In particular, current interest in the near-infrared wavelength region[2-5,19] is explained and a closer look at darkfield microscopy and reflectance confocal microscopy is taken – imaging systems capable of detecting enhanced contrast on the *surface* of cells and tissues.

Since the use of silica-based gold nanoshells as a potential solution for rapid diagnostics is suggested, it is critical to understand the key characteristics of these novel nanoparticles. In Chapter 5, the properties of silica-based gold nanoshells are described, with special attention placed on their optical tunability and ability to be engineered to function as multi-purpose nanoparticles.[20] Also provided is a simplified overview of how these nanoparticles are fabricated and, subsequently, conjugated to antibodies.

The next four chapters review, in detail, the sequence of studies executed to demonstrate and validate that silica-based gold nanoshells may potentially be used as contrast agents for applications where rapid diagnostic information, by means of receptor

overexpression, is desired. Chapter 6 begins by examining the ability of anti-HER2-targeted nanoshells to preferentially label HER2 receptors in an *in vitro* cell study using a time-based analysis.[21] Although former studies have shown successful targeting of HER2-overexpressing cell lines using HER2-targeted nanoshells[3,5], this chapter describes larger, more scattering-based nanoshells designed to enhance HER2-overexpression within only 5 minutes of incubation time. Furthermore, the approximate number of nanoshells bound per cell at both 5 and 60 minutes is determined and it is shown that an estimated 95% of the nanoshells in solution bind within the first 5 minutes of incubation time. This work, which demonstrated the proof of concept that nanoshells may offer rapid labeling opportunities *in vitro*, was subsequently published in 2008 in NanoBiotechnology.

While gold nanoshells have commonly been shown to serve as diagnostic imaging agents for darkfield microscopy[3,5,21], their use as contrast agents under two-photon microscopy has not been as thoroughly studied. In Chapter 7, the two-photon characteristics of two different-sized silica-gold nanoshells are first validated and their wide-spanning emission range under two-photon excitation is shown.[22] Owing to this wide-spanning emission range, the ability to specifically label HER2-overexpressing cells after only 5 minutes is confirmed through a unique co-culture experiment employing two-photon microscopy. In Chapter 9, this relatively new application is revisited when two-photon microscopy is utilized again for the visualization of nanoshells on the surface of intact *ex vivo* breast tissue specimens. This research, which showed the utility of gold nanoshells for two-photon imaging of breast cancer cells, was published in Nanotechnology in 2008.

Formerly, through *in vitro* cell studies, targeted nanoshells were shown as rapid diagnostic imaging agents for HER2-overexpression. However, in order for this new potential application to make its way to the clinical realm, it is imperative that more clinically-geared experiments ensue. Thus, in Chapter 8, this work is advanced to include sectioned breast tissue specimens.[23] Moreover, while previous studies considered nanoshell-enhanced contrast of cells observed through a darkfield microscope, nanoshells' potential as contrast agents for reflectance confocal microscopy, an imaging modality capable of looking at thicker tissue specimens, is revealed. First, nanoshells demonstrated enhanced contrast of HER2-overexpressing cells using reflectance confocal microscopy. Next, a procedure is described for visualizing HER2-overexpression in sectioned breast tissue within only 5 minutes of incubation time with a reflectance confocal microscope. Importantly, labeling results with HER2-targeted nanoshells was supported by immunohistochemistry experiments against the HER2 biomarker.[23] This research was consequently published in the journal Breast Cancer Research and Treatment in 2010.

While the evaluation of tissue sections is the current method of *microscopic* disease verification (as will be described in Chapter 3)[24], the ability to realize the extent of disease *macroscopically* is highly desirable. By doing so, the regions of interest that remain questionable could be minimized without the need for further tissue sectioning and processing. In light of this, Chapter 9 describes the use of silica-gold nanoshells as rapid imaging agents for the widefield imaging of intact human breast tissue specimens through the use of a standard stereomicroscope. Two-photon microscopy is first employed to assess the possible depth of penetration of the nanoshells after 5 minutes of

incubation time. As expected, these nanoshells preferentially targeted and labeled HER2 receptors on the surface of HER2-overexpressing tissue. Furthermore, through the use of a standard stereomicroscope, the rapid labeling of HER2-overexpressing tissue is shown without image manipulation and these results are validated by both reflectance confocal microscopy and immunohistochemistry against HER2. Currently, this work is in preparation for submission to Breast Cancer Research and Treatment.

In conclusion, in Chapter 10, a summary of research findings is presented in addition to the future direction of translating this work into a usable clinical supplement to current diagnostic techniques, in particular for intraoperative tumor margin detection. While several objectives must be met to validate their use as rapid diagnostic imaging agents in the clinic, this unique and additional feature of silica-gold nanoshells, never before thoroughly studied, has been shown. This distinctive characteristic of silica-gold nanoshells is expected to evoke numerous opportunities in the field of biomedical nanophotonics.

Chapter 1 References

1. Bickford LR, Drezek RA, Yu T-K, "Intraoperative techniques and tumor margin status - Room for improvement for cervical cancer patients of childbearing age". Gynecologic Oncology, Vol. 107/1S, S180-186 (2007).

2. Loo C, Hirsh L, Lee MH, Change E, West J, Halas N, and Drezek R. "Gold nanoshell bioconjugates for molecular imaging in living cells". Optics Letters 30(9):1012-1014 (2005).

3. Loo C, Lowery A, Halas N, West J. and Drezek R. "Immunotargeted nanoshells for integrated cancer imaging and therapy". Nano Letters 5(4):709-711 (2005).

4. Gobin AM, Lee MH, Halas NJ, James WD, Drezek RA, and West JL. "Near-infrared resonant nanoshells for combined optical imaging and photothermal cancer therapy". Nano Letters 7(7):1929-1934 (2007).

5. Fu K, Sun J, Bickford LR, Lin AWH, Halas NJ, Yu TK, and Drezek RA. "Measurement of immunotargeted plasmonic nanoparticles' cellular binding: a key factor in optimizing diagnostic efficacy". Nanotechnology 19:045103 (2008).

6. Wu C, Liang X, and Jiang H. "Metal nanoshells as contrast agents in near-infrared diffuse optical tomography". Optics Communications 253:214-221 (2005).

7. Zaman RT et al. "In Vivo Detection of Gold Nanoshells in Tumors Using Diffuse Optical Spectroscopy". IEEE J Selected Top Quantum Elec. 13(6):1715-1720 (2007).

8. Fournelle M, Maass K, Fonfara H, Welsch HJ, Hewener H, Günther C, Lemor R. "Real-time optoacoustic imaging using near-infrared absorbing gold nanoshells for contrast enhancement". IEEE Ultrasonics Symp. 2417-2420 (2007).

9. Agrawal A, Huang S, Lin AWH, Lee MH, Barton J, Drezek RA, and Pfefer TJ. "Quantitative evaluation of optical coherence tomography signal enhancement with gold nanoshells". Journal of Biomedical Optics 11:041121(2006).

10. Park J, Estrada A, Sharp K, Sang K, Schwartz A, Smith DK, Coleman C, Payne JD, Korgel BA, Dunn AK, and Tunnell JW. "Two-photon-induced photoluminescence imaging of tumors using near-infrared excited gold nanoshells". Optics Express 16(3):1590-1599 (2008).

11. Wang Y, Xie X, Wang X, Ku G, Gill KL, O'Neal DP, Stoica G, and Wang L. "Photoacoustic Tomography of a Nanoshell Contrast Agent in the In Vivo Rat Brain". Nano Letters 4(9):1689-1692 (2004).

12. Huang X, Qian W, El-Sayed I H, and El-Sayed MA. "The potential use of the enhanced nonlinear properties of gold nanospheres in photothermal cancer therapy". Lasers Surg. Med. 39(9):747-753 (2007).

13. Nagesha D, Laevsky GS, Lampton P, Banyal R, Warner C, DiMarzio C, and Sridhar S. "In vitro imaging of embryonic stem cells using multiphoton luminescence of gold nanoparticles". Int. J. Nanomedicine 2(4):813-819 (2007).

14. Sokolov K, Follen M, Aaron J, Pavlova I, Malpica A, Lotan R, and Richards-Kortum R. "Real-Time Vital Optical Imaging of Precancer Using Anti-Epidermal Growth Factor Receptor Antibodies Conjugated to Gold Nanoparticles". Cancer Research 63:1999-2004 (2003).

15. El-Sayed IH, Huang X, El-Sayed MA. "Surface Plasmon Resonance Scattering and Absorption of anti-EGFR Antibody Conjugated Gold Nanoparticles in Cancer Diagnostics: Applications in Oral Cancer". Nano Letters 5(5):829-834 (2005).

16. Bouhelier A, Bachelot R, Lerondel G, Kostcheev S, Royer P, and Wiederrecht GP. "Surface plasmon characteristics of tunable photoluminescence in single gold nanorods". Phys. Rev. Lett. 95(26):267405 (2005).

17. Wang H, Huff TB, Zweifel DA, He W, Low PS, Wei A, and Cheng JX. "In vitro and in vivo two-photon luminescence imaging of single gold nanorods". Proc. Natl. Acad. Sci. 102(44):15752-15756 (2005).

18. Durr, NJ, Larson T, Smith DK, Korgel BA, Sokolov K, and Ben-Yakar A. "Two-photon luminescence imaging of cancer cells using molecularly targeted gold nanorods". Nano Letters 7(4):941-945 (2007).

19. Weissleder R. "A clearer vision for in vivo imaging". Nature Biotechnology 19:316-317 (2001).

20. Bickford LR, Day ES, Hu Y, Sun J, Fu K, Chang J, Lewinski NA, Yu T-K, Drezek RA. "Biomedical Applications of Multi-functional Silica-Based Gold Nanoshells" in Biomedical Nanotechnology: Materials for Nanomedicine, edited by Mansoor M. Amiji, RPh, PhD, and Vladimir P. Torchilin, DSc, PhD (Pan Stanford Publishing). In press (2010).

21. Bickford LR, Chang J, Fu K, Sun J, Hu Y, Gobin AM, Yu T-K, Drezek RA, "Evaluation of Immunotargeted Gold Nanoshells as Rapid Diagnostic Imaging Agents for HER2-Overexpressing Breast Cancer Cells: A Time-Based Analysis". NanoBiotechnology, 4(1-4), 1-8 (2008).

22. Bickford LR, Sun J, Fu K, Lewinski N, Nammalvar V, Chang J, Drezek RA, "Enhanced Multi-Spectral Imaging of Live Breast Cancer Cells Using

Immunotargeted Gold Nanoshells and Two-Photon Excitation Microscopy". Nanotechnology, 19, 315102 (2008).

23. Bickford LR, Agollah G, Drezek R, Yu TK, "Silica-gold nanoshells as potential intraoperative molecular probes for HER2-overexpression in ex vivo breast tissue using near-infrared reflectance confocal microscopy". Breast Cancer Research and Treatment, 120(3), 547 (2010).

24. Cabioglu N, Hunt K, Aysegul AS, Kuerer HM, Babiera GV, Singletary SE, Whitman GJ, Ross MI, Ames FC, Feig BW, Buchholz TA, and Meric-Bernstam F. "Role for Intraoperative Margin Assessment in Patients Undergoing Breast-Conserving Surgery". Annals of Surgical Oncology 14(4):1458-1471 (2007).

CHAPTER 2

INTRODUCTION

Currently, breast cancer is the second leading cause of cancer-related deaths in women and it accounts for approximately one-third of all cancers diagnosed in women in the United States.[1] In order to reduce cancer recurrence and progression, cancerous tissue must be completely eliminated, regardless of grade.[2] Treatment decisions are, therefore, absolutely critical. Although some patients may need to undergo mastectomy, which involves complete removal of the entire breast, some patients with less-advanced breast cancer may choose breast-conserving surgery. To reduce the likelihood of cancer recurrence, it is recommended that patients seeking breast conservation therapy, such as lumpectomy, undergo adjuvant radiation treatment.[3] Specifically, Fisher *et al.* determined that lumpectomy (followed by radiation therapy) is just as effective as mastectomy as long as the resected tissue specimens contain negative tumor margins.[3]

The accurate delineation of tumor margins is one of the most significant factors in cancer recurrence and its importance has been documented for several cancers, including breast[4,5], brain[6,7], prostate[8], larynx[9], melanoma[10-12], urothelial[13], oral[14-16] and cervical[17-19] cancers. The presence of a positive surgical margin has been associated with lower rates in patient survival.[20] Due to residual cancer cells being left in many patients that undergo breast conservation therapy, as many as 40% of patients have experienced local breast cancer recurrence near the site of the original tumor.[3]

Current intraoperative tumor margin detection involves the surgeon removing the tissue that he/she visually perceives as cancerous (as well as a region of surrounding

'perceived' normal tissue) and the tissue being sent to pathology where it undergoes further analysis. For tumors that are palpable, the process usually involves inking the breast specimen (to designate *in situ* location) followed by serial sectioning and physical measurement between the edge of the tumor and the margin of the resected tissue. If the margins appear negative, the sample is further processed by permanent paraffin-embedded histology. However, if the margins appear positive, suspicious areas typically undergo frozen sectioning and histology for microscopic confirmation. For tumors that are non-palpable, radiographs are taken of the specimen both before and after serial sectioning (and specimen inking). The distance between the tumor and the resected edge is measured and the specimen is evaluated grossly.

During this evaluation, the surgical team waits for a response from the pathologist while the patient remains anesthetized. Based on the results, the pathologist contacts the surgical team in the operating room and notifies them if enough tissue has been removed ('negative margin'). On occasion, enough tissue has been excised and the surgical team can proceed with suturing the patient. Other times, however, not enough tissue has been removed ('positive margin') and the process continues until the histological sample shows an adequate tumor margin. Clearly, this current practice of determining tumor margins during surgery is expensive and inconvenient.

Once surgeons are able to achieve clear or negative margins, for which there are no histologically visible dysplastic cells surrounding the resected tumor, the primary goal of the surgical procedure has been met. Cases for which a positive margin has been obtained typically result in continued tissue resection until the margins become negative. In some cases, additional tissue removal is not feasible and the procedure terminates with

the possibility of residual dysplasic cells remaining in the body cavity. The purpose of adjuvant radiation treatment in patients undergoing breast conservation surgery is to combat these potential residual cancerous cells and maintain local control.[21]

The aforementioned method of tumor margin detection applies only to specialized tertiary centers, such as The University of Texas M.D. Anderson Cancer Center (MDACC). In community hospitals, however, pathologic analysis of excised tissue does not occur until well after the operation is complete. Those patients who subsequently present with positive tumor margins must return for an additional surgical procedure to remove remaining suspicious tissue, which portends additional risks and costs to the patient. Furthermore, the accuracy of breast cancer diagnosis in community hospitals needs to be addressed; approximately 10,000 cases of misdiagnoses are estimated to occur annually.[22] Due to the existing limitations of current intraoperative tumor margin detection, there is an opportunity to develop superior diagnostic tools to assist in reducing the recurrence and progression of cancer due to inadequate tissue removal during primary surgery.

Chapter 2 References

1. American Cancer Society. Breast Cancer Facts and Figures 2005-2006. Atlanta: American Cancer Society, Inc.

2. Steen RG, A Conspiracy of Cells. New York: Plenum Press (1993).

3. Fisher B, Anderson S, Bryant J, Margolese RG, Deutsch M, Fisher ER, Jeong JH, Wolmark N. "Twenty-year follow-up of a randomized trial comparing total mastectomy, lumpectomy, and lumpectomy plus irradiation for the treatment of invasive breast cancer", New England Journal of Medicine 347(16):1233-1241 (2002).

4. Balch GC, Mithani SK, Simpson JF, Kelley MC. "Accuracy of Intraoperative Gross Examination of Surgical Margin Status in Women Undergoing Partial Mastectomy for Breast Malignancy", Annual Scientific Meeting and Postgraduate Course Program, Southeastern Surgical Congress. Atlanta, GA, 22-27 (2004).

5. Gibson GR, Lesnikoski BA, Yoo J, Mott LA, Cady B, and Barth RJ. "A Comparison of Ink-Directed and Traditional Whole-Cavity Re-Excision for Breast Lumpectomy Specimens With Positive Margins", Annals of Surgical Oncology 8(9):693-704 (2001).

6. Bucci M, Maity A, Janss A, Belasco J, Fisher M, Tochner Z, et al. "Near complete surgical resection predicts a favorable outcome in pediatric patients with nonbrainstem, malignant gliomas: results from a single center in the magnetic resonance imagine era", Cancer 101(4):817-824 (2004).

7. Winger M, Macdonald D, Cairncross J. "Supratentorial anaplastic gliomas in adults. The prognostic importance of extent of resection and prior low-grade glioma", Journal of Neurosurgery 71(4):487-493 (1989).

8. Tsuboi T, Ohori M, Kuroiwa K, Reuter VE, Kattan MW, Eastham JA, et al. "Is Intraoperative Frozen Section Analysis An Efficient Way To Reduce Positive Surgical Margins?" Urology 66:1287-1291 (2005).

9. Lam KH and Wei WI. "Tumor Clearance at Resection Margins in Total Laryngectomy", Cancer 61:2260-2272 (1988).

10. Riker AI, Glass F, Perez I, Cruse CW, Messina J, and Sondak VK. "Cutaneous melanoma: methods of biopsy and definitive surgical excision", Dermatologic Therapy 18:387-393. (2005).

11. Stell VH, Norton HJ, Smith KS, Salo JC, White RL. "Method of Biopsy and Incidence of Positive Margins in Primary Melanoma", Annals of Surgical Oncology 14(2):893-898 (2006).

12. Sober AJ and Balch CM. "Method of Biopsy and Incidence of Positive Margins in Primary Melanoma", Annals of Surgical Oncology 14(2):274-275 (2007).

13. Raj GV, Tal R, Vickers A, Bochner BH, Serio A, Donat SM, et al. "Significance of Intraoperative Ureteral Evaluation at Radical Cystectomy for Urothelial Cancer", Cancer 107:2167-2172 (2006).

14. Ribeiro NFF, Godden DRP, Wilson GE, Butterworth DM, and Woodwards RTM. "Do frozen sections help achieve adequate surgical margins in the resection of oral carcinoma?" Int J Oral Maxillofac Surg 32:152-158 (2003).

15. Sutton DN, Brown JS, Rogers SN, Vaughn ED, and Woolgar JA. "The prognostic implications of the surgical margin in oral squamous cell carcinoma", Int J Oral Maxillofac Surg 32:30-34 (2003).

16. Upile T, Fisher C, Jerjes W, Maaytah ME, Singh S, Sudhoff H, et al. "Recent technological developments: in situ histopathological interrogation of surgical tissues and resection margins", Head & Face Medicine 3(13):1-12 (2007).

17. Carvalho JP, Carvalho FM, Pincerato KM, and Pereyra EAG. "Conization, Frozen Section Examination, and Planned Hysterectomy In The Treatment of High-Grade Cervical Intraepithelial Neoplasia", Rev Hosp Clin Fac Med S Paulo 56(6):169-172 (2001).

18. Cohn DE, Morrison CD, Zanagnolo VL, Goist MM, and Copeland LJ. "Invasive cervical adenocarcinoma immediately following a cone biopsy for adenocarcinoma in situ wiht negative margins", Gynecologic Oncolocy 98:158-160 (2005).

19. Murta EFC, Resende AV, Souza MAH, Adad SJ, and Salum R. "Importance of surgical margins in conization for cervical intraepithelial neoplasia grade III. Archives of Gynecology and Obstetrics", 263:42-44 (1999).

20. Mojica CM, Bastani R, Boscardin WJ, and Ponce NA. "Low-Income Women With Breast Abnormalities: System Predictors of Timely Diagnostic Resolution", Cancer Control 14(2):176-182 (2007).

21. Buckman R. "What You Really Need to Know about Cancer", Baltimore: The Johns Hopkins University Press (1997).

22. Perkins C, Balma D, Garcia R, et al. "Why Current Breast Pathology Practices Must Be Evaluated", A *Susan G. Komen for the Cure* White Paper: June 2006. Breast Journal 13(5):443-447 (2007).

CHAPTER 3[a]

CURRENT METHODS OF MICROSCOPIC BREAST CANCER TUMOR MARGIN DETECTION

3.1 Introduction

As formerly described, during breast conservation surgery, the surgeon initially removes the suspicious breast tissue and, using tactile sensation and visual inspection of both the specimen and region of excision, determines if the entire cancerous region has been removed. The first intraoperative tumor margin detection, therefore, occurs grossly. Used as the only intraoperative tumor margin detection method, gross examination results in positive tumor margins roughly 50% of the time.[1] The identification of any microscopic residual cells located at the margin of the excised specimen occurs subsequently by a pathology lab. In community hospitals, this typically occurs post-operatively and is performed by paraffin-embedded histology. Other specialized cancer centers, however, perform microscopic tumor margin evaluation while the patient remains anesthetized. Regions of the specimen that contain suspicious tumor margins are processed immediately, typically by frozen section histology or touch prep cytology. The remaining tissue sample is later processed by paraffin-embedded histology, which provides the final margin status.[2]

---

[a] Adapted from: Bickford LR, Drezek RA, Yu T-K, "Intraoperative techniques and tumor margin status - Room for improvement for cervical cancer patients of childbearing age"; *Gynecologic Oncology*, Vol. 107/1S, S180-186 (2007).

3.2 Paraffin-Embedded Histology

While paraffin-embedded histology remains the gold standard of tumor margin detection, this method is very lengthy and cannot, therefore, be performed intraoperatively. This lengthy process is due to the series of steps necessary for adequately preserving the tissue. The tissue samples must first be fixed and then prepared for paraffin infiltration by sample dehydration through a series of alcohols. Once the samples are embedded in paraffin, they are sectioned with a microtome, which serially sections the tissue at a designated thickness. Tissue sections must then be stained through a series of additional steps to visualize the cellular morphology of interest. This method of tissue processing continues to be the most accepted due to its reliability, ease of use, and cost.[3]

3.3 Frozen Section Histology

Frozen sections are used frequently for their quick, easy, and least labor intensive diagnosis[3] and have an accuracy as high as 97-99% when compared to paraffin histology.[4,5] The tissue sample is frozen as quickly as possible and is then sectioned using a special microtome called a cryostat. The tissue samples may be fixed or unfixed, depending on the preference of the laboratory. After the specimens are sectioned and mounted to glass slides, they are traditionally stained with hematoxylin and eosin (H&E), which are the most frequently used stains for histology.[6] The use of H&E allows cell nuclei to be stained a blue/black color, while the cell cytoplasm and connective tissue fibers obtain a pink color. Dysplasic cells are distinguished from their normal cell counterparts by their cellular characteristics, including cell and nuclear size, presence of

mitoses, and level of differentiation.[7] Though historically used as a standard procedure, H&E histology for frozen intraoperative tissue analysis has been shown to present several limitations. These limitations include difficulties in processing, such as the development of artifacts[8], as well as sampling error, cost, time needed to achieve diagnosis, reliability as a staging modality, and variability of results with level of operator experience.[9,10] Additionally, Black *et al.* have illustrated that there is not a standard to frozen section analysis once the tissue samples have been collected and that what is considered 'adequate' varies according to surgeon subjectivity.[10]

3.4 Touch-Prep Cytology

Touch-prep cytology has been proposed as an alternative technique for evaluating margin status and has been primarily studied for the diagnosis of breast cancer tumor margins.[8-9,11-13] This method has also been referred to as wet-film cytology, cytologic smear, and imprint cytology. Much like standard frozen histology, touch-prep cytology is regarded as a rapid, simple, and accurate way to determine tumor margins intraoperatively. In this method, a glass slide is pressed up against the specimen margins in question and cells stick to the slide. This technique is performed for each margin of the tissue sample and, after the tissue is imprinted onto glass slides, the slides are fixed and stained with H&E prior to being viewed microscopically. The actual specimen is additionally inked, sectioned, and stained to verify diagnosis. Studies have shown that the accuracy of touch-prep diagnoses varies from 85-99.3%, sensitivity ranges from 80-96.4%, and specificity ranges from 85-100% when compared to paraffin-embedded histology.[8,12] As with frozen section preparation, an experienced pathologist is needed to

assess tumor margin involvement. However, unlike the use of a cryostat which may result in inadequate and unusable tissue sections, loss of tissue is not a concern with the touch-prep method.

Although touch-prep cytology appears to be a superior alternative to frozen section analysis, limitations exist that render this method less promising. A major limitation of touch prep cytology is that only positive margins can be detected and, therefore, the distance between the edge of a negative margin and the edge of the tumor cannot be evaluated.[2] Additionally, touch prep cytology does not seem to dramatically reduce sample processing time; an average of 15 minutes has been reported for cytologic results to become available.[13] This is similar to the amount of time needed to acquire results from frozen section histology (based on physical observations at MDACC).

Chapter 3 References

1. Abraham SC, Fox K, Fraker D, Solin L, and Reynolds C. "Sampling of grossly benign reexcisions: a multidisciplinary approach to assessing adequacy". American Journal of Surgical Pathology 23(3):316-322 (1999).

2. Cabioglu N, Hunt K, Aysegul AS, Kuerer HM, Babiera GV, Singletary SE, Whitman GJ, Ross MI, Ames FC, Feig BW, Buchholz TA, and Meric-Bernstam F. "Role for Intraoperative Margin Assessment in Patients Undergoing Breast-Conserving Surgery". Annals of Surgical Oncology 14(4):1458-1471 (2007).

3. Bancroft JD, Gamble M, editors. "Theory and Practice of Histological Techniques", 5th edition. Edinburgh: Churchill Livingstone (2002).

4. Ord RA and Aisner S. "Accuracy of Frozen Sections in Assessing Margins in Oral Cancer Resection". J Oral Maxillofac Surg 55:663-669 (1997).

5. Kaufman Z, Lew S, Griffel B, Dinbar A. "Frozen-Section Diagnosis in Surgical Pathology". Cancer 57:377-379 (1986).

6. Ross MH, Romrell LJ, Kaye GI. Histology A Text and Atlas. Third ed. Baltimore: Williams & Wilkins (1995).

7. Kumar V, Cotran RS, Robbins SL, editors. Basic Pathology, 6th edition. Philadelphia: W.B. Saunders Company (1997).

8. Creager AJ, Shaw JA, Young PR, and Geisinger KR. "Intraoperative Evaluation of Lumpectomy Margins by Imprint Cytology With Histologic Correlation". Archives of Pathological Laboratory Medicine 2002;126:846-848 (2002).

9. Klimberg VS, Harms S, and Korourian S. "Assessing margin status". Surgical Oncology 8:77-84 (1999).

10. Black C, Marotti J, Zarovnaya E, and Paydarfar J. "Critical Evaluation of Frozen Section Margins in Head and Neck Cancer Resections". Cancer 107:2792-2800 (2006).

11. Balch GC, Mithani SK, Simpson JF, Kelley MC. Accuracy of Intraoperative Gross Examination of Surgical Margin Status in Women Undergoing Partial Mastectomy for Breast Malignancy. Annual Scientific Meeting and Postgraduate Course Program, Southeastern Surgical Congress. Atlanta, GA (2004).

12. Klimberg VS, Westbrook KC, and Korourian S. "Use of Touch Preps for Diagnosis and Evaluation of Surgical Margins in Breast Cancer". Annals of Surgical Oncology 5(3):220-226 (1998).

13. Valdes EK, Boolbol SK, Cohen JM, and Feldman SM. "Intra-operative Touch Preparation Cytology; Does It Have a Role in Re-excision Lumpectomy?" Annals of Surgical Oncology 14(3):1045-1050 (2007).

CHAPTER 4[b]

THE POTENTIAL OF MICROSCOPIC, SCATTERING-BASED IMAGING SYSTEMS AND CONTRAST AGENTS

4.1 Introduction

Medical imaging technologies such as magnetic resonance imaging, mammography, and positron emission tomography have revolutionized the detection of cancer over the last thirty years. Although these tools are invaluable for understanding the normal structure of various tissues and associated irregularities, being able to visualize cancerous abnormalities at the microscopic level is necessary for adequate delineation of tumor margins and thus, prevention of recurrent disease. Various research laboratories are already looking at the potential of using microscopic optical imaging techniques to diagnose oral[1-4], cervical[4-10], skin[11], colon and gastrointestinal[12-15], and breast cancers[16-22]. While several of these laboratories are optimizing and developing instrumentation for the direct imaging of tissues, others are also considering the benefits of utilizing both exogeneous contrast agents in tandem with optical tools. One advantage of using exogenous contrast agents is that detection limits can be significantly improved beyond what is capable with optical instrumentation alone. Additionally, some exogenous contrast agents can be targeted to biomarkers which are overexpressed during

---

[b] Adapted from: Bickford LR, Day ES, Hu Y, Sun J, Fu K, Chang J, Lewinski NA, Yu T-K, Drezek RA. "Biomedical Applications of Multi-functional Silica-Based Gold Nanoshells " in *Biomedical Nanotechnology: Materials for Nanomedicine,* edited by Mansoor M. Amiji, RPh, PhD, and Vladimir P. Torchilin, DSc, PhD (Pan Stanford Publishing). In press (2010).

the multistages of cancer progression. By combining both contrast agents and imaging devices, these biomarkers may be used as tools for intraoperative tumor margin detection, which will require identifying malignant cells among heterogeneous tissue.

Currently, research interest centered on developing optical techniques that combine both contrast agents and imaging devices is focused on diagnostic applications in the near-infrared (NIR) spectral region.[23-27] Since the major absorbers in biological tissue are water, hemoglobin and oxy-hemoglobin, the high absorption peaks of these substances must be avoided so that potentially greater signals can be detected for tissue-based diagnostics.[27] Figure 4.1 illustrates the absorption spectra of tissue absorbers from the visible to the NIR region. Hemoglobin mainly absorbs in wavelength ranges lower than 650 nm, while water mainly absorbs in wavelength ranges greater than 900 nm. Thus, the NIR window of 650 nm - 900 nm is ideal for biological imaging applications.[27]

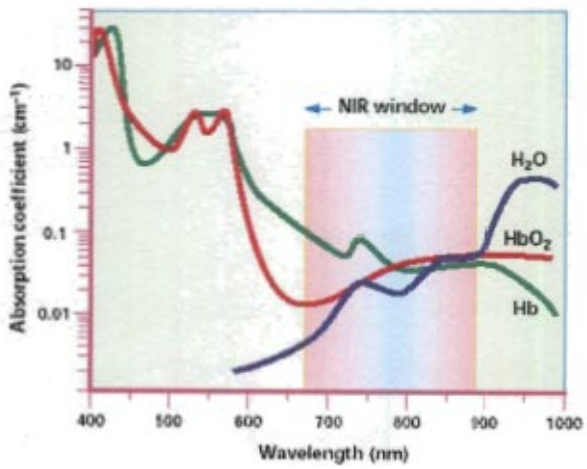

Figure 4.1. Spectra of major tissue absorbers showing that the NIR region ($650<\lambda<900$) is ideal for *in vivo* diagnostic application. Adapted from Reference 27.

Accordingly, utilizing exogenous contrast agents that can scatter or absorb light in the NIR window has become increasingly critical for biomedical researchers. Gold-based

nanoparticles, specifically, have gained increased attention in the area of biomedical diagnostics because of their great potential as such imaging contrast agents.[22-26] Thus far, the most predominantly and thoroughly studied gold-based nanoparticles include nanoshells[21-26,28-34], gold colloid[35-38], and nanorods[39-45]. For the purposes of this thesis, I have chosen to focus on the use of silica-based gold nanoshells, which have previously demonstrated effectiveness as diagnostic imaging agents for HER2-overexpressing breast cancer cells.[22,23,26]

In order to evaluate contrast facilitated by gold nanoparticles, scattering- and absorption-sensitive optical tools must be employed. Absorption-sensitive tools are commonly associated with therapeutic applications and will not be considered here. Scattering-sensitive devices, meanwhile, are typically used for achieving real-time diagnostic results. Although these tools have included darkfield microscopy, optical coherence tomography (OCT), and reflectance confocal microscopy (RCM), darkfield microscopy and RCM are the two scattering-based imaging systems which will be discussed as they are particularly advantageous for visualizing the surface of a particular tissue of interest.

4.2 Darkfield Microscopy

Darkfield microscopy is ideal for imaging strongly-scattering specimens, such as biological cells and nanoparticles, that otherwise have low contrast under standard brightfield microscopy. Under darkfield microscopy, images are formed only by the light that is scattered from the subject of interest.[46] This is possible in part because of a specialized condenser (or stop) that prevents a solid cone of transmitted light from

entering the objective lens, such as in brightfield microscopy (Figure 4.2). In darkfield microscopy, the numerical aperture of the condenser is greater than the numerical aperture of the objective. As can be seen in Figure 4.3, when imaging the single-celled green alga Chlamydomonas with darkfield microscopy under specific illumination conditions, the cells appears bright against a dark background. Visualization of the same cells under standard brightfield microscopy, meanwhile, produces a very different image in which the contrast between the alga and background is more difficult to distinguish.

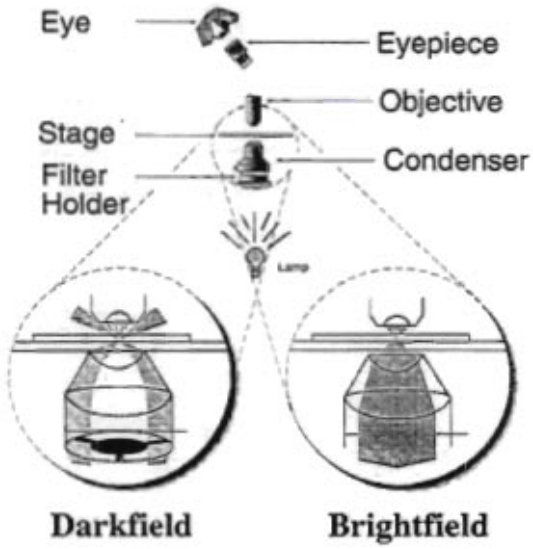

Figure 4.2. Diagram comparing darkfield and brightfield microscopy. Republished from Reference 46.

When imaging cells labeled with immunotargeted nanoshells under darkfield microscopy, the contrast of the cells is enhanced by the attached nanoshells due to the strong scattering signal from the nanoshells, as shown in Figure 4.4.[26] The labeling of cells with nanoshells significantly improves the image contrast in comparison with those images taken of cells without nanoshells.

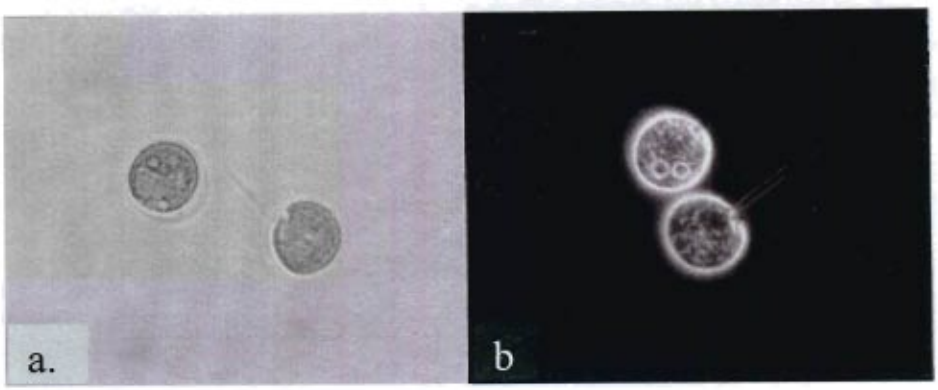

Figure 4.3. (a.) Brightfield and (b.) darkfield images of the single-celled green alga Chlamydomonas. Reproduced from http://www.wsu.edu/~omoto/papers/Fig2.html; accessed on 09/18/2010.

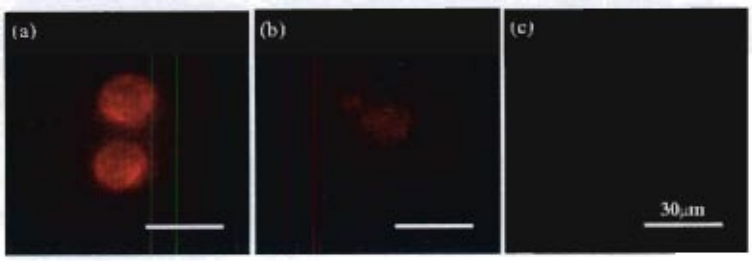

Figure 4.4. Darkfield microscopy images of HER2-positive SK-BR-3 cells with (a) specific anti-HER2-nanoshell targeting, (b) non-specific anti-IgG-nanoshell targeting, and (c) without targeting. Republished from Reference 26.

4.3 Reflectance Confocal Microscopy

Reflectance confocal microscopy is an imaging tool that allows visualization of scattering-based structures at and beyond the surface. By employing the use of point illumination and a specialized pinhole, out-of-focus light can be rejected thus providing a high resolution image of specimens that are thicker than the focal plane (Figure 4.5). Confocal microscopy can also be used to generate 3-D images based on a reconstruction of multiple images taken at various depths throughout a specimen. This imaging modality has found applications in fluorescence imaging, as well as reflectance imaging. Unlike conventional confocal microscopy, which relies on the excitation of endogenous or

exogenous fluorophores, RCM involves the collection of backscattered light at different depths from the tissue of interest, where the confocal pinhole is used to eliminate signals from the out-of-focus planes. Accessibility issues have limited the use of conventional confocal microscopy to areas as the skin[47,48], cornea[49], lip and tongue[50]. Recent advances in fiber optics, however, have made it possible to integrate the components of confocal microscopy into an optical fiber bundle with a miniaturized objective, enabling access to other tissue sites, such as the cervix.[51-53].

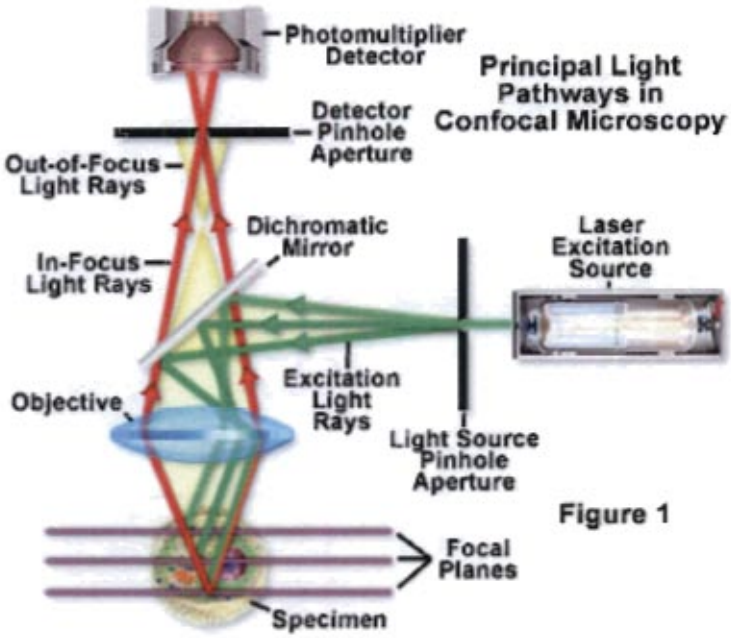

Figure 4.5. Schematic of a confocal microscope. Reproduced from http://www.mikroskopie.org/2008/01/26/types-of-confocal-microscopy/14/; accessed on 08/25/2010.

The use of RCM as a device for assessing tumor margins has previously been shown by Chen *et al.*[54] The authors looked at the use of RCM for assessing lentigo maligna melanoma tumor margins in vivo. Lentigo maligna melanoma is a noninvasive melanoma that is sometimes difficult to assess due to photothermal damage already present on the skin surface. In this study, the authors used RCM to identify the

superficial extent of the tumor and performed punch biopsies and standard H&E histology on the samples to confirm their results. The performance of the confocal microscope was in agreement with the histological evaluation and on follow-up one year later, the patient displayed no evidence of tumor recurrence. Although this study was performed on only one patient, the findings reinforce the use of confocal microscopy as a possible strategy for determining tumor margin involvement.

More recently, Parrish *et al.* demonstrated the use of RCM to characterize mammary ductal structures of wild-type mice and genetically engineered mice with ductal carcinoma in situ.[18] In this study, the researchers utilized acetic acid as a contrast agent in order to enhance visible cellular structures. As can be seen in Figure 4.6, the application of acetic acid to both normal and cancerous mammary tissues resulted in enhanced contrast for the cancerous sample under RCM. Normal tissue appears significantly less reflective. The studies demonstrate that RCM may be a tool for rapid and accurate analysis of mammary gland structures.

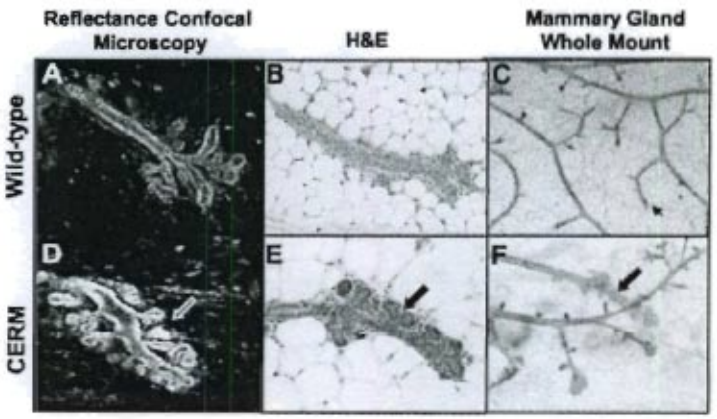

Figure 4.6. Comparison of RCM images with corresponding H&E stained sections of mammary gland tissues. A-C: Normal mouse; D-F: Genetically engineered mouse with ductal carcinoma in situ. C,F: Whole mount images demonstrate lateral budding (black arrows). 5% acetic acid was used as a contrast agent. Adapted from Reference 18.

Tilli *et al.* furthered this application to the characterization of human breast cancer biopsy samples.[20] Again, by implementing the use of acetic acid as a contrast agent, the characteristic features associated with normal and malignant cells (such as nuclear morphology and cancer cell invasion) could be discerned and compared well with corresponding H&E stained sections. Although the results of this study support the use of RCM as a tool for rapid and accurate analysis of mammary gland structures in tandem with acetic acid, the authors indicated that the use of different contrast agents may incur greater resolution and increased detection of cancer cells throughout their multistage progression.

Chapter 4 References

1. Hsu E, Gillenwater A, Hasan M, Williams M, El-Naggar A, and Richards-Kortum R. "Real-time detection of epidermal growth factor receptor expression in fresh oral cavity biopsies using a molecular-specific contrast agent". Int J Cancer 118(12):3062-3071 (2006).

2. Clark A, Gillenwater A, Alizadeh-Naderi R, El-Naggar A, and Richards-Kortum R. "Detection and diagnosis of oral neoplasia with an optical coherence microscope". Journal of Biomedical Optics 9(6):1271-1280 (2004).

3. Clark AL, Gillenwater AM, Collier TG, Alizadeh-Naderi R, El-Naggar AK, and Richards-Kortum R. "Confocal Microscopy for Real-Time Detection of Oral Cavity Neoplasia". Clinical Cancer Research 9:4714-4721 (2003).

4. Clark A, Collier T, Lacy A, Follen M, Malpica A, Gillenwater A, et al. "Detection of dysplasia with near real time confocal microscopy". Biomed Sci Instrum 38:393-398 (2002).

5. Carlson K, Pavlova I, Collier T, Descour M, Follen M, and Richards-Kortum R. "Confocal microscopy: imaging cervical precancerous lesions". Gynecologic Oncolocy 99(3 Suppl 1):S84-88 (2005).

6. Nida DL, Rahman MS, Carlson KD, Richards-Kortum R, and Follen M. "Fluorescent nanocrystals for use in early cervical cancer detection". Gynecologic Oncolocy 99:S89-S94 (2005).

7. Luck B, Carlson K, Bovik A, and Richards-Kortum R. "An Image Model and Segmentation Algorithm for Reflectance Confocal Images of In Vivo Cervical Tissue". IEEE Transactions on Image Processing 14(9):1265-1276 (2005).

8. Luck B, Carlson K, Collier T, and Sung K. "Confocal Microscopy for Detection of Precancerous Cervical Lesions". IEEE Potentials 14-17 (2004).

9. Drezek RA, Richards-Kortum R, Brewer MA, Feld MS, Pitris C, Ferenczy A, et al. "Optical Imaging of the Cervix". Cancer 98(9 Suppl):2015-2027 (2003).

10. Drezek RA, Collier T, Brookner CK, Malpica A, Lotan R, Richards-Kortum R, et al. "Laser scanning confocal microscopy of cervical tissue before and after application of acetic acid". Am J Obstet Gynecol 182(5):1135-1139 (2000).

11. Chen C-SJ, Elias M, Busam K, Rajadhyaksha M, Marghoob AA. "Multimodal in vivo optical imaging, including confocal microscopy, facilitates presurgical margin mappling for clinically complex lentigo maligna melanoma". British Journal of Dermatology 153(5):1031-1036 (2005).

12. Liu J, Mandella M, Friedland S, Soetikno R, Crawford J, Contag C, et al. "Dual-axes confocal reflectance microscope for distinguishing colonic neoplasia". Journal of Biomedical Optics 11(5):054019 (2006).

13. DaCosta R, Wilson B, and Marcon N. "Optical techniques for the endoscopic detection of dysplastic colonic lesions". Curr Opin Gastroenterol 21(1):70-79 (2005).

14. Evans J, Nishioka N. "Endoscopic confocal microscopy". Curr Opin Gastroenterol 21(5):578-584 (2005).

15. MacAulay C, Lane P, and Richards-Kortum R. "In vivo pathology: microendoscopy as a new endoscopic imaging modality". Gastrointest Endosc Clin N Am 14(3):595-620 (2004).

16. Zysk AM and Boppart SA. "Computational methods for analysis of human breast tumor tissue in optical coherence tomography images". Journal of Biomedical Optics 11(5):054015 (2006).

17. Zysk AM, Nguyen FT, Odenburg AL, Marks DL, and Boppart SA. "Optical coherence tomography: a review of clinical development from bench to bedside". Journal of Biomedical Optics 12(5):051403 (2007).

18. Parrish A, Halama E, Tilli MT, Freedman M, and Furth PA. "Reflectance confocal microscopy for characterization of mammary ductal structures and development of neoplasia in genetically engineered mouse models of breast cancer". Journal of Biomedical Optics 10(5):051602 (2005).

19. Tilli MT, Parrish AR, Cotarla I, Jones LP, Johnson MD, and Furth PA. "Comparison of mouse mammary gland imaging techniques and applications: Reflectance confocal microscopy, GFP Imaging, and ultrasound". BMC Cancer 8(21):1-15 (2008).

20. Tilli MT, Cabrera MC, Parrish AR, Torre KM, Sidawy MK, Gallagher AL, Makariou E, Polin SA, Liu MC, and Furth PA. "Real-time imaging and characterization of human breast tissue by reflectance confocal microscopy". Journal of Biomedical Optics 12(5):051901 (2007).

21. Hirsch LR, Gobin AM, Lowery AR, Tam F, Drezek RA, Halas NJ, and West JL. "Metal Nanoshells". Annals of Biomedical Engineering 34(1):15-22 (2006).

22. Loo C, Hirsh L, Lee MH, Change E, West J, Halas N, and Drezek R. "Gold nanoshell bioconjugates for molecular imaging in living cells". Optics Letters 30(9):1012-1014 (2005).

23. Loo C, Lowery A, Halas N, West J. and Drezek R. "Immunotargeted nanoshells for integrated cancer imaging and therapy". Nano Letters 5(4):709-711 (2005).

24. Lin AWH, Lewinski NA, West JL, Halas NJ, and Drezek RA. "Optically tunable nanoparticle contrast agents for early cancer detection: model-based analysis of gold nanoshells". Journal of Biomedical Optics 10(6):064035 (2005).

25. Gobin AM, Lee MH, Halas NJ, James WD, Drezek RA, and West JL. "Near-infrared resonant nanoshells for combined optical imaging and photothermal cancer therapy". Nano Letters 7(7):1929-1934 (2007).

26. Fu K, Sun J, Bickford LR, Lin AWH, Halas NJ, Yu TK, and Drezek RA. "Measurement of immunotargeted plasmonic nanoparticles' cellular binding: a key factor in optimizing diagnostic efficacy". Nanotechnology 19:045103 (2008).

27. Weissleder R. "A clearer vision for in vivo imaging". Nature Biotechnology 19:316-317 (2001).

28. Lowery AR, Gobin AM, Day ES, Halas NJ, and West JL. "Immunonanoshells for targeted photothermal ablation of tumor cells". Int J. Nanomedicine 1(2):149-154 (2006).

29. Wu C, Liang X, and Jiang H. "Metal nanoshells as contrast agents in near-infrared diffuse optical tomography". Optics Communications 253:214-221 (2005).

30. Zaman RT et al. "In Vivo Detection of Gold Nanoshells in Tumors Using Diffuse Optical Spectroscopy". IEEE J Selected Top Quantum Elec. 13(6):1715-1720 (2007).

31. Fournelle M, Maass K, Fonfara H, Welsch HJ, Hewener H, Günther C, Lemor R. "Real-time optoacoustic imaging using near-infrared absorbing gold nanoshells for contrast enhancement". IEEE Ultrasonics Symp. 2417-2420 (2007).

32. Agrawal A, Huang S, Lin AWH, Lee MH, Barton J, Drezek RA, and Pfefer TJ. "Quantitative evaluation of optical coherence tomography signal enhancement with gold nanoshells". Journal of Biomedical Optics 11:041121(2006).

33. Park J, Estrada A, Sharp K, Sang K, Schwartz A, Smith DK, Coleman C, Payne JD, Korgel BA, Dunn AK, and Tunnell JW. "Two-photon-induced photoluminescence imaging of tumors using near-infrared excited gold nanoshells". Optics Express 16(3):1590-1599 (2008).

34. Wang Y, Xie X, Wang X, Ku G, Gill KL, O'Neal DP, Stoica G, and Wang L. "Photoacoustic Tomography of a Nanoshell Contrast Agent in the In Vivo Rat Brain". Nano Letters 4(9):1689-1692 (2004).

35. Huang X, Qian W, El-Sayed I H, and El-Sayed MA. "The potential use of the enhanced nonlinear properties of gold nanospheres in photothermal cancer therapy". Lasers Surg. Med. 39(9):747-753 (2007).

36. Nagesha D, Laevsky GS, Lampton P, Banyal R, Warner C, DiMarzio C, and Sridhar S. In vitro imaging of embryonic stem cells using multiphoton luminescence of gold nanoparticles. Int. J. Nanomedicine 2(4):813-819 (2007).

37. Sokolov K, Follen M, Aaron J, Pavlova I, Malpica A, Lotan R, and Richards-Kortum R. "Real-Time Vital Optical Imaging of Precancer Using Anti-Epidermal Growth Factor Receptor Antibodies Conjugated to Gold Nanoparticles". Cancer Research 63:1999-2004 (2003).

38. El-Sayed IH, Huang X, El-Sayed MA. "Surface Plasmon Resonance Scattering and Absorption of anti-EGFR Antibody Conjugated Gold Nanoparticles in Cancer Diagnostics: Applications in Oral Cancer". Nano Letters 5(5):829-834 (2005).

39. Bouhelier A, Bachelot R, Lerondel G, Kostcheev S, Royer P, and Wiederrecht GP. "Surface plasmon characteristics of tunable photoluminescence in single gold nanorods". Phys. Rev. Lett. 95(26):267405 (2005).

40. Imura K, Nagahara T, and Okamoto H. "Near-field two-photon-induced photoluminescence from single gold nanorods and imaging of plasmon modes". J. Phys. Chem. B 109(27):13214-13220 (2005).

41. Wang H, Huff TB, Zweifel DA, He W, Low PS, Wei A, and Cheng JX. "In vitro and in vivo two-photon luminescence imaging of single gold nanorods". Proc. Natl. Acad. Sci. 102(44):15752-15756 (2005).

42. Huff TB, Hansen MN, Zhao Y, Cheng JX, and Wei A. "Controlling the cellular uptake of gold nanorods". Langmuir 23(4):1596-1599 (2007).

43. Huang X, El-Sayed IH, Qian W, and El-Sayed MA. "Cancer cell imaging and photothermal therapy in the near-infrared region by using gold nanorods". J. Am. Chem. Soc. 128(6):2115-2120 (2006).

44. Durr, NJ, Larson T, Smith DK, Korgel BA, Sokolov K, and Ben-Yakar A. "Two-photon luminescence imaging of cancer cells using molecularly targeted gold nanorods". Nano Letters 7(4):941-945 (2007).

45. Yu, C, Nakshatri, H, and Irudayaraj J. "Identity profiling of cell surface markers by multiplex gold nanorod probes". Nano Letters 7(8):2300-2306 (2007).

46. Omoto CK, Folwell JA. "Using Darkfield Microscopy To Enhance Contrast". The American Biology Teacher 61(8):621-624 (1999).

47. Corcuff P, Chaussepied C, Madry G, and Hadjur C. "Skin optics revisited by in vivo confocal microscopy: melanin and sun exposure". J. Cosmet. Sci. 52(2):91-102 (2001).

48. Rajadhyaksha M, Anderson RR, and Webb RH. "Video-rate confocal scanning laser microscope for imaging human tissues in vivo". Applied Optics 38(10):2105-2115 (1999).

49. Masters B and Thaer AA. "Real-time scanning slit confocal microscopy of the in vivo human cornea". Applied Optics 33(4):695-701 (1994).

50. White WM, Rajadhyaksha M, Gonzalez S, Fabian RL, and Anderson RR. "Noninvasive imaging of human oral mucosa in vivo by confocal reflectance microscopy". Laryngoscope 109(10):1709-1717 (1999).

51. Sung KB, Liang C, Descour M, Follen M, Malpica A, and Richards-Kortum R. "Near real time in vivo fibre optic confocal microscopy: sub-cellular structure resolved". Journal of Microscopy 207(Pt 2):137-145 (2002).

52. Sung KB, Liang C, Descour M, Collier T, Follen M, and Richards-Kortum R. "Fiber-optic confocal reflectance microscope with miniature objective for in vivo imaging of human tissues". IEEE Trans. Biomed. Eng. 49(10):1168-1172 (2002).

53. Sung KB, Richards-Kortum R, Follen M, Malpica A, Liang C, and Descour MR. "Fiber optic confocal reflectance microscopy: a new real-time technique to view nuclear morphology in cervical squamous epithelium in vivo". Optics Express 11(24):3171-3181 (2003).

54. Chen CSJ, Elias M, Busam K, Rajadhyaksha M, Marghoob AA. "Multimodal in vivo optical imaging, including confocal microscopy, facilitates presurgical margin mappling for clinically complex lentigo maligna melanoma". British Journal of Dermatology 153(5):1031-1036 (2005).

CHAPTER 5[c]

PROPERTIES OF SILICA-GOLD NANOSHELLS

5.1 Introduction

As mentioned previously, various gold-based nanoparticles have been explored as agents for biomedical applications. For the ultimate purpose of rapid tumor margin detection, gold nanoshells will act as optical contrast agents that are specifically targeted to molecular surface markers of breast cancer cells that can be used directly in the operating room to enhance current detection methods. Nanoshells are advantageous for biomedical applications because they are highly biocompatible, they possess ideal optical properties for imaging, and they can be readily conjugated with antibodies that bind to specific markers that are overexpressed in certain types of cancer.[1-3]

Based on the core-to-shell ratio, nanoshells can be designed to preferentially absorb or scatter light. Absorbed energy is dissipated in the form of heat, which enables gold nanoshells to be used for applications such as photo-thermal therapy.[4] Meanwhile, scattered light permits nanoshells to serve as contrast agents by enhancing optical contrast for several imaging applications, such as the aforementioned darkfield microscopy[5], reflectance confocal microscopy[6], and optical coherence tomography[3,7]. The optical extinction spectra of nanoshells can be calculated by employing the Mie

---

[c] Adapted from: Bickford LR, Day ES, Hu Y, Sun J, Fu K, Chang J, Lewinski NA, Yu T-K, Drezek RA. "Biomedical Applications of Multi-functional Silica-Based Gold Nanoshells " in *Biomedical Nanotechnology: Materials for Nanomedicine,* edited by Mansoor M. Amiji, RPh, PhD, and Vladimir P. Torchilin, DSc, PhD (Pan Stanford Publishing). In press (2010).

solution to Maxwell's equations for concentric spheres.[8,9] Energy-level-dependent gold properties can be obtained from Johnson and Christy.[10]

Figure 5.1 illustrates the extinction, absorption, and scattering results from sample calculations performed for a common-sized nanoshell with a core diameter of 260 nm and a shell thickness of 20 nm immersed in water. The extinction peak observed in Figure 5.1 is also known as the plasmonic resonance of the nanoshell. Plasmon resonances are a result of the oscillation of the incompressible electron gas in the conducting gold shell. Such resonance enhance the amount of the scattered or absorbed light, which may yield an extinction cross-section several times larger than the physical dimension of the particle itself.

One particularly unique feature of nanoshells is their agile optical tunability. This allows one to engineer the nanoshell extinction peak to coincide with the NIR optical window for biological applications. The optical tunability can best be understood both qualitatively and quantitatively by the theory of plasmon hybridization between shell and cavity.[11] The shell thickness determines the strength of the interaction between the plasmons on the inner and outer surface of the gold shell. Jain *et al.* recently explained that the plasmon resonant wavelength decays near-exponentially as the interparticle gap (ie. shell thickness) is scaled by the particle size.[12] This is illustrated in Figure 5.2 with the spectra of five groups of nanoshells that have an identical outer diameter but distinct core diameter-to-shell thickness ratios. The extinction peak is readily tuned in the entire visible-NIR spectrum without changing the overall particle size.

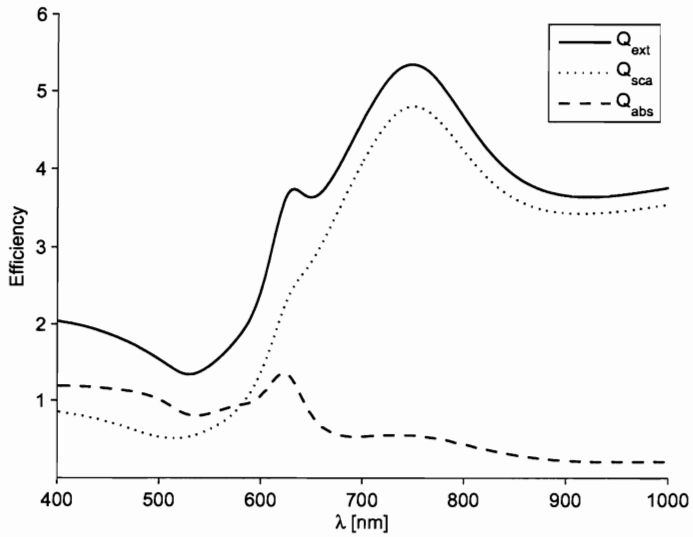

Figure 5.1. Spectra for nanoshells with a silica core diameter of 260 nm and a shell thickness of 20 nm suspended in water. Image provided courtesy of Ying Hu.

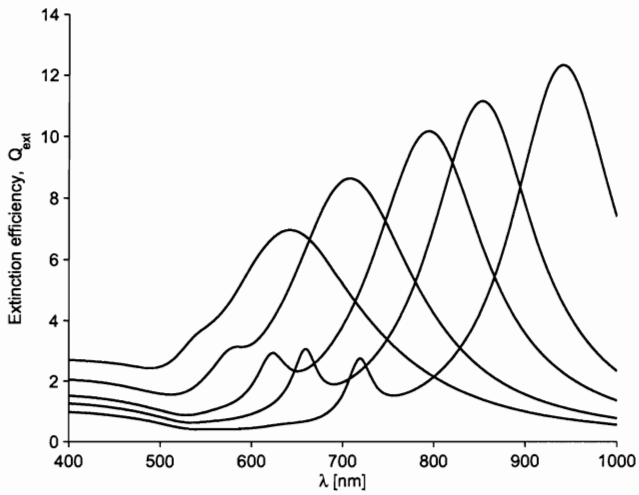

Figure 5.2. Extinction spectra for different groups of nanoshells in water, all with a total diameter of 130 nm. From left to right, the inner core diameter changes as follows: 80, 100, 110, 114, and 118 nm. Image provided courtesy of Ying Hu.

5.2 Nanoshell Fabrication

As previously published by Loo *et al.*[13], the synthetic protocol developed for the fabrication of gold nanoshells consists of three basic steps:

I. grow or obtain silica nanoparticles dispersed in solution,

II. attach very small (1-2 nm) metal "seed" colloids to the surface of the nanoparticles via molecular linkages; these seed colloids cover the dielectric nanoparticle surfaces with a discontinuous metal colloid layer,

III. grow additional metal onto the "seed" metal colloid adsorbates via chemical reduction solution.

Various stages in the growth of a gold metallic shell onto a functionalized silica nanoparticle are shown in Figure 5.3.

First, cores of silica nanoparticles are fabricated as described by Stöber *et al.*[14] in which tetraethyl orthosilicate (TEOS) is reduced in ammonium hydroxide (NH_4OH) in ethanol. Next, the silica surface is aminated by reaction with aminopropyltriethoxysilane (APTES) in ethanol. Gold shells are then grown using the method of Duff *et al.*[15] Briefly, small gold colloid (1-3 nm) is adsorbed onto the animated silica nanoparticle surface. More gold is then reduced onto these colloid nucleation sites using potassium carbonate and hydrogen tetrachloroaurate trihydrate ($HAuCl_4$ $3H_2O$) in the presence of formaldehyde. Gold nanoshell formation and dimensions are typically assessed with a UV-VIS spectrophotometer and scanning electron microscopy (SEM). The original description of metallodielectric nanoshell synthesis can be found in Oldenburg *et al.*[16]

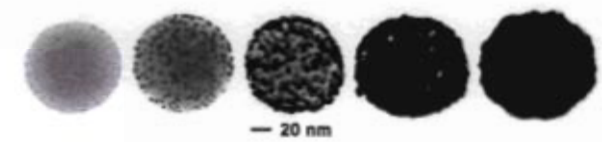

Figure 5.3. Transmission electron microscope images of gold/silica nanoshells during shell growth. Republished from Reference 13.

5.3 Nanoshell-Antibody Conjugation

Loo *et. al.*[13] formerly introduced the history of bioconjugation as it pertains to gold nanoshells as well as a description of how nanoshells are conjugated to other biological molecules. In order to conjugate antibodies to nanoshells, an ortho-pyridyl-disulfide-*n*-hydroxysuccinimide polyethylene glycol (PEG) polymer (OPSS-PEG-NHS) is used to tether antibodies onto the surfaces of the gold nanoshells. The amidohydroxysuccinimide group (NHS) enables conjugation of the PEG linker to the antibodies through amide linkages; the remaining end of the PEG linker, OPSS, allows binding to the nanoshell gold surfaces through sulfur groups. Using sodium bicarbonate, OPSS-PEG-NHS is typically resuspended to a volume equal to that of either specific or non-specific antibodies. The reaction is allowed to proceed on ice overnight. Excess unbound polymer may then be removed by membrane dialysis. PEGylated antibody is then added to the nanoshells for at least 1 hour to facilitate targeting. Following antibody conjugation, nanoshell surfaces are further modified with PEG-thiol (PEG-SH) to block non-specific adsorption sites and to enhance biocompatibility.

5.4 Conclusion

Silica-based gold nanoshells offer exciting optical properties that are not otherwise conventionally available, including large extinction cross-sections and flexible optical tunability. These characteristics render gold nanoshells as exceptional optical agents for numerous biomedical practices. For this thesis, nanoshells will be conjugated to anti-HER2 antibodies. This particular antibody has been selected as a model surface tumor target due to its association with more aggressive breast cancers seen in 15-25% of

all breast cancer cases.[17] Additionally, studies in our laboratory have previously demonstrated the effectiveness of using nanoshells as diagnostic imaging agents for HER2-overexpressing cancer cells.[1,2,5] Nanoshells will further be evaluated at the tissue-level for more clinically-relevant applications. Based on the results of this research, the combined use of nanoparticles and optical imaging tools may offer promise for rapid intraoperative tumor detection.

Chapter 5 References

1. Loo C, Hirsh L, Lee MH, Change E, West J, Halas N, and Drezek R. "Gold nanoshell bioconjugates for molecular imaging in living cells". Optics Letters 30(9):1012-1014 (2005).

2. Loo C, Lowery A, Halas N, West J. and Drezek R. "Immunotargeted nanoshells for integrated cancer imaging and therapy". Nano Letters 5(4):709-711 (2005).

3. Gobin AM, Lee MH, Halas NJ, James WD, Drezek RA, and West JL. "Near-infrared resonant nanoshells for combined optical imaging and photothermal cancer therapy". Nano Letters 7(7):1929-1934 (2007).

4. Lowery AR, Gobin AM, Day ES, Halas NJ, and West JL. "Immunonanoshells for targeted photothermal ablation of tumor cells". Int J. Nanomedicine 1(2):149-154 (2006).

5. Fu K, Sun J, Bickford LR, Lin AWH, Halas NJ, Yu TK, and Drezek RA. "Measurement of immunotargeted plasmonic nanoparticles' cellular binding: a key factor in optimizing diagnostic efficacy". Nanotechnology 19:045103 (2008).

6. Loo C. Gold Nanoshells: "Contrast Agents for Molecular Imaging". Ph.D Thesis, Rice University, Houston,Texas (2006).

7. Agrawal A, Huang S, Lin AWH, Lee MH, Barton J, Drezek RA, and Pfefer TJ. "Quantitative evaluation of optical coherence tomography signal enhancement with gold nanoshells". Journal of Biomedical Optics 11:041121 (2006).

8. van de Hulst HC. Light Scattering by Small Particles. Dover Publications, Inc., New York (1981).

9. Bohren CF and Huffman DR. Absorption and Scattering of Light by Small Particles, John Wiley & Sons, New York (1983).

10. Johnson PB and Christy RW. "Optical Constants of the Noble Metals". Physical Review B 6(12):4370-4379 (1972).

11. Prodan E, Radloff C, Halas NJ, and Nordlander P. "A hybridization model for the plasmon response of complex nanostructures". Science 302(5644):419-422 (2003).

12. Jain PK and El-Sayed MA. "Universal scaling of plasmon coupling in metal nanostructures: extension from particle pairs to nanoshells". Nano Letters 7(9):2854-2858 (2007).

13. Loo C, Lin A, Hirsch L, Lee MH, Barton J, Halas N, West J, and Drezek R. "Nanoshell-enabled photonics-based imaging and therapy of cancer". Technology in Cancer Research & Treatment 3(1):33-40 (2004).

14. Stöber W and Fink A. "Controlled Growth of Monodisperse Silica Spheres in the Micron Size Range". Journal of Colloid and Interface Science 26:62-69 (1968).

15. Duff DG, Baiker A, and Edwards PP. "A new hydrosol of gold clusters. 1. Formation and particle size variation". Langmuir 9(9):2301-2309 (1993).

16. Oldenburg SJ, Averitt RD, Westcott SL, and Halas NJ. "Nanoengineering of optical resonances". Chemical Physics Letters 288(2):243-247 (1998).

17. *Breast Cancer Treatment Guidelines for Patients*. National Comprehensive Cancer Network; Version IX; (July 2007).

CHAPTER 6[d]

INVESTIGATE THE USE OF GOLD NANOSHELLS AS RAPID DIAGNOSTIC IMAGING AGENTS *IN VITRO*

The previous chapters have introduced the need for superior diagnostic imaging tools for intraoperative tumor margin detection and have provided a foundation for understanding key properties of silica-based gold nanoshells and the imaging systems capable of observing their scattering-signatures. In this chapter, the aforementioned backgrounds come together in order to examine the efficacy of using gold nanoshells as rapid diagnostic imaging agents in the most fundamental and imperative proof of concept experiments: *in vitro* cell studies.

6.1 Introduction

Several nanoparticles have been explored for potential applications in cancer diagnosis, including nanoshells[1-4], gold colloid[5,6], quantum dots[7,8], carbon dots[9], nanorods[10-12] and nanocrystals[13]. For *in vivo* applications, several steps will need to be taken to ensure the safe delivery of nanoparticles before they can be used in a clinical setting. However, several opportunities still exist for *in vitro* applications in which the cytotoxicity of nanoparticles is immaterial. Numerous *in vitro* technologies that have shown promise for point-of-care diagnostic testing may allow clinicians to provide user-

---

[d] Adapted from: Bickford LR, Chang J, Fu K, Sun J, Hu Y, Gobin AM, Yu T-K, Drezek RA, "Evaluation of Immunotargeted Gold Nanoshells as Rapid Diagnostic Imaging Agents for HER2-Overexpressing Breast Cancer Cells: A Time-Based Analysis"; *NanoBiotechnology*, 4(1-4), 1-8 (2008).

friendly, cost effective, and rapid results at the patient bedside. Currently, these technologies involve analyzing biological fluids to detect DNA or protein amplification through the use of microarrays or biochip devices[14-16]. In addition to fluid-based modalities, these microscopic advancements can also be used to analyze larger biological components, such as excised tumor specimens, for cancer screening and diagnosis. One particular area of application is the diagnosis of cancer from biopsy samples. For example, after a breast biopsy, the specimen is sent to a pathology laboratory where it is processed and examined microscopically for morphological abnormalities and sometimes analyzed for the presence of molecular biomarkers of disease, such as hormone receptor expression[17]. This process can take up to several days, during which the patient must cope with the fear of an unknown diagnosis and the potential of treatment delay. Mojica *et al.* showed that delays between initial breast cancer symptoms and treatment are associated with lower survival rates[18]. Consequently, delays in breast cancer diagnosis top the list of liability claims made against physicians[19].

Another area of opportunity for advancement in point-of-care microscopic analysis of tumor specimens involves the assessment of intraoperative tumor margins. During a lumpectomy, for instance, the surgeon removes the suspected cancerous lesion with a margin of normal tissue. Judgment of the width of this margin is largely based on tactile sensation and visible, macroscopic abnormalities. In advanced hospital systems, the sample is excised and immediately subjected to pathologic analysis to ensure the surgical margins are tumor-free before the procedure is completed. The need to achieve negative margins is critical to minimizing cancer recurrence and progression, particularly for patients undergoing breast conservation therapy[20]. The presence of a positive surgical

margin has been associated with lower rates in patient survival[18]. Due to residual cancer cells being left in many patients that undergo breast conservation therapy, as many as 40% of patients have experienced local breast cancer recurrence near the site of the original tumor[21]. Positive margins in a surgical specimen, therefore, necessitate the resection of additional tissue until the margins do not contain tumor. Even if the specimens are examined immediately, this extends the period of anesthesia and hence increases both the cost and risk to the patient. Furthermore, many county hospitals must by necessity process tissue samples after the surgery is completed. In that case, the identification of positive surgical margins requires that the patient undergo another surgical procedure to excise the remaining tissue, which further delays the start of adjuvant treatment and increases the risk of cancer recurrence and subsequent patient mortality.

With the expansion of nanotechnology-driven research, opportunities for the use of fast and accurate diagnostic tests outside of the hospital laboratory are likely to increase. To realistically use nanoparticles as a point-of-care tool for the immediate assessment of key cancer gene signatures in excised tissue samples, the time needed to achieve optical contrast must be minimized. Thus far, few published reports have focused on minimizing the time needed to achieve suitable contrast of cancer cells incubated with nanoparticles. Previous studies demonstrating the effectiveness of using gold-based nanoparticles targeted to extracellular cancer biomarkers have involved incubation times ranging from 30 to 90 minutes[1,3,5,6,10-12]. The objective of this study was to demonstrate the feasibility of using gold nanoshells targeted to anti-HER2 antibodies to achieve sufficient optical contrast in a HER2-overexpressing breast cancer

cell line (SK-BR-3) after a series of incubation times. Overexpression of the HER2 receptor is associated with greater cancer progression and is seen in approximately 15-25% of all breast cancer cases[17]. The nanoshells, made of dielectric silica particles covered with a thin gold shell, were fabricated to scatter strongly in the near-infrared spectrum through manipulation of the silica core:gold shell ratio. We compared the contrast that could be achieved by incubating the nanoshells with both normal and cancerous cells. Our results demonstrate that gold nanoshells targeted to this cell-surface marker can produce enhanced contrast after only 5 minutes of incubation. This proof of concept supports the initial feasibility of using gold nanoshells for potential point-of-care diagnostic applications.

6.2 Materials and Methods

6.2.1 Nanoshell Fabrication

Nanoshells were developed and bioconjugated as described in Chapter 5. The final silica particles were measured by scanning electron microscopy (SEM) to obtain the average silica core diameter of 254 nm. The spectrum of the completed nanoshells was analyzed with a UV-vis spectrophotometer (Varian Cary 300). The relationship between the extinction spectrum obtained by UV-vis spectroscopy and that obtained by application of the Mie scattering theory can be used to approximate the size of the nanoparticles in solution (Figure 6.1). Subsequently, Mie Theory can be used to derive the absorption, scattering, and extinction coefficients for nanoparticles of a specific size, and a standard known concentration can be acquired for a particular optical density. In addition to using Mie scattering theory for multilayer spheres, we also used SEM to

confirm the size of the nanoshells. The nanoshells used in this study had an average diameter of 292 nm, a peak surface plasmon resonance at 778 nm and a concentration of approximately 1.6×10^9 particles/mL.

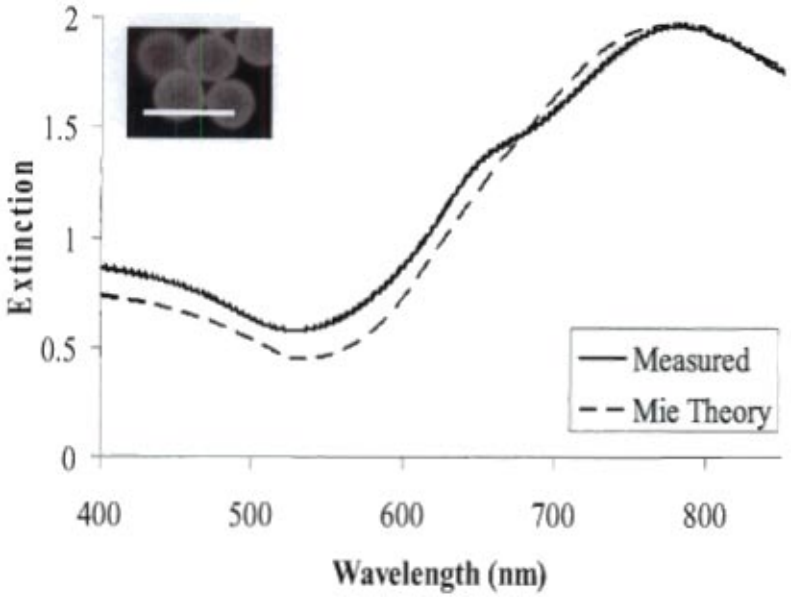

Figure 6.1. Measured spectra of nanoshells (core radius 127 nm, shell thickness 19 nm) as compared with that estimated using the Mie scattering theory; the insert depicts the corresponding image from scanning electron microscopy. Scale bar represents 500 nm.

6.2.2 Nanoshell Surface Modification

To target the prepared nanoparticles to molecular markers associated with HER2-overexpression, antibodies were first prepared by methods described in Chapter 5. Briefly, anti-HER2 antibodies (C-erbB-2/HER-2/*neu* Ab-4, Lab Vision Corporation) were conjugated to the heterobifunctionalized polyethylene glycol linker orthopyridyl-disulfide-PEG-N-hydroxysuccinimide ester (OPSS-PEG-NHS, MW = 2kD, CreativeBiochem Laboratories) by reaction at a molar ratio of 1:3 in sodium bicarbonate (100 mM, pH 8.5) overnight on ice. Aliquots were stored at -80°C. The nanoshells (1.6×10^9 particles/mL) were incubated with the prepared anti-HER2-PEG solution (0.4

mg/mL) for 1 hour at 4°C. The newly conjugated nanoshells were subsequently incubated with a 10 μM polyethylene glycol-thiol solution (PEG-SH, MW = 5kD, Nektar) for 2 additional hours at 4°C, which stabilized the nanoshells by blocking any unoccupied adsorption sites. The nanoshells were then centrifuged to remove unbound antibodies, resuspended in ultrapure water, and stored at room temperature until use. Before being incubated with cells, the nanoshell solution was supplemented with bovine serum albumin (BSA) and phosphate-buffered saline (PBS) at final concentrations of 1% each.

6.2.3 Preparation of Cells

Two cell types were analyzed for this study: the HER2-overexpressing epithelial breast cancer cell line SK-BR-3 and the normal mammary epithelial cell line MCF10A (American Type Culture Collection). The SK-BR-3 cells were grown in McCoy's 5A medium supplemented with 10% fetal bovine serum (FBS) and 1% penicillin-streptomycin and maintained at 37°C in a 5% CO_2 atmosphere. The MCF10A cells were cultured in Mammary Epithelial Basal Medium (MEBM) supplemented with a BulletKit (Clonetics) and also maintained at 37°C in 5% CO_2. Both cell lines were grown in 25-cm^2 culture flasks until confluent. At that time, cells were rinsed once with 1x PBS and incubated with trypsin-EDTA for 5 minutes at 37°C to detach the cells from the substrate, after which trypsin was neutralized with the appropriate medium and the cells were counted. Approximately $6x10^5$ cells were placed in each of four conical tubes per cell line for each time point under investigation. The cells were then centrifuged at 115 x g for 3 minutes. For each cell line and each time point of interest, three cell pellets were

resuspended in the bioconjugate-nanoshell solution and one was resuspended in an equal amount of PBS as a control. The nanoshell-cell suspensions and controls were then incubated in a hybridization chamber (VWR International) at 37°C and a motor speed of 7 rpm for 5, 10, 30, or 60 minutes. After incubation, the suspensions were centrifuged at 115 x g for 3 minutes and the unbound nanoshells were collected with a pipette. Cells were then rinsed once with 1x PBS, centrifuged, and the unbound nanoshells were again collected. A small volume (5 μL) of 10% glucose mixed with PBS was added to the remaining cell pellets to prevent cell death during imaging. Approximately 7 μL of each pellet was placed on a glass slide and coverslipped for immediate microscopic analysis.

6.2.4 Darkfield Imaging and Processing

Images of the two cell types incubated with nanoshells were obtained with a Zeiss Axioskop 2 darkfield microscope outfitted with a color camera (Zeiss AxioCam MRc5). Darkfield microscopy depends on light scattering to achieve contrast. All images were taken under the same lighting conditions and magnification (20x). Optical intensity was quantified by using a MATLAB code. Based on this code, an image with a value of 0 was designated pure black and that with a value of 255 pure white. An increase in intensity, therefore, corresponded to an image with a higher numerical value. Average intensity values for each time point and each cell line were calculated from 10 independent cell samples that were devoid of scattering influences from neighboring cells and unbound nanoshells. Sample normality was assessed by using Minitab to evaluate the error distribution for all data points. A normal probability plot of the residuals verified that the samples followed a normal distribution (data not shown). F-tests were

also used to determine the equality of variance before applying two-tailed paired Student's t-tests to evaluate significance.

6.2.5 Derivation of Bound Nanoshell Concentration Using Spectroscopy

According to the Beer-Lambert law, the absorbance of particles in solution is directly related to the concentration of those particles in that solution. To validate the ability of spectroscopy to predict the concentration of a solution of nanoshells of known size, we used linear regression analysis. Nanoshells of known concentration, based on the Mie Theory calculations, were serially diluted and the corresponding peak absorbance values were measured. We considered a concentration of approximately 2.0×10^9 particles/mL (optical density = 2.4) as a 100x concentration. From this analysis, an equation relating the peak absorbance (independent variable) to each known nanoshell concentration (dependent variable) was used to approximate the number of nanoparticles in subsequent solutions of unknown concentration. This derivation was necessary to calculate the approximate number of bound nanoparticles per cell at the different time points.

To determine and compare the number of nanoshells bound after 5 minutes and 60 minutes of incubation, the collected unbound nanoshells were centrifuged at 255 x g for 20 minutes, resuspended in ultrapure water, transferred to cuvettes and sonicated briefly before being measured with a UV-vis spectrophotometer. The spectrum was recorded and the peak absorbance documented for each sample. Based on the original concentration of nanoshells, the number of cells used, and the concentration of the collected unbound nanoshells, the approximate number of nanoshells bound to each

cancer cell was derived. An F-test was also used to determine the equality of variance before applying a two-tailed paired Student's t-test to evaluate significance.

6.3 Results and Discussion

We evaluated the contrast that could be achieved by incubating nanoshells targeted to HER2 receptors with normal breast epithelial cells (MCF10A) or breast cancer cells (SK-BR-3) for four intervals: 5, 10, 30, and 60 minutes. All procedures were done with triplicate samples and included a control condition (cells to which no nanoshells had been added). Figures 6.2 and 6.3 illustrate original and enlarged images obtained at all four time points for both cells lines and for cells incubated without nanoshells (designated as 0 minutes). Because the optical peak resonance for the fabricated nanoparticles occurred at 778 nm, the nanoshells scattered strongly in the near-infrared range and could be visualized under darkfield illumination as red particles. Qualitative assessment of the imaging results revealed that the MCF10A cells showed little enhanced scattering at any period of incubation with the bioconjugate-nanoshell solution compared with both controls or the cancer cells. However, the SK-BR-3 cancer cells showed enhanced contrast after as little as 5 minutes of incubation. Typically, SK-BR-3 cells express about $8x10^5$ receptors per cell and normal MCF10A cells about $1x10^4$.[22,23] The targeted bioconjugated nanoshells apparently bound to cell surface receptors on both cell types; however, because the cancer cells had higher numbers of receptors, the contrast that could be achieved was considerably greater with those HER2-overexpressing cells. Other evidence of the superior contrast achieved with the SK-BR-3 cells was apparent from the difference in the numbers of unbound nanoshells between the

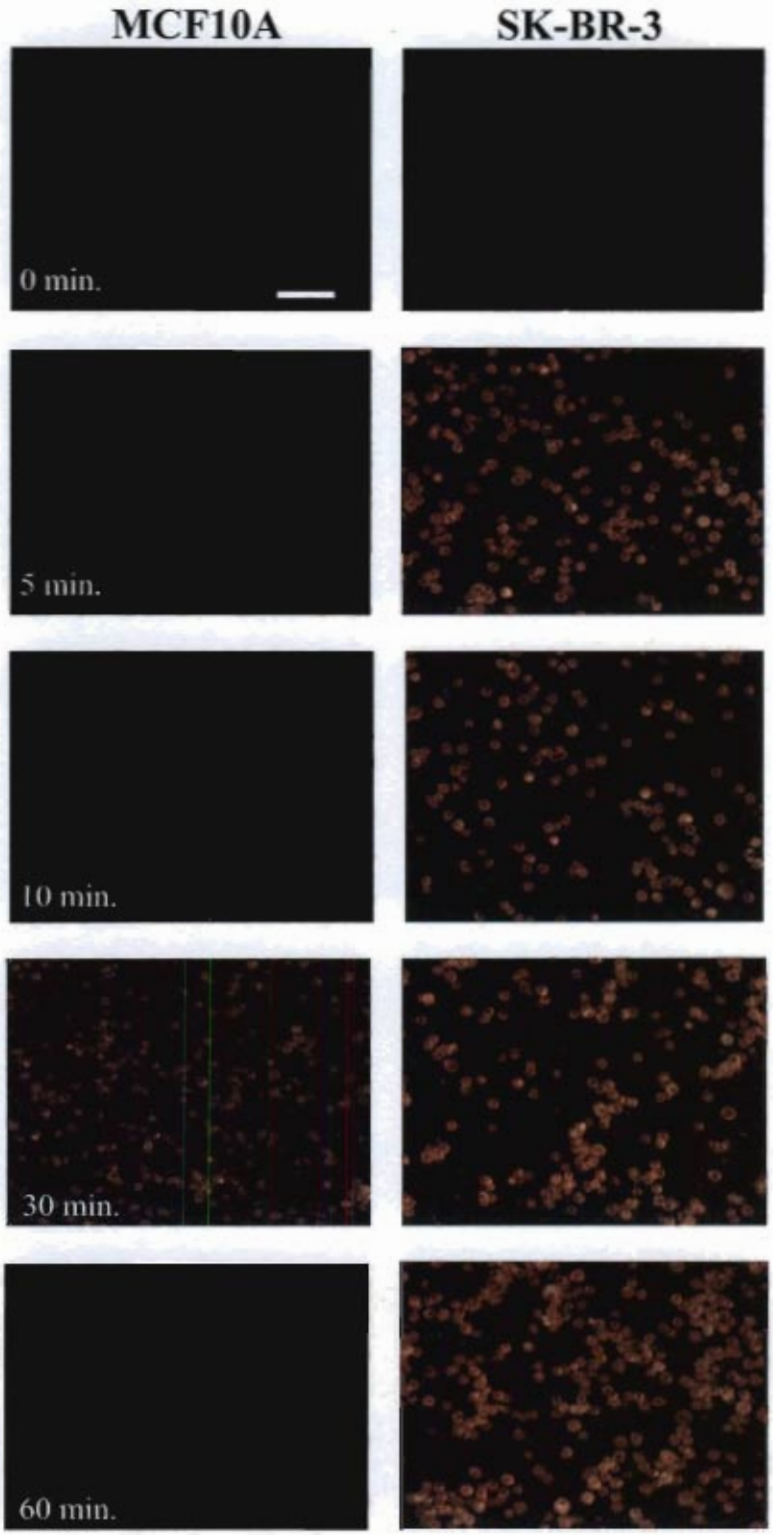

Figure 6.2. Darkfield images of MCF10A and SK-BR-3 cells incubated with bioconjugated nanoshells for the indicated times. Images were obtained at 20x. Scale bar represents 125 μm.

two cell types. In the images of the MCF10A cells, several unbound nanoshells could be seen between cells despite our attempts at removing unbound nanoshells and rinsing the cells. Considerably fewer such nanoshells were present in the SK-BR-3-nanoshell images (Figure 6.2).

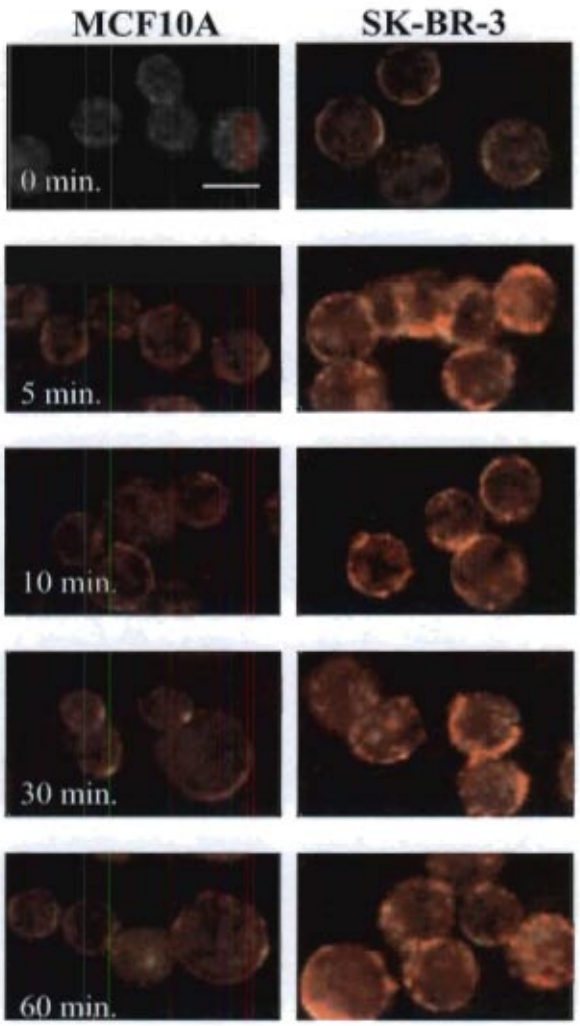

Figure 6.3. Enlarged darkfield images of MCF10A and SK-BR-3 cells incubated with the bioconjugated nanoshells for the indicated times. Original images taken at 20x. Scale bar represents 20 μm.

To quantitatively assess the increase in contrast between the normal and cancerous cells at each time point, we used a MATLAB code to evaluate the average

intensity 10 cells from each condition; an intensity value of 0 was considered pure black and 255 pure white. Statistical analyses indicated no difference between either cell type incubated with only PBS (the control condition) ($P>0.1$). However, differences between the MCF10A cells and the SK-BR-3 cells were significant at all four incubation times ($P<0.001$) (Figure 6.4). An additional analysis of variance showed no differences in the mean intensity of the SK-BR-3 cells at any of the four incubation times ($P>0.5$).

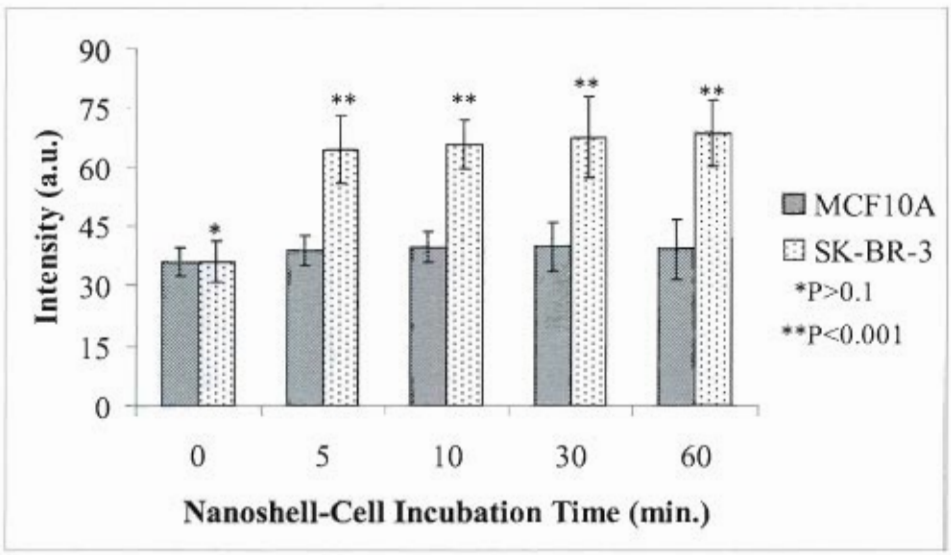

Figure 6.4. Mean quantitative intensity values for samples of MCF10A and SKBR3 cells incubated with nanoshells for the indicated times. Differences between cell types incubated without nanoshells were not statistically significant ($P>0.1$, $n=10$). Differences between cell types incubated with nanoshells were statistically significant at all time points ($P<0.001$, $n=10$). Error bars indicate standard deviations.

To further compare the differences between contrast that could be achieved at 5 minutes and 60 minutes for the SK-BR-3 cells, we examined the number of bound nanoshells at both time points. To do so, we first developed a simple UV-vis spectroscopy method to determine the concentration of nanoshells in solution. On the basis of dilutions of known nanoshell concentrations, we used linear regression to

estimate the concentration of nanoshells in a given solution (Figure 6.5). We confirmed the existence of a linear relationship between absorbance and corresponding concentration of nanoshells for concentrations ranging from 9.8×10^7 to 2.0×10^9 particles/mL. With a goodness-of-fit (R^2) value of 0.986, we concluded that the absorbance accurately predicts the concentration of an unknown suspension of nanoparticles that falls within this range.

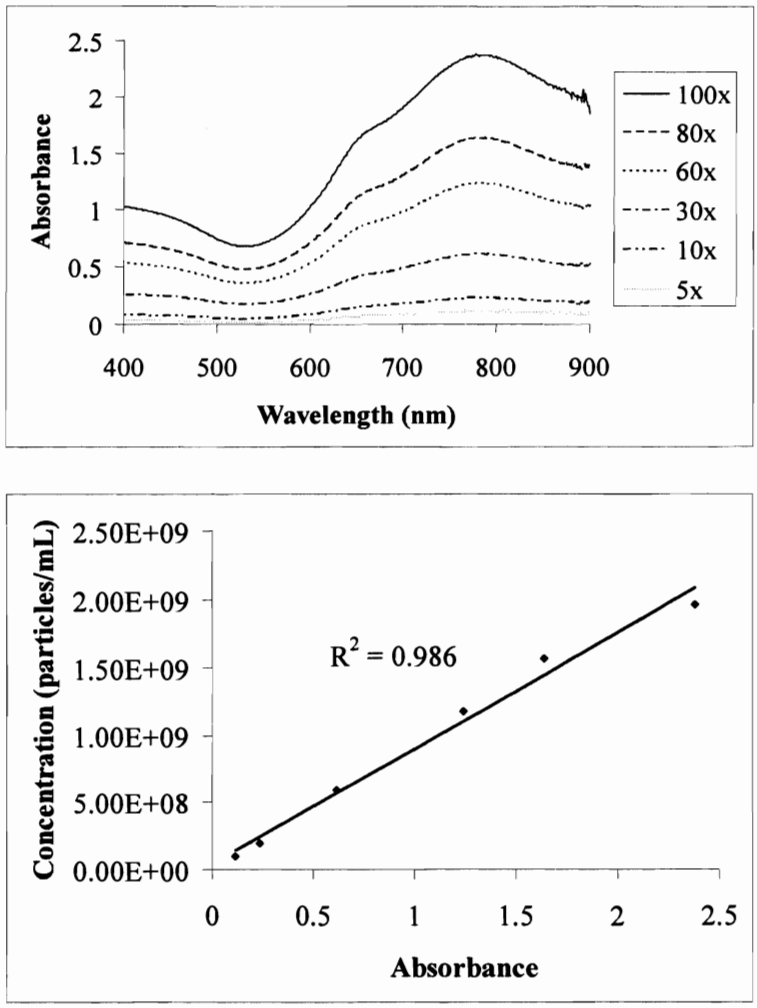

Figure 6.5. Top, spectra of serial dilutions of known nanoshells concentrations in suspension. Bottom, linear regression analysis of known nanoshell concentrations vs. the corresponding peak absorbance values.

We next used this relationship between absorbance and concentration to measure the absorbance of unbound nanoshells collected after incubation and cell rinsing and subsequently resuspended in a volume of water equal to that of the diluted samples of known concentration. Knowing the initial number of nanoshells and cells, we could derive the approximate number of nanoshells bound to each cell, which we did for the triplicate samples of nanoshells plus cells after 5 minutes and 60 minutes of incubation. At 5 minutes of incubation, 1593 ± 121 nanoshells were bound per cell; at 60 minutes, that range was 1686 ± 40 nanoshells per cell ($P>0.1$, not significant) (Figure 6.6). Thus, roughly 95% of the binding noted at 60 minutes had occurred within the first 5 minutes of incubation. Our imaging results suggest that this 5% difference did not seem to affect contrast.

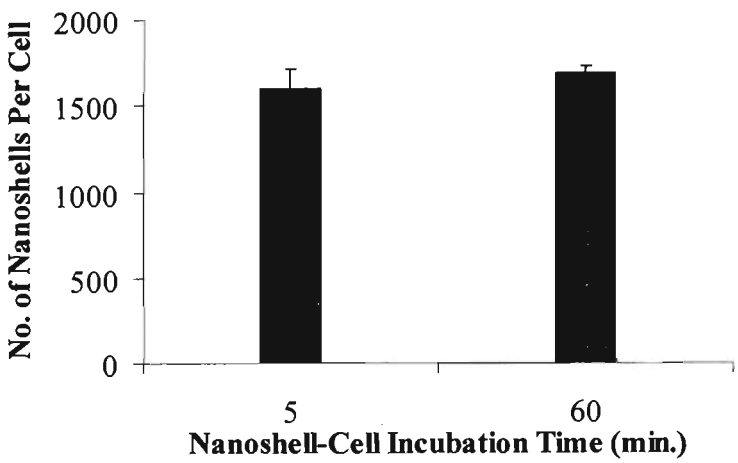

Figure 6.6. Number of nanoshells bound per SK-BR-3 cell after 5 minutes and 60 minutes of incubation. Values shown are the means of triplicate measurements. Error bars indicate standard deviations.

6.4 Conclusions

These findings support the proof of concept that optical contrast of HER2-overexpressing breast cancer cells can be achieved by brief periods of incubating those cells with nanoshells. Although the ability to detect malignancy by such means is critical for *in vivo* applications and for *in vitro* applications associated with biological fluids, other opportunities exist for using such techniques to diagnose solid tumor specimens *in vitro*. The time between diagnosis and treatment could be drastically shortened by use of microscopic evaluations of excised tissue samples that provide rapid and reliable results. We have shown both qualitatively and quantitatively that nanoshells can be used to achieve discernible contrast between cancerous and normal breast cells in 5 minutes. These results suggest that gold nanoshells can be designed and optimized to enhance the scattering signatures of cancer cells at minimal incubation times necessary for potential applications in point-of-care cancer diagnostic imaging. Subsequent studies extend these findings from the cellular level to tumor specimen models.

Chapter 6 References

1. Loo C, Lowery A, Halas N, West J, and Drezek R. "Immunotargeted nanoshells for integrated cancer imaging and therapy", Nano. Lett. 5(4), 709-711 (2005).

2. Loo C, Hirsch L, Lee MH, Chang E, West J, Halas N, and Drezek R. "Gold nanoshell bioconjugates for molecular imaging in live cells", Opt. Lett. 30(9):1012-1014 (2005).

3. Lowery AR, Gobin AM, Day ES, Halas NJ, and West JL. "Immunonanoshells for targeted photothermal ablation of tumor cells", Int. J. Nanomedicine. 1(2):149-154 (2006).

4. Gobin AM, Lee MH, Halas NJ, James WD, Drezek RA, and West JL. "Near-infrared resonant nanoshells for combined optical imaging and photothermal cancer therapy", Nano. Lett. 7(7):1929-1934 (2007).

5. Sokolov K, Follen M, Aaron J, Pavlova I, Malpica A, Lotan R, and Richards-Kortum R. "Real-time vital optical imaging of precancer using anti-epidermal growth factor receptor antibodies conjugated to gold nanoparticles", Cancer Res. 63(9):1999-2004 (2003).

6. El-Sayed IH, Huang X, El-Sayed MA. "Surface plasmon resonance scattering and absorption of anti-EGFR antibody conjugated gold nanoparticles in cancer diagnostics: applications in oral cancer", Nano Lett. 5(5):829-834 (2005).

7. Sun J, Zhu MQ, Fu K, Lewinski N, and Drezek R. "Lead sulfide near-infrared quantum dot bioconjugates for targeted molecular imaging", Int. J. Nanomed. 2(2):235-240 (2007).

8. Gao X, Cui Y, Levenson, RM, Chung LW, and Nie S. "In vivo cancer targeting and imaging with semiconductor quantum dots", Nat Biotechnol. 22(8):969-976 (2004).

9. Cao L, et al. "Carbon Dots for Multiphoton Bioimaging", J. Am. Chem. Soc. 129(37):11318-11319 (2007).

10. Huang X, El-Sayed IH, Qian W, and El-Sayed MA. "Cancer cell imaging and photothermal therapy in the near-infrared region by using gold nanorods", J. Am. Chem. Soc. 128(6):2115-2120 (2006).

11. Durr NJ, Larson T, Smith DK, Korgel BA, Sokolov K, Ben-Yakar A. "Two-photon luminescence imaging of cancer cells using molecularly targeted gold nanorods", Nano. Lett. 7(4):941-945 (2007).

12. Yu C, Nakshatri H, Irudayaraj J. "Identity profiling of cell surface markers by

multiplex gold nanorod probes", Nano Lett. 7(8):2300-2306 (2007).

13. Sukhanova A, Devy J, Venteo L, Kaplan H, et al. "Biocompatible fluorescent nanocrystals for immunolabeling of membrane proteins and cells", Anal. Biochem. 324:60-67 (2004).

14. Zajac A, Song D, Qian W, and Zhukov T. Colloids Surf. B Biointerfaces. 58:309-314 (2007).

15. Weigum SE, Floriano PN, Christodoulides N, and McDevitt JT. "Cell-based sensor for analysis of EGFR biomarker expression in oral cancer", Lab. Chip. 7(8):995-1003 (2007).

16. Culha M, Stokes DL, Griffin GD, Vo-Dinh T. "Screening for the breast cancer gene (BRCA1) using a biochip system and molecular beacon probes immobilized on solid surfaces", J. Biomed. Opt. 9(3):439-443 (2004).

17. National Comprehensive Cancer Network. Breast Cancer Treatment Guidelines for Patients. Version IX (2007).

18. Mojica CM, Bastani R, Boscardin WJ, and Ponce NA. "Low-income women with breast abnormalities: system predictors of timely diagnostic resolution", Cancer Control. 14(2):176-182 (2007).

19. Guthrie TH. "Breast cancer litigation: A retrospective analysis", Breast J. 1(6):376-379 (1995).

20. Klimberg VS, Harms S, and Korourian S. "Assessing margin status", Surg. Oncol. 8(2):77-84 (1999).

21. Fisher B, Anderson S, Bryant J, Margolese RG, Deutsch M, Fisher ER, Jeong JH, Wolmark N. "Twenty-year follow-up of a randomized trial comparing total mastectomy, lumpectomy, and lumpectomy plus irradiation for the treatment of invasive breast cancer", N Engl. J Med. 347(16):1233-1241 (2002).

22. Hayes DF, Walker TM, Singh B, Vitetta ES, Uhr JW, Gross S, Rao C, Doyle GV, Terstappen LWMM., "Monitoring expression of HER-2 on circulating epithelial cells in patients with advanced breast cancer", Int. J. Oncol. 21(5):1111-1117 (2002).

23. Kornilova ES, Taverna D, Hoeck W, and Hynes NE. "Surface Expression of ERBB-2 Protein is Posttranscriptionally Regulated in Mammary Epithelial-Cells By Epidermal Growth-Factor and By The Culture Density", Oncogene 7(3):511-519 (1992).

CHAPTER 7[e]

INVESTIGATE THE USE OF GOLD NANOSHELLS AS CONTRAST AGENTS FOR TWO PHOTON MICROSCOPY

Based on successful experiments demonstrating that gold nanoshells could be used to enhance contrast of HER2-overexpressing cancer cells within 5 minutes of incubation time, this chapter focuses on a new characteristic of these nanoparticles (two-photon-induced luminescence) which is subsequently utilized to validate the ability to preferentially target HER2-positive cancer cells in a heterogeneous cell population.

7.1 Introduction

Accurate cancer diagnosis through its multistage progression is critical for developing effective and selective cancer treatments. In order to provide clinicians with functional diagnostic results, knowledge of the molecular signatures of carcinogenesis is necessary. Due to their over-expression during the development of cancer, several biomarkers have been identified as a biological means of characterizing these signatures.[1] Although the acquisition of molecular-specific data is typically associated with gene arrays and proteomics[2], there is an opportunity to use such biomarkers as tools for both *in vitro* and *in vivo* diagnostic evaluations of tissue specimens, such as during surgery, in order to identify malignant cells among heterogeneous tissue.

---

[e] Adapted from: Bickford LR, Sun J, Fu K, Lewinski N, Nammalvar V, Chang J, Drezek RA, "Enhanced Multi-Spectral Imaging of Live Breast Cancer Cells Using Immunotargeted Gold Nanoshells and Two-Photon Excitation Microscopy"; *Nanotechnology*, 19, 315102 (2008).

Silica-based gold nanoshells, which are advantageous for several biological applications due to their unique optical tunability and potential as multi-modal agents, have previously demonstrated enhanced diagnostic imaging potential of carcinogenesis at the microscopic scale through the use of extracellular biomarkers[3-6]. By manipulation of the size of their silica cores and gold outer shells, nanoshells can be optically tuned to absorb or scatter light from wavelengths ranging from the visible to the near-infrared, allowing for both imaging and therapy applications[7]. Achieving optimal contrast of gold nanoshells for biological diagnostics includes a combination of developing nanoshells that are tuned to scatter or absorb light in the near-infrared (NIR), where biological chromophores absorb minimal light, and the use of NIR-based imaging systems.

Although several optical devices have been used to validate applications of gold nanoshells as viable contrast agents[3-15], none have focused on evaluating the effectiveness of using immunotargeted nanoshells as contrast agents for cell surface biomarkers using nonlinear excitation microscopy. Nonlinear optics has been used extensively for analyzing fluorescent signals in animal models and tissue samples[16-20]. By using a femtosecond pulsed laser, two photons can be used simultaneously to excite tissue molecules similar to the excitation generated by a single photon, but with twice the energy. Only the molecules at the focus of the femtosecond laser will be excited, resulting in greater resolution than that achievable with single photon systems, such as conventional confocal microscopy. Additionally, unlike conventional confocal microscopy, a pinhole is not required to reject out-of-focus light and the inherent excitation at only the focal plane means that biological tissue undergoes less photodamage[20]. Although multiphoton microscopy has frequently been used for

enhancing fluorescent signals[16,20], studies have demonstrated that metal particles display photoluminescence as a result of excitation by such multiphoton systems[21,22]. This photoluminescence is induced by a significant field enhancement that occurs upon multi-photon excitation of the metallic molecules[21]. Thus far in the literature, metallic nanoparticles analyzed for two-photon imaging potential have included gold colloid spheres[23,24], gold nanorods[25-29], and gold nanoshells[14]. A recent publication on the use of two photon microscopy for evaluating nanoshell contrast focused on potential dual imaging and therapy applications where unlabeled nanoshells were delivered to murine tumors through extravasations due to the presence of leaky vasculature[14]. However, since nanoshell dimensions are fundamentally variable[7], it is important to further elucidate and confirm the two-photon properties of these highly tunable nanoparticles despite differences in size. Furthermore, since cancer undergoes a multistage progression, the ability to track molecular signatures through the over-expression of biomarkers is crucial in obtaining functional and accurate diagnostic results. Therefore, the goal of our study was to demonstrate the nonlinear properties of very different-sized nanoshells and validate the proof of concept that immunotargeted nanoshells can be used to enhance contrast of malignant human cells *in vitro* through nonlinear excitation prior to our evaluation of this system in excised tissue specimens. Additionally, through the use of two-photon excitation and multi-spectral imaging, the simultaneous acquisition of images at different emission wavelengths was obtained to ascertain the optimal imaging parameters for this system.

We demonstrate the two-photon luminescence properties of two different sizes of gold nanoshells designed with a similar plasmon resonance in the near-infrared. We

evaluate the enhanced contrast by comparing HER2-overexpressing breast cancer cells to normal breast cells with and without targeted anti-HER2-bioconjugated gold nanoshells at five different emission wavelength ranges: 451-483 nm, 483-515 nm, 515-547 nm, 558-579 nm, and 590-644 nm. By evaluating imaging results under different ranges, we explore the broad emission properties of silica-based gold nanoshells under two-photon induced luminescence. The anti-HER2 antibody was selected as a model for surface tumor targeting due to the association of HER2-overexpression with more aggressive breast cancers seen in 15-25% of all breast cancer cases[30]. Additionally, studies in our laboratory have previously demonstrated effectiveness of using immunotargeted nanoshells as diagnostic imaging agents for HER2-overexpressing cancer cells[3,5-6,13]. We show that for immunotargeted nanoshells with a silica core diameter of 254 nm and a gold shell thickness of 19 nm imaged with our specific system (set at 10% of maximum excitation power), enhanced contrast of HER2-overexpressing breast cancer cells can be visualized from 451 nm – 644nm. Under similar conditions, normal breast cells are not detectable. Using this information, we also demonstrate the ability to selectively label HER2-overexpressing cells with anti-HER2 nanoshells in a heterogeneous cell population.

7.2 Methods and Materials

7.2.1 Multiphoton Imaging System

A Zeiss Laser Scanning Microscope (LSM) 510 META multi-photon system was used in conjunction with a Coherent Chameleon femtosecond mode locked Ti:Sapphire laser to collect two-photon data (Figure 7.1). The wavelength of the polarized output

laser beam was tunable between 720-950 nm with pulse width of 140 fs at a repetition rate of 90 MHz. A short-pass dichroic mirror (KP700/488, Zeiss) was used to reflect the incident NIR excitation light onto the sample through a 20x or 63x objective and to collect the two-photon-induced luminescence data. To further eliminate the background signal of the excitation light, a wave plate and an IR-blocking filter (BG39, Zeiss) were placed in front of the META detector. The Zeiss LSM META system allowed simultaneous multi-spectral imaging and recording of up to eight emission channels. The maximum output power of the Chameleon femtosecond laser was around 1640 mW for excitation at 780 nm. Based on data from the manufacturer, less than 10% of this power was incident on the sample. The excitation wavelength of 780 nm was chosen as it was within 10 nm of the extinction peak for both nanoshell sizes.

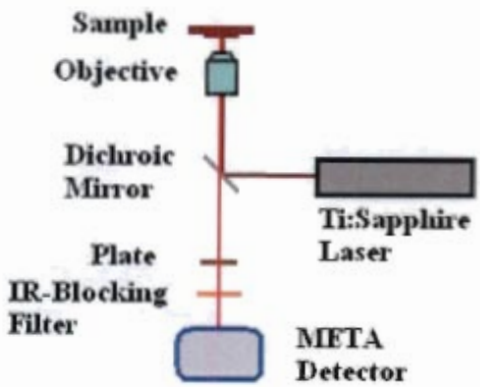

Figure 7.1. Schematic of Zeiss LSM 510 META Multiphoton System Configuration.

7.2.2 Nanoshell Fabrication

Nanoshells were developed as described previously. The two different-sized groups of silica particles were measured by scanning electron microscopy (SEM) as having diameters of 130 nm and 254 nm. The two finished groups of nanoshells were

spectrally analyzed using a Varian Cary 300 UV-vis spectrophotometer (Figure 7.2). The final sizes of the nanoshells were determined using SEM imaging (Figure 7.2, insert) and confirmed using Mie Theory simulation for multilayer spheres. The smaller nanoshells had an average gold shell thickness of 21 nm. The larger nanoshells had an average shell thickness of 19 nm. Nanoshells were stored in deionized water at 4°C until further use.

7.2.3 Nanoshell Surface Modification and Bioconjugation

For live cell imaging, the larger nanoshells were used and targeted to HER2-overexpressing cells through conjugations with anti-HER2 antibodies. In order to prepare the immunotargeted nanoshells, a heterobifunctionalized polyethylene glycol linker (orthopyridyl-disulfide-PEG-N-hydroxysuccinimide ester, OPSS-PEG-NHS, MW = 2kD, CreativeBiochem Laboratories) was first conjugated to anti-HER2 antibodies (C-erbB-2/HER-2/*neu* Ab-4, Lab Vision Corporation) as described in Chapter 5. This reaction proceeded at a 3:1 molar ratio in sodium bicarbonate (100 mM, pH 8.5) on ice overnight. Aliquots of the 'PEGylated' antibodies, at a concentration of 0.4 mg/mL, were stored at -80°C until use. Conjugation of the nanoshells to the PEGylated antibodies was performed by incubating the nanoshells, at a concentration of 1.6×10^9 particles/mL, with the PEGylated antibodies for one hour under refrigeration (4°C). In order to block vacant adsorption sites, the nanoshells were further incubated with a 10 μM polyethylene glycol-thiol cocktail (PEG-SH, MW = 5kD, Nektar) for 2 additional hours under refrigeration. Unbound antibodies were then removed by centrifugation and the immunotargeted nanoshells were then resuspended in deionized water. Prior to incubation with cells, the immunotargeted nanoshell solution was further modified by the

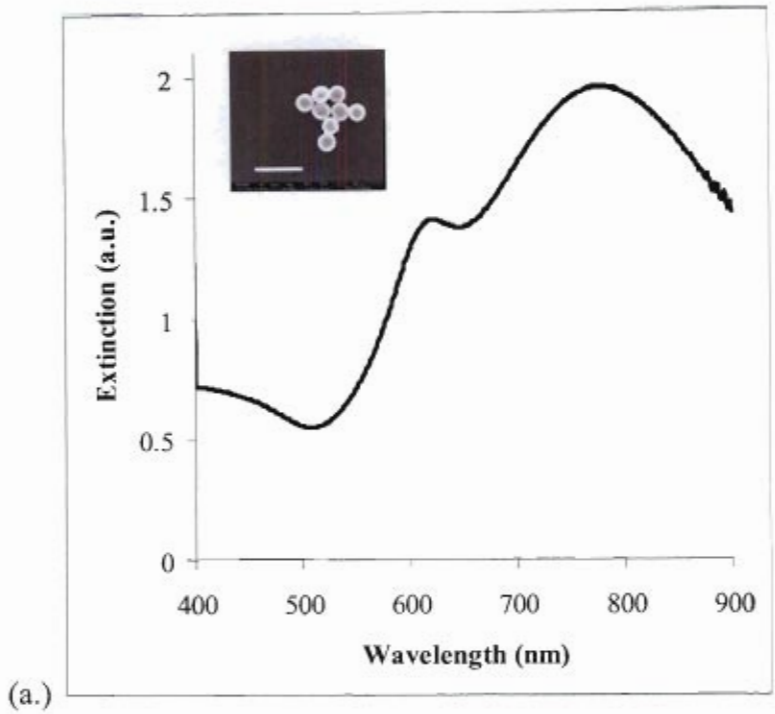

(a.)

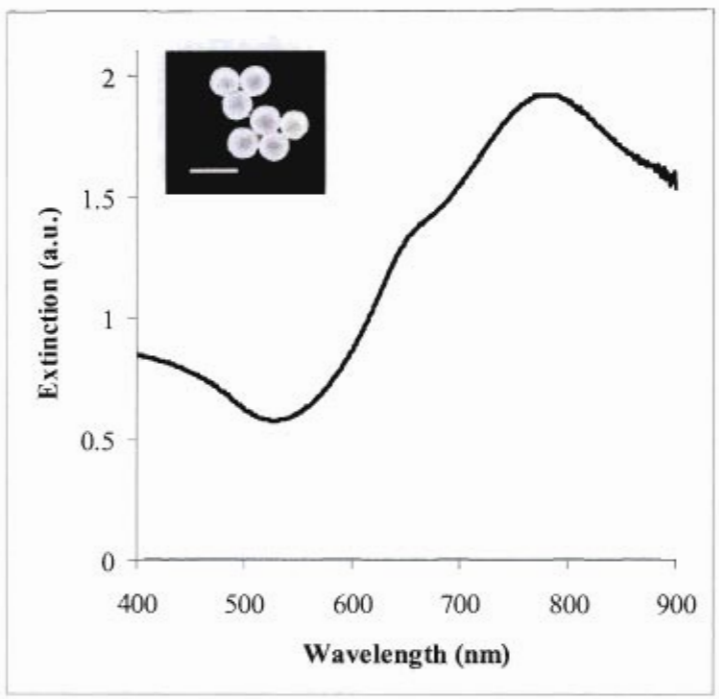

(b.)

Figure 7.2. Measured extinction spectra of nanoshells. (a.) Nanoshells of average core diameter 130 nm and average shell thickness of 21 nm. (b.) Nanoshells of average core diameter 254 nm and average shell thickness of 19 nm. Inserts depict corresponding images from scanning electron microscopy. Scale bars represent 450 nm.

addition of bovine serum albumin (BSA) and phosphate-buffered saline (PBS) to a final concentration of 1% each.

7.2.4 Cell Preparation for Visualization of Enhanced Contrast

SK-BR-3 cells (American Type Culture Collection, ATCC) were grown at 37°C in a 5% CO_2 atmosphere using McCoy's 5A growth medium supplemented with 1% antibiotics and 10% fetal bovine serum (FBS). MCF10A cells (ATCC) were also grown at 37°C in a 5% CO_2 atmosphere using Mammary Epithelial Basal Medium (MEBM) supplemented with a BulletKit (Clonetics) and 1% antibiotics. Both cell lines were grown in 25-cm^2 culture flasks until confluent, rinsed once with 1xPBS, and incubated with trypsin-EDTA for 5 minutes at 37°C in a 5% CO_2 atmosphere. The trypsin-EDTA was then neutralized with the appropriate culture medium and the cells were subsequently counted using a hemacytometer. For each cell line, an estimated $6x10^5$ cells were placed in each of two 15-mL conical tubes and then centrifuged at 115 x g for 3 minutes. One cell pellet was resuspended in the immunotargeted nanoshell solution and the other pellet was resuspended in an equal volume of 1xPBS. The cells were then incubated at 37°C in a hybridization chamber (VWR International) and rotated under a motor speed of 7 rpm for 10 minutes. Post incubation, the cells were centrifuged at 115 x g for 3 minutes, the supernatant was removed, and the cells were rinsed once with 1xPBS. Following rinsing, cells were resuspended in 10% glucose in 1xPBS in order to maintain cell viability during imaging. The cell suspensions were then placed on chambered coverglasses (Fisher Scientific) prior to two-photon imaging.

7.2.5 Cell Preparation for Validation of Nanoshell-Specific Labeling

SK-BR-3 cells and MCF10A cells were grown and cultured as stated above. Similarly, the cells were grown to confluence and counted with a hemacytometer. For each cell line, an estimated $3x10^5$ cells were placed in each of two 15-mL conical tubes and then centrifuged at 120 x g for 3 minutes. After supernatant was removed, the SK-BR-3 cells were resuspended in 2 ml of hexidium iodide (Invitrogen, 15 μM) and the MCF10A cells were resuspended in an equal volume of 1 x PBS. Samples were then incubated at 37°C (under a motor speed of 7 rpm) in the hybridization chamber used previously for 15 minutes. The SK-BR-3 samples were then centrifuged at 120 x g for 3 minutes and resuspended in 1 x PBS. Next, all samples were centrifuged at 120 x g for 3 minutes. Nanoshells (1.6×10^9 particles/mL) were then added to one tube from each cell line and then both of these cell populations were combined into one 15-ml conical tube. The remaining tubes were resuspended in an equal volume of 1 x PBS (1 ml) and similarly combined (control condition). All samples were then incubated at 37°C (under a motor speed of 7 rpm) in the hybridization chamber for 5 minutes. Post-incubation, both tubes of heterogeneous cells were centrifuged at 15 g for 3 minutes and resuspended in 1 ml of a 1:1 SK-BR-3:MCF10A media solution. An aliquot of cells (~10 μl) was evaluated for cell viability using Trypan Blue (Sigma Aldrich).

7.3 Results and Discussion

By manipulation of the core-to-shell ratio, nanoshells can be designed to strongly absorb or scatter light upon near-infrared excitation. In order to validate the two-photon characteristics of silica-based gold nanoshells, we designed two different sizes of

nanoshells with a similar peak surface plasmon resonance in the near-infrared. After fabrication of two different-sized silica cores, their average diameters were confirmed through scanning electron microscopy (SEM) as 130 nm and 254 nm. Once the gold shell was added, the nanoshells were measured by SEM and their optical properties were assessed by UV-Vis spectroscopy. The smaller nanoshells had an average diameter of 172 nm and a peak surface plasmon resonance at 772 nm; for the larger nanoshells, the average diameter was 292 nm, with a peak surface plasmon resonance occurring at 778 nm (both shown previously in Figure 7.2). Two-photon luminescence properties of the gold nanoshells were then observed using a Zeiss LSM 510 META multiphoton system with the configuration shown in Figure 7.1. The two-photon properties were verified by evaluating the dependence of increasing logarithmic emission intensity on increasing logarithmic excitation power. Aliquots of both sizes of bare nanoshells suspended in deionized water were well dispersed with sonication and separately placed on chambered coverglasses (Fisher Scientific). Data was recorded at an excitation wavelength of 780 nm which corresponded to the peak plasmon resonance of the nanoshells for both sample sizes. The excitation power was varied from 2% to 15% of the maximum laser power with a detection spectral band of 494 – 634 nm. By using the image processing software inherent in the LSM 510 META system, the average intensities of the nanoshell suspensions were obtained. Dependence of luminescence intensity on excitation power at 780 nm for both smaller- and larger-sized nanoshells was determined (Figure 7.3). The slopes of the fitted linear curves are estimated as 2.02 and 2.18 for the smaller and larger nanoshells, respectively, in accordance with the characteristic two-photon-induced quadratic dependence of emission intensity on excitation power[14,16,20]. Specifically,

Wang *et al.* demonstrated that the dependence of luminescence intensity on excitation power for gold nanorods ranged from 1.97 to 2.17.[27] This disparity was attributed to possible nanoparticle melting after increasing the power on the nanorod sample and, subsequently, decreasing the power on the same sample. However, in our study, since a difference in quadratic dependence exists for two sizes of gold nanoshells treated under the same conditions, we believe the nanoshells may actually undergo photophysics which are not yet fully elucidated.

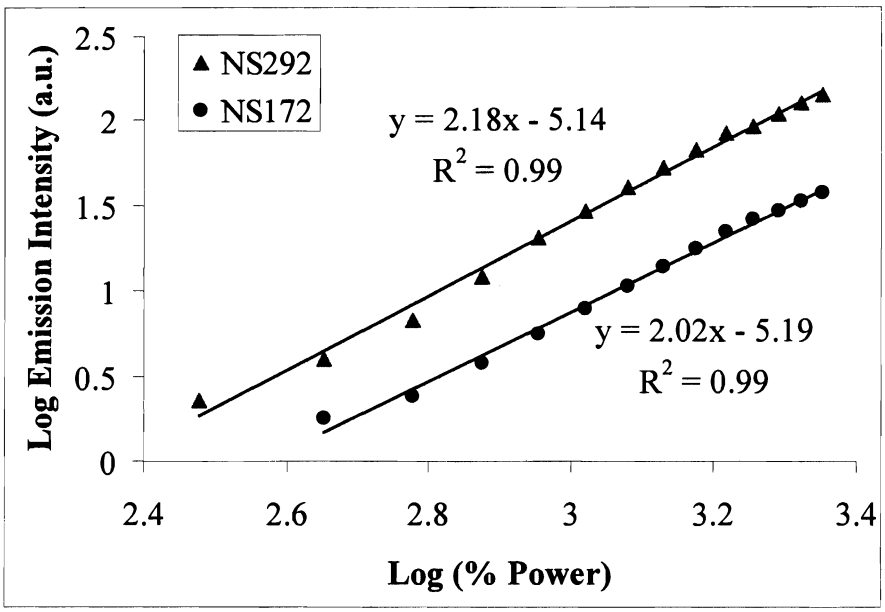

Figure 7.3. Quadratic dependence of luminescence intensity on excitation power at 780 nm for two different-sized nanoshells. Nanoshells of core diameter of 130 nm and shell thickness of 21 nm are designated as NS172. Nanoshells of core diameter of 254 nm and shell thickness of 19 nm are designated as NS292. Data was recorded with a 20x objective.

In order to demonstrate the enhanced two-photon optical signatures of breast cancer cells labeled with immunotargeted nanoshells, the HER2-overexpressing epithelial breast cancer cell line, SK-BR-3, was analyzed and compared to the normal breast

epithelial cell line, MCF10A, which does not overexpress HER2. For this component of the study, the cells were incubated with the larger nanoshells which were conjugated to anti-HER2 antibodies. Images were taken of the SK-BR-3 cancer cells under three conditions: labeled with nanoshells at 10% of maximum laser power, unlabeled at 10% of maximum laser power, and unlabeled at 100% of maximum laser power. An excitation wavelength of 780 nm was used for all images and five different emission wavelength ranges were analyzed: 451-483 nm, 483-515 nm, 515-547 nm, 558-579 nm, and 590-644 nm. Additionally, images were taken of the MCF10A normal cells under the same labeling and imaging conditions. As shown in Figure 7.4a, bright two-photon luminescence signals from nanoshells targeted to cell surface receptors provided clear visualization of the SK-BR-3 cancer cells under only 10% of maximum laser power. However, under the same power, unlabeled cancer cells were not perceivable (data not shown due to lack of detectable signal). By increasing the laser power to 100%, the spectral-resolved two-photon-induced autoflorescence is evident at emission wavelengths ranging from 451 to 547 nm (Figure 7.4b). However, this autoflorescence, which is only visible at the maximized power, cannot be discerned beyond an emission wavelength of 547 nm. With regard to the normal MCF10A cells labeled with immunotargeted nanoshells under 10% of maximum laser power, clear visualization of the cells is not possible and only a few targeted cell surface receptors can be distinguished (Figure 7.4c). Due to the differences in HER2 cell surface receptor expression, which is approximately $8x10^5$ receptors per SK-BR-3 cancer cell[31] and about $1x10^4$ receptors per normal MCF10A cell[32], the contrast was dramatically increased in the cancer cells due to the overexpression of HER2. Similar to the unlabeled SK-BR-3 cancer cells, unlabeled

MCF10A cells imaged at 10% of maximum laser power were not detectable (data not shown due to lack of detectable signal). Furthermore, images collected at 100% of maximum laser power demonstrated that the MCF10A cells exhibited low levels of two-photon-induced autoflorescence (Figure 7.4d). Wang *et al.*[27] and Durr *et al.*[29] have previously shown two-photon imaging results using gold nanorods. However, the images collected were taken over a single emission wavelength range from 400 nm to approximately 700 nm. Based on spectral-resolved image acquisition, however, the unique widely-spanning luminescence properties of gold nanoshells demonstrate great flexibility in selecting the emission wavelengths necessary to minimize the influence of background autofluorescence. Photobleaching was also not observed under the two-photon-induced nanoshell luminescence. Based on a comparison of live cell brightfield images observed before and after laser exposure, morphological changes were not detected as a result of the aforementioned laser conditions and, in particular, all cell membranes remained visible and intact.

Exploiting the wide-spanning emission range of the aforementioned (larger) gold nanoshells, the ability to preferentially label HER2-overexpressing cells in a heterogeneous cell population was evaluated. Hexidium iodide, a nucleic acid stain, displays a maximum excitation/emission wavelength at 518/600 nm upon binding to DNA. Under two photon excitation (at a laser wavelength of 780 nm), hexidium iodide fluoresces strongly from 590 nm to 644 nm. By prelabeling SK-BR-3 cells with hexidium iodide prior to incubation with anti-HER2 nanoshells, confirmation of preferential nanoshell labeling to these HER2-overexpressing cells over normal cells can be easily visualized. Figure 7.5 demonstrates the ability to distinguish MCF10A cells

from SK-BR-3 cells in a heterogeneous mixture simply by adjusting the emission channels in view using the 510 META detector system. The SK-BR-3 cells, which were incubated with hexidium iodide, appear green when the appropriate emission channel for hexidium iodide (590 nm – 640 nm) is selected. As shown in Figure 7.5(a.), when the emission channel is restricted to the wavelength range spanning 450 nm – 515 nm, only cells labeled with nanoshells (which appear red) can be visualized. Once the range is expanded to include both the nanoshell- and fluorescence-emission channels, the ability to specifically target the SK-BR-3 cells with the HER2-targeted nanoshells becomes evident, as only the SK-BR-3 cells are labeled and the MCF10A cells are only perceivable due to the overlay of the phase contrast image (Figure 7.5.(b.), right panel).

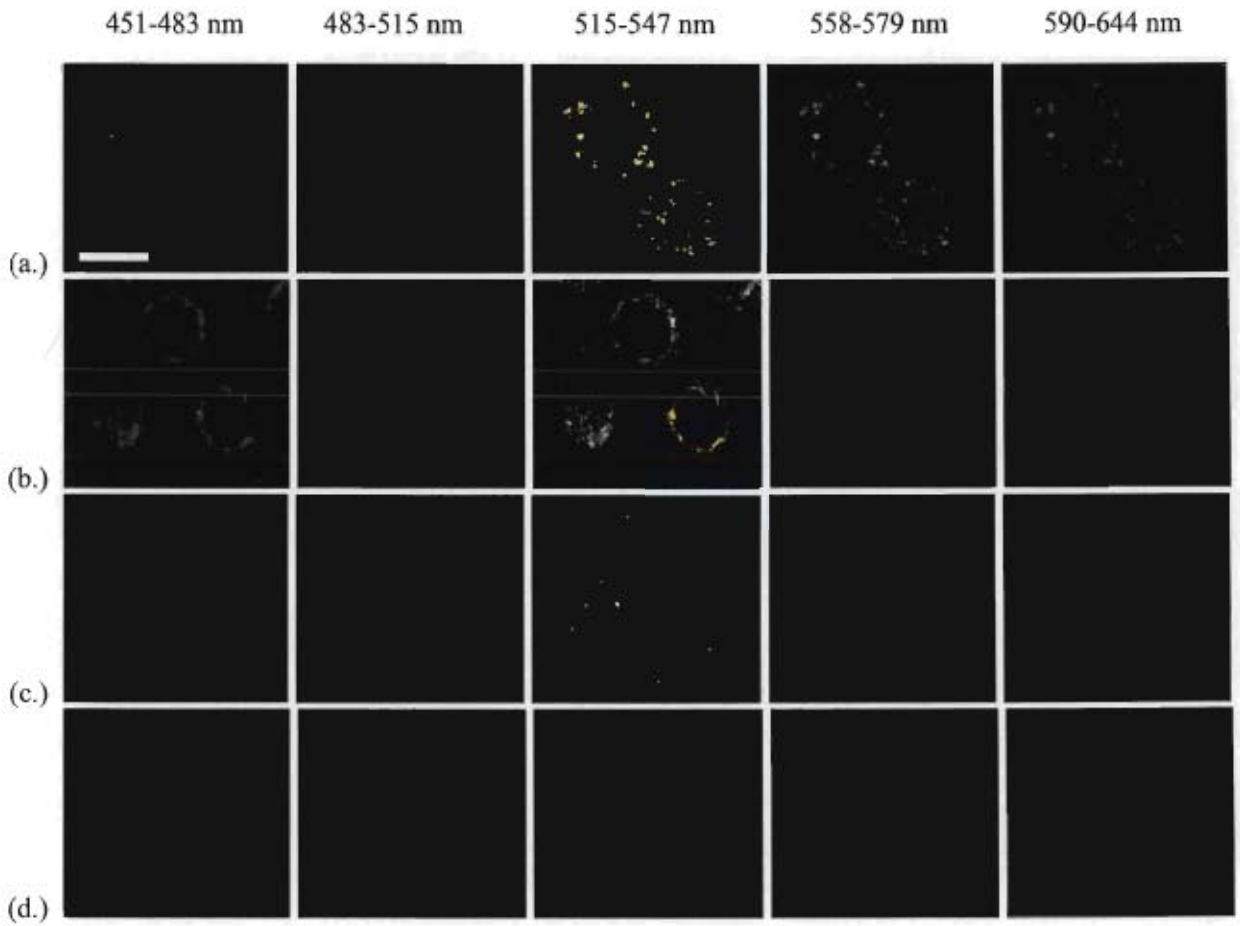

Figure 7.4. Two-photon images (pseudo color) of live SK-BR-3 cancer cells and MCF10A normal cells in suspension taken at different emission wavelengths. (a.) Cancer cells labeled with larger nanoshells at 10% of maximum excitation power. (b.) Unlabeled cancer cells at 100% of maximum excitation power. (c.) Normal cells labeled with larger nanoshells at 10% of maximum excitation power. (d.) Unlabeled normal cells at 100% of maximum excitation power. Images taken at 63x. Scale bar represents 20 μm.

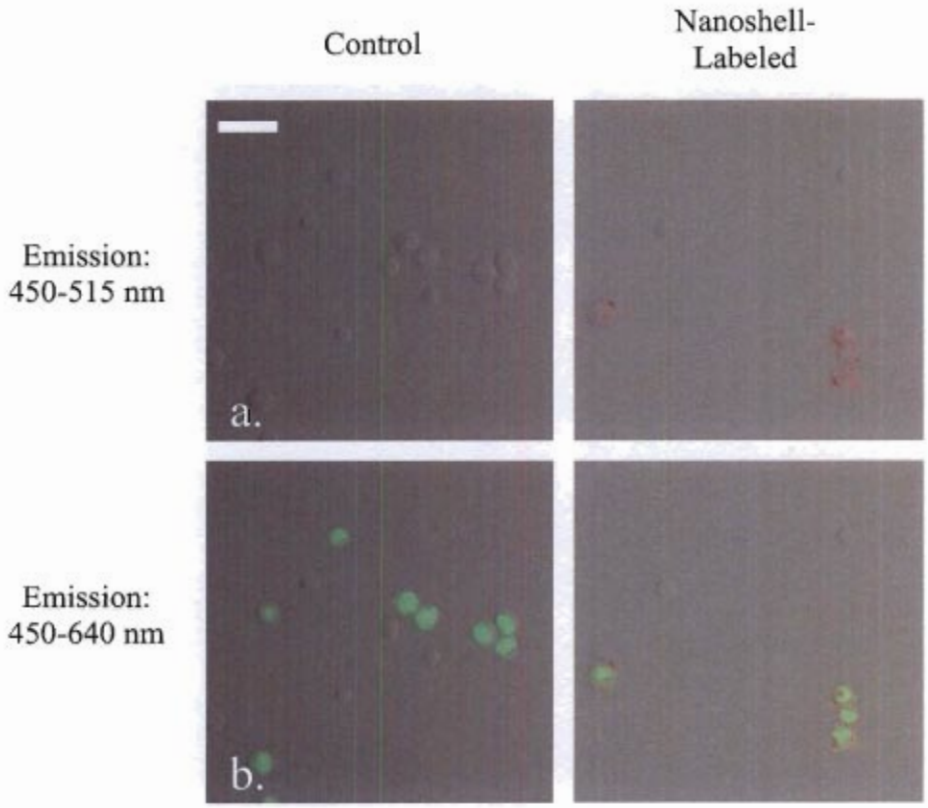

Figure 7.5. Merged two-photon and phase contrast images of control and nanoshell-labeled cell suspensions at 63x. Images take with (a.) nanoshell-emission channel only and (b.) combined nanoshell- and fluorescence-emission channels. Nanoshell luminescence appears red and hexidium iodide fluorescence appears green. Scale bar represents 40 μm.

7.4 Conclusions

Two-photon microscopy is a powerful tool for diagnostic research applications. With advancements in gold-based contrast agent development and flexibility in two-photon excitation wavelength selection readily achieved through tunable laser sources, the potential to use multi-photon imaging for assessment of molecular signatures of malignancy is substantial. In this study, we demonstrate the first use of immunotargeted gold nanoshells as *in vitro* contrast agents for biomarkers of disease using two-photon

microscopy. Additionally, we confirm broad luminescence from gold nanoshells using multi-spectral images to visualize the optical contrast provided by anti-HER2-nanoshells targeted to live HER2-overexpressing breast cancer cells. Using this broad luminescence attribute, we further demonstrate the ability to visualize selective targeting of HER2-overexpressing cells with HER2-labeled nanoshells in a heterogeneous cell population. Our study identifies an additional application of immunotargeted nanoshells and suggests their potential future use as multi-functional probes for molecular imaging.

Chapter 7 References

1. Hawk E, Viner JL, and Lawrence JA. 'Biomarkers as surrogates for cancer development', Curr. Oncol. Rep. 2(3):242-250 (2000).

2. Weinberg RA. the biology of CANCER (New York: Taylor and Francis) pp 727-732 (2007).

3. Loo C, Hirsch L, Lee MH, Chang E, West J, Halas N, and Drezek R. "Gold nanoshell bioconjugates for molecular imaging in live cells", Opt. Lett. 30(9):1012-1014 (2005).

4. Lowery AR, Gobin AM, Day ES, Halas NJ, and West JL. "Immunonanoshells for targeted photothermal ablation of tumor cells", Int. J. Nanomedicine. 1(2):149-154 (2006).

5. Loo C, Lowery A, Halas N, West J, and Drezek R. "Immunotargeted nanoshells for integrated cancer imaging and therapy", Nano. Lett. 5(4), 709-711 (2005).

6. Fu K, Sun J, Bickford LR, Lin AWH, Halas NJ, Yu TK, and Drezek RA. "Measurement of immunotargeted plasmonic nanoparticles' cellular binding: a key factor in optimizing diagnostic efficacy", Nanotechnology 19(4):045103 (2008).

7. Hirsh LR, Gobin AM, Lowery AR, Tam F, Drezek RA, Halas NJ, and West JL. "Metal nanoshells", Ann. Biomed. Eng. 34(1):15-22 (2006).

8. Gobin AM, Lee MH, Halas NJ, James WD, Drezek RA, and West JL. "Near-infrared resonant nanoshells for combined optical imaging and photothermal cancer therapy", Nano. Lett. 7(7):1929-1934 (2007).

9. Wu C, Liang X, and Jiang H. "Metal nanoshells as a contrast agent in near-infrared diffuse optical tomography", Optics Comm. 253(1-3):214-221 (2005).

10. Zaman RT, et al. "In vivo detection of gold nanoshells in tumors using diffuse optical spectroscopy", IEEE J Selected Top Quantum Elec. 13(6):1715-1720 (2007).

11. Fournelle M, Maass K, Fonfara H, Welsch HJ, Hewener H, Günther C, Lemor R. "P6A-5 real time optoacoustic imaging using near infrared absorbing gold nanoshells for contrast enhancement", IEEE Ultrasonics Symp. 2417-2420 (2007).

12. Agrawal A, Huang S, Lin AWH, Lee MH, Barton J, Drezek RA, and Pfefer TJ. "Quantitative evaluation of optical coherence tomography signal enhancement with gold nanoshells", J Biomed. Opt. 11(4):041121 (2006).

13. Loo C. Ph.D. Thesis. Rice University, Houston, Texas (2006).

14. Park J, Estrada A, Sharp K, Sang K, Schwartz A, Smith DK, Coleman C, Payne JD, Korgel BA, Dunn AK, and Tunnell JW. "Two-photon-induced photoluminescence imaging of tumors using near-infrared excited gold nanoshells", Opt. Exp. 16(3):1590-1599 (2008).

15. Wang Y, Xie X, Wang X, Ku G, Gill KL, O'Neal DP, Stoica G, and Wang L. "Photoacoustic tomography of a nanoshell contrast agent in the in vivo rat brain", Nano. Lett. 4(9):1689-1692 (2004).

16. Zipfel WR, Williams RM, and Webb WW. "Nonlinear magic: multiphoton microscopy in the biosciences", Nat. Biotechnol. 21(11):1369-1377 (2003).

17. Denk W, Strickler JH, and Webb WW. "2-photon laser scanning fluorescence microscopy", Science 248(4951):73-76 (1990).

18. Hell SW, Booth M, Wilms S, Schnetter CM, Kirsch AK, Arndt-Jovin DJ, and Jovin TM. "Two-photon near- and far-field fluorescence microscopy with continuous-wave excitation", Opt. Lett. 23(15):1238-1240 (1998).

19. Lewis MK, Wolanin P, Gafni A, and Steel DG. "Near-field scanning optical microscopy of single molecules by femtosecond two-photon excitation", Opt. Lett. 23(14):1111-1113 (1998).

20. Piston DW. "Imaging living cells and tissue by two-photon excitation microscopy", Trends Cell. Biol. 9(2):66-69 (1999).

21. Boyd GT, Yu ZH, and Shen YR. "Photoinduced luminescence from the noble-metals and its enhancement on roughened surfaces", Phys. Rev. B Condens. Matter 33(12):7923-7936 (1986).

22. Mooradian A. "Photoluminescence of metals", Phys. Rev. Lett. 22:185-187 (1969).

23. Huang X, Qian W, El-Sayed IH, and El-Sayed MA. "The potential use of the enhanced nonlinear properties of gold nanospheres in photothermal cancer therapy", Lasers Surg. Med. 39(9):747-753 (2007).

24. Nagesha D, Laevsky GS, Lampton P, Banyal R, Warner C, DiMarzio C, and Sridhar S. "In vitro imaging of embryonic stem cells using multiphoton luminescence of gold nanoparticles", Int. J. Nanomedicine. 2(4):813-819 (2007).

25. Bouhelier A, Bachelot R, Lerondel G, Kostcheev S, Royer P, Wiederrecht GP. "Surface plasmon characteristics of tunable photoluminescence in single gold nanorods", Phys. Rev. Lett. 95(26):267405 (2005).

26. Imura K, Nagahara T, and Okamoto H. "Near-field two-photon-induced photoluminescence from single gold nanorods and imaging of plasmon modes", J. Phys. Chem. B 109(27):13214-13220 (2005).

27. Wang H, Huff TB, Zweifel DA, He W, Low PS, Wei A, and Cheng JX. "In vitro and in vivo two-photon luminescence imaging of single gold nanorods", Proc. Natl. Acad. Sci. 102(44):15752-15756 (2005).

28. Huff TB, Hansen MN, Zhao Y, Cheng JX, Wei A. "Controlling the cellular uptake of gold nanorods", Langmuir 23(4):1596-1599 (2007).

29. Durr NJ, Larson T, Smith DK, Korgel BA, Sokolov K, Ben-Yakar A. "Two-photon luminescence imaging of cancer cells using molecularly targeted gold nanorods", Nano. Lett. 7(4):941-945 (2007).

30. National Comprehensive Cancer Network. Breast Cancer Treatment Guidelines for Patients. 2007, Version IX.

31. Hayes DF, Walker TM, Singh B, Vitetta ES, Uhr JW, Gross S, Rao C, Doyle GV, Terstappen LWMM., "Monitoring expression of HER-2 on circulating epithelial cells in patients with advanced breast cancer", Int. J. Oncol. 21(5):1111-1117 (2002).

32. Kornilova ES, Taverna D, Hoeck W, and Hynes NE. "Surface Expression of ERBB-2 Protein is Posttranscriptionally Regulated in Mammary Epithelial-Cells By Epidermal Growth-Factor and By The Culture Density", Oncogene 7(3):511-519 (1992).

CHAPTER 8[f]

ASSESS THE RAPID DETECTION OF CANCER CELLS IN HUMAN BREAST TISSUE SECTIONS

The proof of concept that nanoshells can label HER2-overexpressing cells preferentially over normal (nonneoplastic) cells within 5 minutes of incubation time has set the groundwork for potentially invoking these particles as rapid diagnostic imaging agents. In this chapter, we next focus our attention to bringing these findings one step closer to clinical practice by evaluating the efficacy of gold nanoshells as rapid imaging agents for HER2-overexpressing human tissue sections.

8.1 Introduction

The accurate assessment of breast cancer cells at the surgical margins (positive margin) is one of the most important factors that can prevent local recurrence in patients undergoing breast conservation therapy (BCT)[1,2]. The presence of positive margin predicts for the presence of residual disease still present in the breast near the surgical margin. More importantly, it has been associated with significantly increased risk of local recurrence after BCT[3-5].

---

[f] Adapted from: Bickford LR, Agollah G, Drezek R, Yu TK, "Silica-gold nanoshells as potential intraoperative molecular probes for HER2-overexpression in *ex vivo* breast tissue using near-infrared reflectance confocal microscopy"; *Breast Cancer Research and Treatment*, 120(3), 547 (2010).

Currently, breast cancer tumor margins are initially examined intraoperatively by the surgeon. This gross examination method, if used alone, can result in positive tumor margins roughly 50% of the time[6]. In specialized centers, intraoperative pathology evaluation of microscopic tumor margins can be obtained of the resected specimen while the patient remains anesthetized. Regions of the specimen that contain suspicious tumor margins are processed by either frozen section histology or touch prep cytology[1], which may take as long as 20 minutes. In many community hospitals, this service is not available, so the resected specimens are analyzed post-operatively. This process takes approximately 24-48 hours to complete due to the series of steps necessary for adequately preserving the tissue.

To enhance visualization of malignancy without the need for lengthy sample preparations, optical imaging tools such as reflectance confocal microscopy (RCM)[8-11] and optical coherence tomography[12-17] have been studied for both *in vivo* and *ex vivo* applications. Although results have been promising, authors have noted difficulty in distinguishing between normal tissue stroma and cancerous tissue when OCT was used alone[13] and it has been suggested that incorporating contrast agents targeted to molecular markers of disease may incur greater resolution and increased detection of cancer cells throughout their multistage progression[10,18]. Subsequent studies have also evaluated the use of targeted metal nanoparticles in tandem with RCM to enhance contrast of cancerous cells and tissues[19-24]. While these results support the ability to improve visualization of key cancer signatures with nanoparticle-based imaging, the minimum time utilized to achieve a diagnostic conclusion ranged from 30 minutes to 2 hours[19-24] for *ex vivo* investigations.

In order to realistically improve upon the current standard of tumor margin detection in the operating room, the time to achieve a diagnostic result must be kept at a minimum. Previously, we demonstrated that targeted gold nanoshells can be used to increase contrast of cancer cells that overexpress HER2 receptors within 5 minutes of incubation[25]. Gold nanoshells, which have a silica core and a thin, gold outer shell, are beneficial nanoparticles for this application because of their tunable optical properties and their ability to be conjugated to antibodies. In this study, we translate our previous findings to conditions more characteristic of intraoperative tumor margin assessment. First, we validate the use of gold nanoshells as effective imaging probes for RCM by evaluating contrast enhancement of diverse populations of HER2-overexpressing cells. Importantly, we also confirm that these nanoshells, after 5 minutes of incubation time, can be used as rapid diagnostic imaging agents for human tissue sections that overexpress HER2 receptors.

8.2 Materials and Methods

8.2.1 Breast Cancer Cell Lines and Ex Vivo Human Breast Tissues

Three separate breast cancer cell lines that are known to overexpress different levels of HER2 receptors were analyzed in this study: SK-BR-3, HCC1419, and JIMT-1. The normal mammary epithelial cell line, MCF10A, was also analyzed as a control that does not overexpress the HER2 antigen. All cell lines were purchased from the American Type Culture Collection with the exception of the JIMT-1 cell line, which was purchased from DSMZ (Germany). The SK-BR-3, HCC1419, and JIMT-1 cell lines were grown with medium (McCoy's 5A, RPMI-1640, and Dulbecco's Modified Essential

Medium, respectively) supplemented with 10% fetal bovine serum (FBS) and 1% penicillin-streptomycin. The MCF10A cells were cultured in Mammary Epithelial Basal Medium (MEBM) supplemented with a BulletKit (Clonetics). The cells were maintained at 37°C in 5% CO_2 atmosphere.

The human normal and cancerous (HER2+ and HER2-) breast tissue specimens were obtained from the Cooperative Human Tissue Network under an Institutional Review Board-approved protocol. Cancerous and HER2 status were determined by pathologists located at the medical centers where the respective tissues were procured. These tissue specimens were initially snap-frozen in liquid nitrogen prior to shipment and then immediately stored at -80°C until use.

8.2.2 Quantification of HER2 Antigen on Cell Surface by Flow Cytometry

Each cell line was grown to confluency, trypsinized and then counted using a hemocytometer. The cells were then incubated with either media alone, PE anti-human CD340 (erbB2/HER-2) antibody (BioLegend), or PE mouse IgG1 isotype control antibody (BioLegend) for 30 minutes on ice in the dark. The cells were then washed, resuspended in 500 µl of cell staining buffer (BioLegend), and stored on ice until they were analyzed at The University of Texas M.D. Anderson Cancer Center (MDACC) flow cytometry core for the immunofluorescence intensity of HER2 expression levels. In order to determine the mean immunofluorescence intensity for each cell line, we used a commercially available kit including PE Anti-Human CD340 (erbB2/HER-2) Antibody, cell staining buffer, and a PE Mouse IgG1 Isotype Control (BioLegend) for background signal correction. The immunofluorescence intensity was converted into antigen binding

capacity using the Quantum Simply Cellular anti-Mouse IgG kit (Bangs Laboratories, Inc.). This kit utilizes four different samples of microbeads with a predetermined number of antigen binding sites which correlates with respective immunofluorescence intensity. A linear scale is then generated and used for the interpretation of antigen binding sites on cell samples of known intensity.

8.2.3 Nanoshell Fabrication and Surface Modification

Nanoshells were fabricated as described in Chapter 5 using previous published procedures.[25-29] Briefly, silica cores were generated using the Stöber method[30] and surfaces were terminated with amine groups. The final silica particles were measured by scanning electron microscopy (SEM) to obtain the average radius of 138 nm. Gold colloid of 1-3 nm in diameter was again prepared[31] and adsorbed onto the silica cores through the amine groups (nanoshell 'seeds'). The gold shell overlay was completed by mixing the nanoshell seeds with additional gold solution, potassium carbonate and formaldehyde. A UV-vis spectrophotometer (Varian Cary 300) was used to analyze the spectrum of the completed nanoshells (Figure 8.1.). Mie Theory was then used to derive the absorption, scattering, and extinction coefficients and, subsequently, the concentration of nanoshells in solution. As confirmed by SEM, the nanoshells had an average radius of 175 nm, a peak surface plasmon resonance at 840 nm and a concentration of approximately 2.3×10^9 particles/mL.

To create molecularly-targeted particles, the nanoshell surfaces were first modified by the addition of either specific or non-specific antibodies (anti-HER2/neu or anti-IgG, respectively) as previously described. The same custom made

heterobifunctionalized polyethylene glycol linker used previously, orthopyridyl-disulfide-PEG-N-hydroxysuccinimide ester (OPSS-PEG-NHS, MW = 2kD, CreativeBiochem Laboratories), was incubated this time with either anti-HER2 antibodies (C-erbB-2/HER-2/*neu* Ab-4, Lab Vision Corporation) or anti-rabbit-IgG (Sigma Aldrich) at a molar ratio of 3:1 in sodium bicarbonate (100 mM, pH 8.5) overnight on ice and under refrigeration. All aliquots were then stored at -80°C.

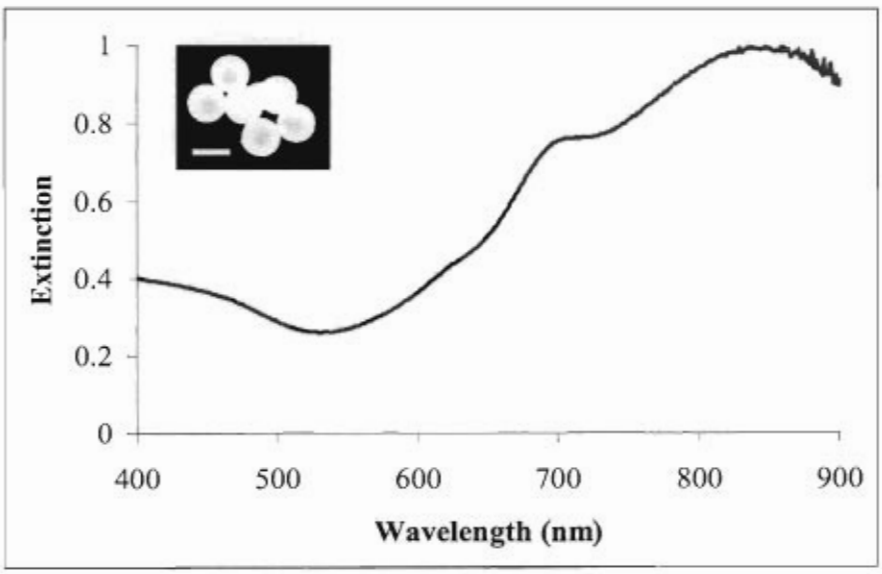

Figure 8.1. Measured spectra of nanoshells (core radius 138 nm, total radius 175 nm). The insert depicts the corresponding image of the nanoshells from scanning electron microscopy. Scale bar represents 350 nm.

In order to perform biological studies, the nanoshells (2.3×10^9 particles/mL) were incubated with the prepared anti-HER2-linker or anti-IgG-liker solution for 1 hour under refrigeration and further stabilized by incubation with a 10 mM polyethylene glycol-thiol solution (PEG-SH, MW = 5kD, Nektar) overnight under refrigeration. Nanoshells were then centrifuged to remove unbound antibodies and resuspended in water. Prior to experimental studies, the nanoshells were brought to room temperature and a solution of

bovine serum albumin (BSA) and phosphate-buffered saline (PBS) was added at a final concentration of 1% each. Samples were vortexed briefly before use.

8.2.4 Imaging Breast Cancer Cell Lines With Nanoshells

Approximately $6x10^5$ cells of each cell line (MCF10A, SK-BR-3, HCC1419, and JIMT-1) were isolated, washed and incubated with a 2 ml solution of either PBS alone, anti-HER2 targeted nanoshells ($2x10^9$ particles), or anti-IgG targeted nanoshells ($2x10^9$ particles). The nanoshell-cell suspensions and controls were then incubated in a hybridization chamber (VWR International) at 37°C and 7 rpm for 15 minutes. After incubation, the suspensions were centrifuged and rinsed two times with PBS to remove unbound nanoshells. The cell pellets were resuspended in 60 μL of the appropriate cell media. This solution was then aliquoted onto a glass slide fitted with a 0.12 mm deep spacer (Invitrogen) and then coverslipped. Images of the different cell types were obtained with a Lucid VivaScope 2500 inverted confocal microscope using a 830 nm source with a lateral resolution < 2μm. The Lucid VivaScope 2500 is a portable, FDA approved system used to assess freshly excised tissue in clinics. Images were taken at the same distance from the glass surface for each condition and at a power of 1.4 mW.

The optical intensity of the reflectance of the cells was measured using ImageJ processing software. An image of pure black was designated with a value of 0 and that of pure white with a value of 255. Average intensity values for each cell line under each condition were calculated from 7 independent areas of the respective glass slide used for imaging. Images used for this component of the study contained areas where no cells were present; therefore, although the intensity of individual cells incubated with HER2-

targeted nanoshells approach 255 (data not shown), this was not possible for widespread images due to the diluted sample allowing certain areas to be void of cells (as seen in Figure 8.2). Sample normality was assessed to evaluate the error distribution for all data points. A normal probability plot of the residuals verified that the samples followed a normal distribution (data not shown). F-tests were also used to determine the equality of variance before applying two-tailed paired Student's t-tests to evaluate significance in the difference in reflectance intensity of cells between two treatment conditions.

8.2.5 Imaging Human Breast Tissue Sections With Nanoshells

Prior to use, samples were thawed briefly in a 37°C water bath and then cut and measured to maintain size consistency. Each cut specimen used ranged from 0.21 - 0.26 grams with dimensions of 5 x 6 mm (length x width) and a thickness of 6 mm. Samples were then embedded in frozen section media (BBC Biochemical) and rapidly frozen on dry ice. A Leica CM1850 UV cryostat was used to section the tissues at a thickness of 20 μm. Four sections were cut per specimen. Normal specimens were sectioned at -35°C and cancerous specimens were sectioned at -20°C. The sections were placed on superfrost slides (Fisher Scientific) and allowed to air dry for 10 seconds. After drying, a 20 mm diameter, 1.0 mm deep silicone isolator with adhesive (Invitrogen) was placed over each section. The sections were then rinsed twice with PBS prior to incubation with blocking reagent (Super Block, ScyTek Laboratories) for 3 minutes at room temperature in order to reduce non-specific binding.

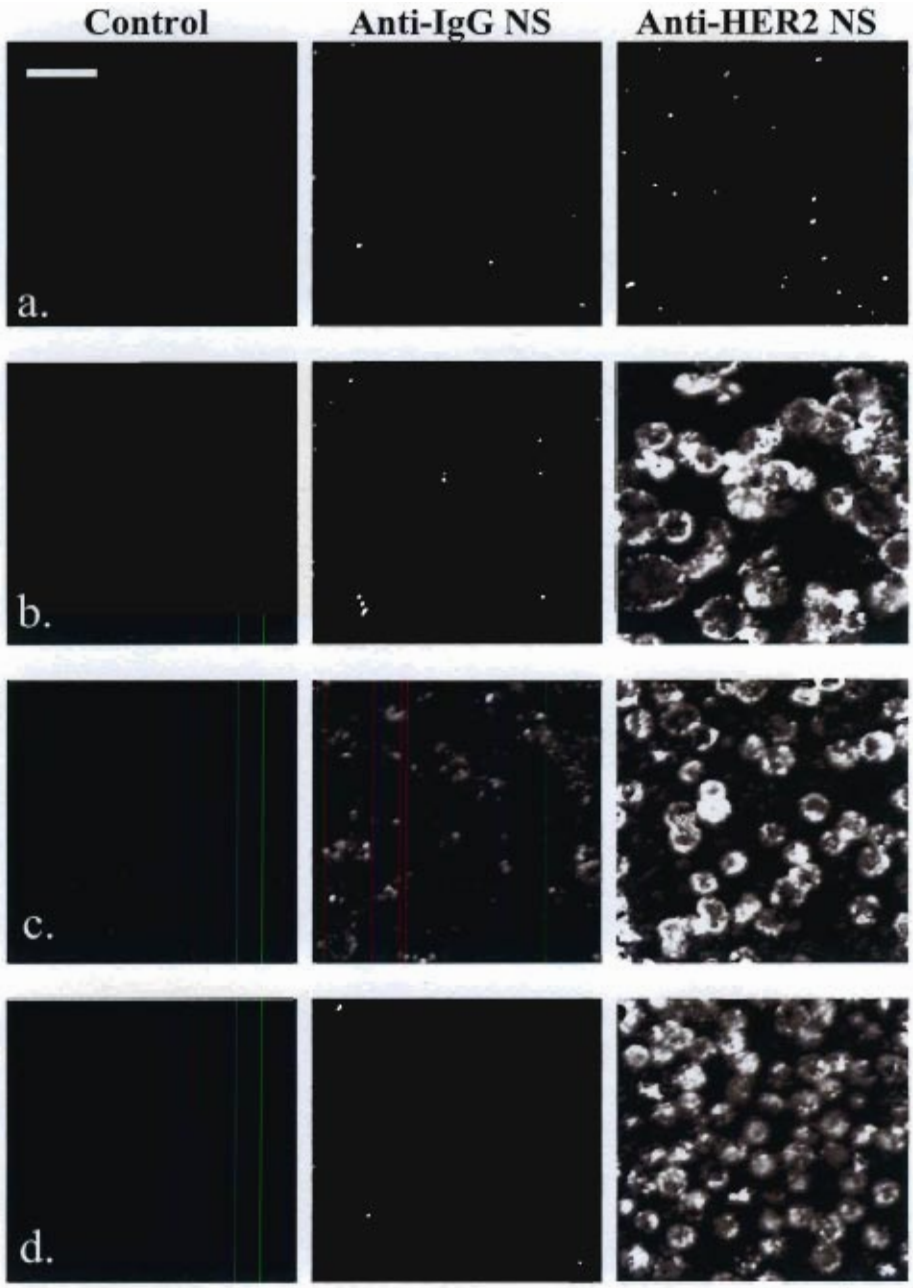

Figure 8.2. Reflectance confocal microscopy images of (a.) MCF10A, (b.) HCC1419, (c.) SK-BR-3, and (d.) JIMT-1 cells incubated with PBS only, nanoshells conjugated to a nonspecific biomarker, or nanoshells conjugated to HER2 antibodies. Power at 1.4 mW. Scale bar represents 50 μm.

After blocking, each of three sections received $1.2x10^9$ particles of the anti-HER2 conjugated nanoshells and one section received an equal volume (325 μl) of PBS. Samples were then coverslipped and placed on an orbital mixer placed in a 37°C incubator for 5 minutes. After incubation, coverslips were removed and samples were rinsed four times with PBS to remove unbound nanoshells. Sections were then covered with immunomount (Thermo Scientific) and coverslipped for imaging.

The Lucid VivaScope 2500 inverted reflectance confocal microscope was used for image acquisition. For each slide, images were taken at three different locations, at the same distance from the glass surface (~16 μm) and at a power of 0.4 mW to validate consistency. After reflectance imaging, coverslips and silicone isolators were removed and a new coverslip was placed over the tissue specimens for brightfield imaging. Brightfield images were obtained using a Zeiss Axioskop 2 microscope outfitted with a color camera (Zeiss AxioCam MRc). All images were taken under the same lighting conditions and magnification (20x).

8.2.6 Immunohistochemistry Staining

For each frozen specimen, 5 μm sections of tissue were also collected for immunohistochemistry (IHC) and hemotoxylin and eosin (H&E) staining. IHC for the HER2 antigen was performed using the Histostain Plus (AEC) Broad Spectrum Kit (Zymed Laboratories) per manufacturer's instructions. H&E staining was performed using the alcoholic Eosin Y solution protocol per manufacturer's instructions (Sigma Aldrich). Brightfield images were acquired using the Zeiss Axioskop 2 microscope as

described above. All images were taken under the same lighting conditions and magnification (20x) to maintain consistency.

8.3 Results and Discussion

8.3.1 Enhanced Optical Imaging of Breast Cancer Cell Lines Using Nanoshells

The goal of this study was to determine if gold nanoshells conjugated to anti-HER2 antibodies can optically enhance the identification of breast cancer cells that overexpress HER2 receptors. Therefore, three breast cancer cell lines (HCC1419, SK-BR-3, and JIMT-1) that are known to overexpress HER2 and a normal mammary epithelial cell line (MCF10A) were chosen to optimize the binding conditions and evaluate specificity of targeted nanoshells. Using flow cytometry, the calculated number of HER2-antigen binding sites, along with the 95% confidence interval for each cell line, was determined and is shown in Table 8.1. Specifically, the breast cancer cell lines were found to have significantly higher (17 to 77 times more) binding sites than the normal breast epithelial cells (MCF10A).

Table 8.1. Average number of HER2-antigen binding sites and the respective 95% confidence intervals for four different breast cell lines.

Number of HER2-Antigen Binding Sites Per Cell	
Cell Line	**Average**
MCF10A	2.2E4 ± 3.4E3
SK-BR-3	1.7E6 ± 7.7E4
HCC1419	1.3E6 ± 5.1E4
JIMT-1	3.8E5 ± 1.6E4

The capacity of the nanoshells to provide optical contrast of the breast cancer cell lines was then assessed using a Lucid VivoScope reflectance confocal microscope, a portable reflectance imaging system that is currently used in clinics. Since the nanoshells are made with a gold shell and have an optical peak resonance at 840 nm, the cells that are bound with the nanoshells clearly reflected more light using reflective confocal microscopy than the cells that are not bound to nanoshells. Qualitatively, the reflective confocal microscopy images in Figure 8.2 demonstrate that the nanoshells conjugated to anti-HER2 antibody bound the most to the three breast cancer cell lines. Most of the cell surface could be visualized. The labeling of the cancer cells was very specific against the HER2 receptor since the nanoshells conjugated with non-specific IgG resulted in only punctate labeling of the same cells. Similarly, only punctate labeling of MCF10A normal epithelial cells was imaged by the nanoshells conjugated with anti-HER2 antibody. This low level of reflectance is likely due the presence of the low level of HER2 receptors present on MCF10A cells, as shown in Table 8.1.

Quantitatively, the reflectance intensity from each breast cancer cell line with HER2 overexpression that was treated with nanoshells conjugated with anti-HER2 antibody was 5 times higher than the reflectance from normal human breast epithelial cells (MCF10A) treated with the same nanoshells ($P<0.001$, Figure 8.3). For each cell line, the binding of nanoshells appeared to be dependent upon the anti-HER2 antibody because the reflectance intensity of the cells was 3 to 5 fold higher when the cells were treated with nanoshells conjugated to anti-HER2 antibody than to non-specific IgG ($P<0.001$). There was no difference in reflectance intensity between any cell type

incubated with only PBS (the control condition) (P>0.1) or with IgG-targeted nanoshells (P>0.1).

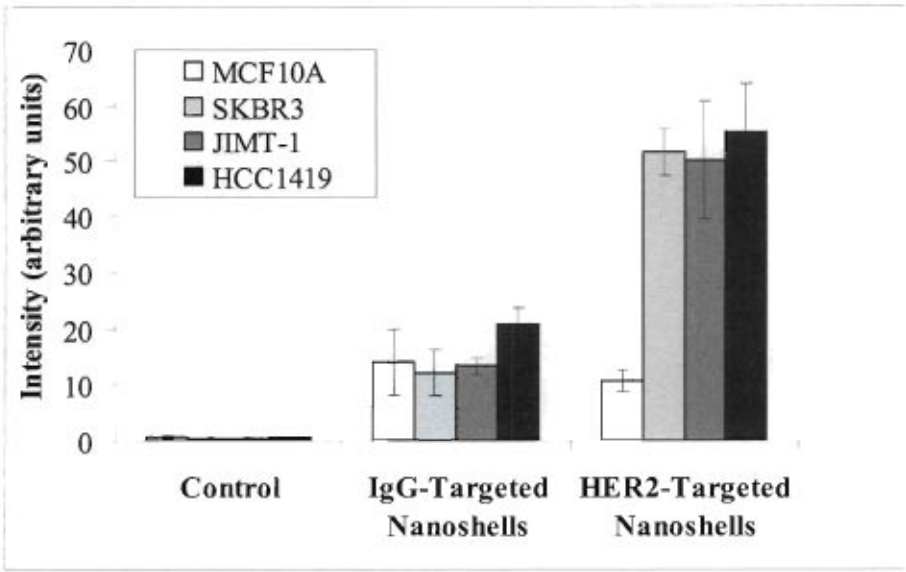

Figure 8.3. Mean quantitative intensity values for samples of MCF10A, HCC1419, SK-BR-3, and JIMT-1 cells incubated with PBS only, nanoshells conjugated to a nonspecific biomarker, or nanoshells conjugated to anti-HER2 antibodies. Differences between cell types incubated with HER2-targeted nanoshells were not statistically significant (P>0.1, n=7). Differences between HER2-overexpressing cell types incubated with HER2-targeted nanoshells and normal cells incubated with HER2-targeted nanoshells were statistically significant (P<0.001, n=7). Error bars indicate standard deviations.

8.3.2 Enhanced Optical Imaging of Human Breast Cancer Tissue Sections Using Nanoshells

As RCM revealed that HER2-targeted nanoshells could be used to enhance contrast in HER2-overexpressing cell lines, we assessed the ability of these nanoparticles to visualize breast cancer cells that overexpressed HER2 receptors using *ex vivo* human tissue sections. Specifically, human breast cancer tissues with and without HER2 receptor overexpresssion (HER2+ and HER2-, respectively) that were resected from patients were incubated with HER2-targeted nanoshells or with PBS for 5 minutes.

Normal breast tissue was used as a control. As shown in Figure 8.4a, tissue sections incubated with PBS showed cells with no perceivable contrast using reflectance confocal microscopy. Similarly, qualitative assessment of the imaging of normal and cancerous HER2- tissue sections incubated with HER2-targeted nanoshells showed little enhanced scattering. However the cancerous HER2+ tissue showed dramatically enhanced contrast after only 5 minutes of incubation with HER2-targeted nanoshells (Figure 8.4b.).

Since tissue without targeted nanoshells shows minimal contrast under reflectance confocal microscopy, we also took brightfield images of the same tissue specimens to validate the distribution of the nanoshells with respect to the tissue surfaces. As can be seen in Figure 8.4c., the nanoshell-targeting seen with brightfield microscopy is consistent with the labeling seen in images taken by RCM. The normal tissue section shows the least amount of targeting due to the prevalence of adipose tissue, which presents as holes within the tissue when cryosectioned. Both cancerous HER2- and HER2+ tissues primarily consist of abnormal tissue structures characteristic of malignancy. Furthermore, the location and arrangement of the HER2-targeted nanoshells corresponds to the results obtained by performing IHC against HER2 (Figure 8.4d.). In order to demonstrate the characteristic morphologic variations associated with normal and cancerous tissue, H&E stained sections have also been included (Figure 8.4e.).

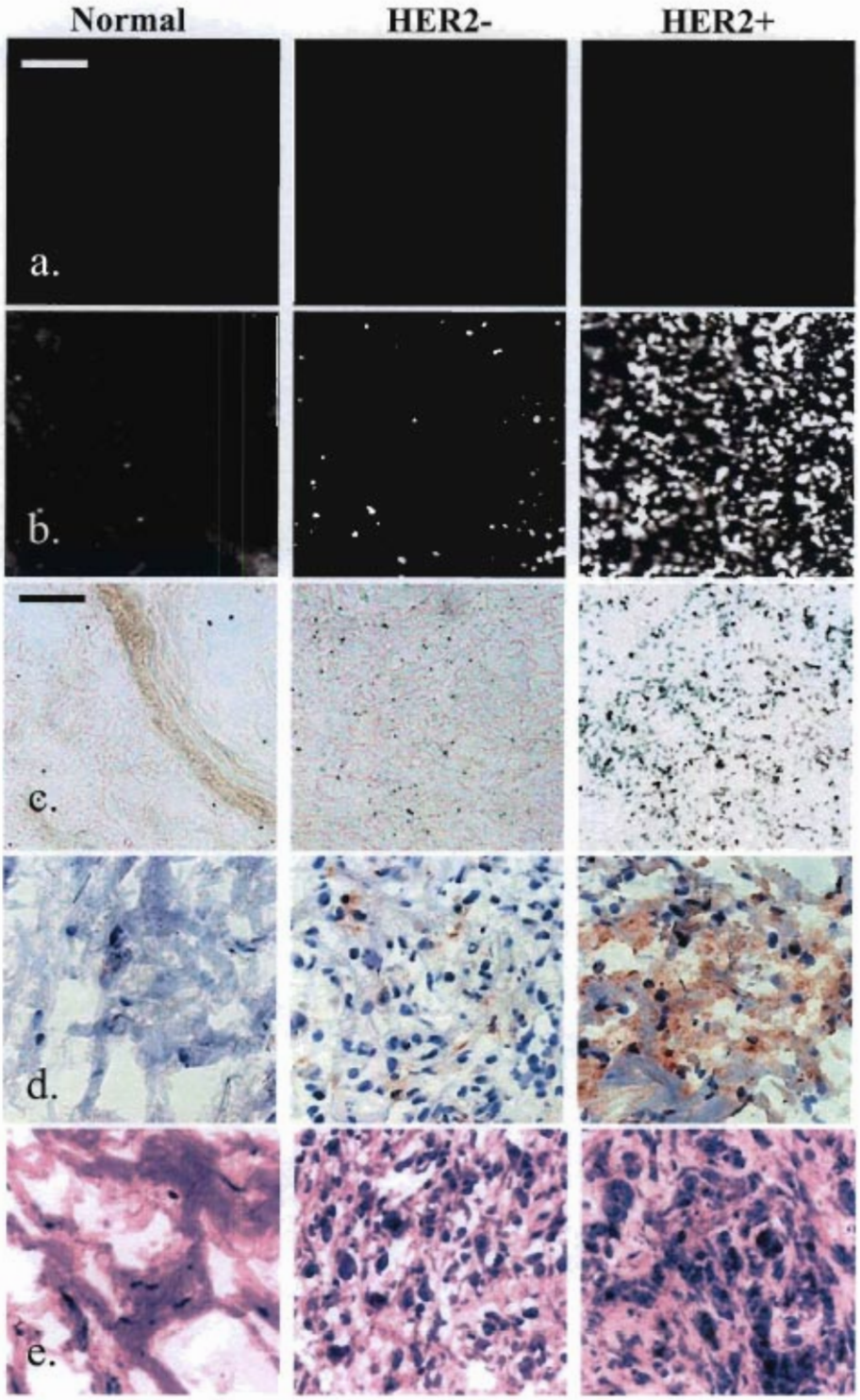

Figure 8.4. (a.,b.) Reflectance confocal microscopy images of normal, HER2- cancerous, and HER2+ cancerous human tissue samples incubated with (a.) PBS or (b.) HER2-targeted nanoshells for 5 minutes. (c.) Respective images from (b.) taken under brightfield microscopy under 20x magnification. (d.) Respective HER2/neu immunohistochemistry results taken under brightfield under 20x magnification. (e.)

Respective H&E results taken under brightfield microscopy under 20x magnification. Power for (a.) and (b.) at 0.4 mW and corresponding scale bar represents 50 μm. Scale bar for (c.), (d.), and (e.) also represents 50 μm.

A major challenge in intraoperative tumor margin detection is the ability to achieve a rapid diagnostic result at the microscopic level directly in the operating room. Although tertiary care centers currently address the evaluation of tumor margins during surgery, non-specialized institutions do not have access to intraoperative pathology assessment. By employing a direct guidance system for the surgeon capable of functioning at the point of care, the amount of time patients spend in surgery and the need for repeat procedures may be reduced. Additionally, the likelihood of achieving tumor resection with negative margins should be improved. Directed re-excision with high sensitivity and specificity may also reduce the amount of tissue that would be removed and, correspondingly, result in superior cosmesis. In this study, targeted gold nanoshells were shown to be an effective contrast agent to improve optical visualization of breast cancer cells. The nanoshells specifically bound to breast cancer cells that overexpressed HER2 receptors with enhanced intensity of up to 5 fold.

Earlier studies have evaluated enhanced contrast in cells and tissues by using targeted metal nanoparticles visualized under reflectance imaging[19-24] as well as quantum dots visualized under fluorescence imaging[32]. However, these studies examined results after long incubation times. In many specialized institutions, intraoperative immediate frozen section histology is used to assess surgical tumor margin status. Since the incubation times in these studies exceeded the time required to perform frozen section histology, the nanoparticles used in those studies are not likely to be clinically advantageous. Previously, we showed that silica-based nanoshells could be used to

enhance contrast in HER2-overexpressing cells within 5 minutes of incubation time[25]. Here, we show that these targeted nanoparticles can also be used to enhance contrast in human tissue sections with an incubation time of only 5 minutes. In fact, these results corresponded to the results obtained with IHC stained against HER2 receptors.

8.4 Conclusions

Since nanoshells can be conjugated to a variety of biomarkers, this system could potentially be used for several biomarkers associated with breast malignancy. In order to translate these findings further into a more immediate diagnostic result in the operating room, studies are currently underway to examine the ability to enhance contrast in resected human tissue without physical sectioning. Since we propose the assessment of tumor margins using the monoclonal antibody HER2 as a molecular marker, we must also understand the distribution of HER2 receptors throughout tissue that is considered HER2 positive. Specifically, the heterogeneity of this biomarker at the margins of tumors from a diverse group of patients who have undergone various neoadjuvant therapies must be studied. Our data suggests that the combined use of targeted nanoshells and reflective confocal microscopy may provide a more immediate assessment of tumor margins based on HER2-expression levels and offer a rapid supplement to current diagnostic techniques.

Chapter 8 References

1. Balch GC, Mithani SK, Simpson JF, Kelley MC. "Accuracy of Intraoperative Gross Examination of Surgical Margin Status in Women Undergoing Partial Mastectomy for Breast Malignancy", Am Surg 71(1):22-27 (2005).

2. Gibson GR, Lesnikoski BA, Yoo J, Mott LA, Cady B, Barth RJ. "A Comparison of Ink-Directed and Traditional Whole-Cavity Re-Excision for Breast Lumpectomy Specimens With Positive Margins", Ann Surg Oncol 8(9):693-704 (2001).

3. Cabioglu N, Hunt KK, Singletary SE, Stephens TW, Marcy S, Meric F, Ross MI, Babiera GV, Ames FC, Kuerer HM. "Surgical Decision Making and Factors Determining a Diagnosis of Breast Carcinoma in Women Presenting with Nipple Discharge", J Am Coll Surg 197(4):697-698 (2003).

4. Vicini FA, Goldstein NS, Pass H, Kestin LL. "Use of Pathologic Factors to Assist in Establishing Adequacy of Excision Before Radiotherapy in Patients Treated with Breast-Conserving Therapy", Int J Radiat Oncol Biol Phys 60(1):86-94 (2004).

5. Smitt MC, Nowels K, Carlson RW, Jeffrey SS. "Predictors of Reexcision Findings and Recurrence After Breast Conservation", Int J Radiat Oncol Biol Phys 57(4):979-985 (2003).

6. Abraham SC, Fox K, Fraker D, Solin L, Reynolds C. "Sampling of grossly benign reexcisions: a multidisciplinary approach to assessing adequacy", Am J Surg Pathol 23(3):316-322 (1999).

7. Cabioglu N, Hunt K, Aysegul AS, Kuerer HM, Babiera GV, Singletary SE, Whitman GJ, Ross MI, Ames FC, Feig BW, Buchholz TA, Meric-Bernstam F. "Role for Intraoperative Margin Assessment in Patients Undergoing Breast-Conserving Surgery", Ann Surg Oncol 14(4):1458-1471 (2007).

8. Parrish A, Halama E, Tilli MT, Freedman M, Furth PA. "Reflectance confocal microscopy for characterization of mammary ductal structures and development of neoplasia in genetically engineered mouse models of breast cancer", J Biomed Opt 10(5):051602 (2005).

9. Tilli MT, Parrish AR, Cotarla I, Jones LP, Johnson MD, Furth PA. "Comparison of mouse mammary gland imaging techniques and applications: Reflectance confocal microscopy, GFP Imaging, and ultrasound", BMC Cancer 8(21):1-15 (2008).

10. Tilli MT, Cabrera MC, Parrish AR, Torre KM, Sidawy MK, Gallagher AL, Makariou E, Polin SA, Liu MC, Furth PA. "Real-time imaging and

characterization of human breast tissue by reflectance confocal microscopy", J Biomed Opt 12(5):051901 (2007).

11. Chen CSJ, Elias M, Busam K, Rajadhyaksha M, Marghoob AA. "Multimodal in vivo optical imaging, including confocal microscopy, facilitates presurgical margin mappling for clinically complex lentigo maligna melanoma", Br J Dermatol 153(5):1031-1036 (2005).

12. Clark A, Gillenwater A, Alizadeh-Naderi R, El-Naggar A, Richards-Kortum R. "Detection and diagnosis of oral neoplasia with an optical coherence microscope", J Biomed Opt 9(6):1271-1280 (2004).

13. Zysk AM, Boppart SA. "Computational methods for analysis of human breast tumor tissue in optical coherence tomography images", J Biomed Opt 11(5):054015 (2006).

14. Wilder-Smith P, Jung W, Brenner M, Osann K, Beydoun H, Messadi D, Chen Z. "In vivo optical coherence tomography for the diagnosis of oral malignancy", Lasers Surg Med 35(4):269-275 (2004).

15. Cobb M, Chen Y, Bailey S, Kemp C, Li X. "Non-invasive imaging of carcinogen-induced early neoplasia using ultrahigh-resolution optical coherence tomography", Cancer Biomark 2(3-4):163-173 (2006).

16. Zuluaga A, Follen M, Boiko I, Malpica A, Richards-Kortum R. "Optical coherence tomography: a pilot study of a new imaging technique for noninvasive examination of cervical tissue", Am J Obstet Gynecol 193(1):83-88 (2005).

17. Boppart S, Brezinksi M, Pitris C, Fujimoto J. "Optical coherence tomography for neurosurgical imaging of human intracortical melanoma", Neurosurgery 43(4):834-841 (1998).

18. Boppart SA. "Advances in Contrast Enhancement for Optical Coherence Tomography", Conf Proc IEEE Eng Med Biol Soc 1:121-124 (2006).

19. Sokolov K, Follen M, Aaron J, Pavlova I, Malpica A, Lotan R, Richards-Kortum R. "Real-Time Vital Optical Imaging of Precancer Using Anti-Epidermal Growth Factor Receptor Antibodies Conjugated to Gold Nanoparticles", Cancer Res 63(9):1999-2004 (2003).

20. Javier DJ, Nitin N, Levy M, Ellington A, Richards-Kortum R. "Aptamer-Targeted Gold Nanoparticles As Molecular-Specific Contrast Agents for Reflectance Imaging", Bioconjugate Chem 19(6):1309-1313 (2008).

21. Aaron J, Nitin N, Travis K, Kumar S, Collier T, Park SY, Jose-Yacaman M, Coghlan L, Follen M, Richards-Kortum R. "Plasmon resonance coupling of metal

nanoparticles for molecular imaging of carcinogenesis in vivo", J Biomed Opt 12(3):034007 (2007).

22. Kah JCY, Olivo MC, Lee CGL, Sheppard CJR. "Molecular contrast of EGFR expression using gold nanoparticles as a reflectance-based imaging probe", Mol Cell Probes 22(1):14-23 (2008).

23. Nitin N, Javier DJ, Roblyer DM, Richards-Kortum R. "Widefield and high-resolution reflectance imaging of gold and silver nanospheres", J Biomed Opt 12(5):051505 (2007).

24. Javier DJ, Nitin N, Roblyer D, Richards-Kortum R. "Metal-based nanorods as molecular-specific contrast agents for reflectance imaging in 3D tissues", J Nanophotonics 2(1):023506 (2008).

25. Bickford LR, Chang J, Fu K, Sun J, Hu Y, Gobin AM, Yu T-K, Drezek RA. "Evaluation of Immunotargeted Gold Nanoshells as Rapid Diagnostic Imaging Agents for HER2-Overexpressing Breast Cancer Cells: A Time-Based Analysis", NanoBiotechnology 4(1-4), 1-8 (2008).

26. Loo C, Lin A, Hirsch L, Lee MH, Barton J, Halas N, West J, Drezek R. "Nanoshell-enabled photonics-based imaging and therapy of cancer", Technol Cancer Res Treat 3(1):33-40 (2004).

27. Loo C, Hirsh L, Lee MH, Change E, West J, Halas N, Drezek R. "Gold nanoshell bioconjugates for molecular imaging in living cells", Opt Lett 30(9):1012-1014 (2005).

28. Loo C, Lowery A, Halas N, West J, Drezek R "Immunotargeted nanoshells for integrated cancer imaging and therapy", Nano Lett 5(4):709-711 (2005).

29. Fu K, Sun J, Bickford LR, Lin AWH, Halas NJ, Yu TK, Drezek RA. "Measurement of immunotargeted plasmonic nanoparticles' cellular binding: a key factor in optimizing diagnostic efficacy", Nanotechnology 19:045103 (2008).

30. Stöber W, Fink A. "Controlled Growth of Monodisperse Silica Spheres in the Micron Size Range", J Colloid Interface Sci 26:62-69 (1968).

31. Duff DG, Baiker A, Edwards PP. "A new hydrosol of gold clusters. 1. Formation and particle size variation", Langmuir 9(9):2301-2309 (1993).

32. Wang J, Yong WH, Sun Y, Vernier PT, Koeffler HP, Gundersen MA, Marcu L. "Receptor-targeted quantum dots: fluorescent probes for brain tumor diagnosis", J Biomed Opt. 12(4):044021 (2007).

CHAPTER 9[g]

ASSESS THE USE OF GOLD NANOSHELLS AS RAPID IMAGING CONTRAST AGENTS FOR INTACT *EX VIVO* BREAST TISSUE SPECIMENS

Though previous studies have shown that gold nanoshells can rapidly afford enhanced contrast of HER2-overexpression in both *in vitro* cell studies and *ex vivo* tissue sections, the ultimate objective is to discern HER2-overexpressing tissue from nonneoplastic tissue *without* the need for physical sectioning. Therefore, in this chapter, we examine the ability to macroscopically and microscopically visualize HER2 biomarker overexpression in intact *ex vivo* human breast tissue specimens.

9.1 Introduction

Macroscopic visualization of questionable tissue is attractive for enhancing the sensitivity and specificity of tumor margin delineation. If the number of suspicious regions that require further microscopic processing can be reduced, surgeons and pathologists can focus their attention and resources on areas that remain inconclusive. Currently, macroscopic evaluation occurs for breast cancer specimens that involve microcalcifications or nonpalpable masses and does not occur for palpable breast

[g] Adapted from: Bickford LR, Thekkek N, Agollah G, Drezek RA, "Rapid Stereomicroscopic Imaging of HER2-Overexpression in Ex Vivo Breast Tissue Using Topically Applied Silica-Based Gold Nanoshells"; *Breast Cancer Research and Treatment*, In Preparation.

masses.[1] For nonpalpable masses that have been resected, the specimen is first oriented with sutures prior to delivery to pathology. The whole specimen is then radiographed and then inked by pathologists to further orient the specimen as to *in situ* location (superior, lateral, etc., surfaces). The tissue is next sectioned serially and those sections are subsequently radiographed and followed by gross examination. The radiographic images are used to determine the extent of the breast disease and the proximity to the resected margins. An adequate margin of 1 cm is considered sufficient under standards used at MDACC.[1] Although specimen radiography appears to increase the accuracy of tumor margin detection, limitations have been noted. For instance, microcalcifications are not necessarily associated with malignancy and areas that appear as tumor on radiographic images may actually be areas of lymphocytic accumulation due to nonneoplastic conditions.[2] Additionally, the microscopic extent of the tumor may actually be misjudged by radiography.[2] In order to increase the sensitivity and specificity associated with macroscopic evaluations, the use of contrast agents targeted to specific biomarkers associated with disease may present superior opportunities.

In preceding studies, we confirmed that silica-based gold nanoshells targeted to anti-HER2 receptors could be used for the rapid contrast enhancement of both cells[3] and tissue sections[4] which overexpress HER2 biomarkers. To facilitate prompt tumor margin detection intraoperatively, the ability to assess tumor margins without the need for physical sectioning is highly desirable. Thus, in this study, we advance our previous findings by examining the ability to rapidly target HER2 receptors quickly in intact *ex vivo* human breast tissue specimens without sectioning. We first investigate the potential depth of penetration of the targeted nanoshells in intact tissue to confirm the

predominance of surface targeting and preferential labeling of HER2-positive tissue. Then, we demonstrate the proof of concept that anti-HER2 targeted gold nanoshells can be used as rapid diagnostic imaging agents for HER2-overexpression in intact breast tissue specimens using a standard stereomicroscope and confirm these results through reflectance confocal microscopy and immunohistochemistry.

9.2 Materials and Methods

9.2.1 Nanoshell Fabrication and Antibody Conjugation

Nanoshells were fabricated as formerly described.[5-7] Silica cores were again made using the Stöber method[8] followed by subsequent termination of the silica surface with amine groups. The final particles were measured by direct light scattering (DLS) to have an average diameter of 276 nm. Next, the aforementioned gold colloid (diameter of ~1-3 nm) was again fabricated and adsorbed onto the surface of the silica cores via the amine groups.[9] After the gold shell layer over the silica cores was completed, the spectrum of the final nanoshell solution was visualized using a UV-vis spectrophotometer (Varian Cary 300) (Figure 9.1.).

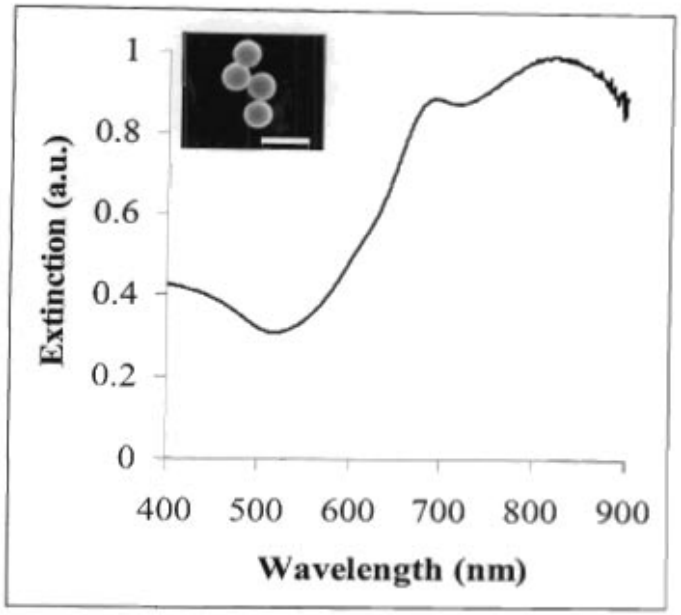

Figure 9.1. Measured extinction spectra of nanoshells with an average core diameter of 276 nm and average shell thickness of 19 nm. Insert depicts corresponding image from scanning electron microscopy. Scale bar represents 500 nm.

In order to determine the concentration of nanoshells in solution, the absorption, scattering, and extinction coefficients were determined using Mie Theory. The average size of the nanoshells, as validated by Scanning Electron Microscopy (SEM), was a diameter of 314 nm with a peak surface plasmon resonance at 840 nm. The concentration of the working nanoshell solution was approximately 2.0×10^9 particles/mL.

Nanoshells were next targeted to biological HER2-antigens by linking the surfaces of the nanoshells to anti-HER2/neu antibodies using previously described methods[5]. Prior to their experimental use, nanoshells (2.0×10^9 particles/mL) were incubated with the anti-HER2-linker cocktail for 2 hours at 4°C. For the purpose of complete nanoparticle stabilization in biological media, the nanoshells were next incubated with a 1 mM polyethylene glycol-thiol solution (PEG-SH, MW = 5kD, Nektar) for 12-16 hours at 4°C. Next, unbound antibodies and excess PEG-SH were removed

from the nanoshells by centrifugation. Supernatant was removed and, just prior to experimental tissue studies, the nanoshells were resuspended in antibody diluent (IHC World, pH 7.4) by gentle pipetting to a final volume of 165 μl.

9.2.2 Ex Vivo Human Breast Tissue Specimens

Normal (nonneoplastic) and cancerous (HER2-negative and HER2-positive) breast tissue specimens were supplied by the Cooperative Human Tissue Network (CHTN) through a protocol approved by the Institutional Review Board (IRB). Tissues were previously designated as normal or cancerous by pathologists at the medical centers where the tissue samples were obtained. Additionally, HER2/neu status was also previously determined by pathologists at the respective medical centers prior to the patients undergoing any form of medical treatment. The tissues, which arrived as pre-frozen in liquid nitrogen, were immediately placed in a -80°C freezer.

Prior to use, samples were thawed briefly in a 37°C water bath and then cut using a disposable cutting board with a 5 mm punch biopsy in order to maintain size consistency. At least two punch biopsies were taken from each specimen for control and experimental conditions. Each cut specimen used was 5 mm in diameter with an average thickness of 1 mm. Tissue samples were subsequently incubated in prewarmed antibody diluent (IHC World, pH 7.4) for 1 minute at room temperature with gentle agitation in a 24-well plate. After pre-rinsing, the samples were incubated in either antibody diluent or the aforementioned targeted-nanoshell cocktail (volume = 165 μl) in polyethylene sample vials (Sigma Aldrich). The vials were then placed on a nutator in an incubator set at 37°C for 5 minutes. After incubation, the tissue samples were removed from the vials and

rinsed 3x in 1xPBS briefly (in a 24-well plate). Samples were then moved to a clean well of 1 x PBS prior to imaging.

9.2.3 *Two Photon Imaging of Human Breast Tissue Specimens*

For two photon imaging of intact breast tissue specimens, both HER2-negative cancerous and HER2-positive cancerous samples were evaluated for surface labeling of HER2-targeted nanoshells as well as their potential depth of penetration. Samples were placed directly on a glass coverslip (Fisher Scientific) and an additional coverslip was placed on top of the tissue in order to facilitate moderate tissue compression. For image acquisition, a Zeiss laser scanning microscope (LSM) 510 META multi-photon system was used in tandem with a Coherent Chameleon femtosecond-pulsed, mode-locked Ti:sapphire laser. This system was set to operate at an excitation wavelength of 780 nm and a power of 10% of the maximum excitation power. The collected emission wavelength range spanned from 451 nm to 697 nm. Images were collected at a magnification of 20x and a z-stack (depth) increment of 5 μm. In order to calculate the percentage of area covered by nanoshells, Image J imaging software was used. An intensity threshold of 30 (on a scale of 0 to 255, where 0 represents pure black and 255 represents pure white) was used to distinguish areas with and without nanoshells. For areas that did not contain nanoshells, the associated intensities did not exceed the threshold.

9.2.4 Widefield Imaging of Human Breast Tissue Specimens

Normal (nonneoplastic) and HER2-positive cancerous breast tissue specimens (from patients who had and had not received previous neoadjuvant chemotherapy) were imaged using a Zeiss Discovery.V8 stereomicroscope equipped with a VisiLED MC1000 light source. This microscope provides enhanced visualization of specimens in three dimensions ranging from 1x to 8x magnification. For macroscopic imaging of breast tissue specimens, a thin black pad (taken from a Maestro imaging system) was placed beneath a 22x22 glass coverslip (Fisher Scientific) to enable ease of tissue placement and to provide a consistent black background among all samples. The specimens (controls and respective nanoshell-labeled counterparts) were placed alongside each other on top of the coverslip. Images were taken at both 1x and 2x magnification under the same lighting conditions.

9.2.5 Reflectance Confocal Microscopy Imaging of Human Breast Tissue Specimens

Following widefield imaging, the aforementioned samples were prepared for microscopic imaging under reflectance confocal microscopy. For this component of the study, a Lucid VivaScope 2500 inverted confocal microscope was employed, which uses an 830 nm light source and has a lateral resolution of less than 2μm. Samples were placed directly on glass slides (Fisher Scientific) which were modified by the addition of an adhesive 1-mm-deep, 20-mm-diameter silicon isolator (Invitrogen). In order to compress the tissue slightly and consistently among samples, an adhesive tissue cassette (Lucid, Inc.) was placed directly on top of the silicone isolators above the tissue specimens. Multiple images were taken at a power of 0.4 mW and at the same distance

from the glass surface for tissue samples incubated in either antibody diluent alone or the HER2-targeted nanoshells. After reflectance imaging, coverslips and silicone isolators were removed and the samples were prepared for histological processing. Additionally, reflectance intensity measurements were recorded using Image J processing software as described previously.[4]

9.2.6 Immunohistochemistry and Histology

Once images were collected under both stereomicroscopy and RCM imaging systems, normal (nonneoplastic) and HER2-positive cancerous samples (with and without previous neoadjuvant chemotherapy) were embedded in OCT media (BBC Biochemical) and frozen rapidly over dry ice. Sections were then made of all specimens using a Leica CM1850 UV cryostat. At least 20 sections were cut from each specimen at a thickness of 5 μm. Cancerous specimens were sectioned at -20°C and normal specimens were sectioned at -30°C, as suggested by Leica for maintaining optimal tissue morphology. The sections were immediately placed on superfrost slides (Fisher Scientific) and allowed to air dry overnight. The next day, multiple sections from each specimen of interest were prepared for either immunohistochemistry (IHC) or hemotoxylin and eosin (H&E) staining. IHC for the HER2-antigen was executed using the Histostain Plus AEC Broad Spectrum Kit (Invitrogen) per manufacturer's instructions. H&E staining was also performed using the manufacturer's instructions (Sigma Aldrich) for the alcoholic Eosin Y solution. For image acquisition, a standard brightfield microscope (Zeiss Axioskop 2 equipped with a Zeiss Axiocam MRc5 color camera) was used at a magnification of 20x under the same lighting conditions.

9.3 Results and Discussion

9.3.1 Distribution and Penetration of Gold Nanoshells In Intact Human Breast Tissue

The goal of this study was to evaluate the distribution of anti-HER2-conjugated gold nanoshells through resected intact tissue specimens. For comparison, the nanoshell labeling between HER2-positive and HER2-negative tissue samples was evaluated. In order to do this, a two photon imaging system was employed. As shown previously, this imaging system is capable of enhancing and capturing the luminescence signature of the gold nanoshells[10] while also creating a stack of images taken in the z-direction throughout the depth of the tissue of interest. Figures 9.2 and 9.3 represent the z-stack images of HER2-positive and HER2-negative tissues, respectively, incubated with HER2-targeted nanoshells. Each sequential increment in the z-direction represents 5 μm into the tissue. Qualitatively, the first image in Figure 9.2 demonstrates that the nanoshells preferentially label HER2-receptors on the surface of the tissue. Although the tissue was incubated with nanoshells for only 5 minutes, the subsequent z stack images illustrate that some targeted nanoshells do penetrate the tissue surface up to approximately 20-25 microns, though considerable nanoshell penetration is diminished after 10 microns. Based on a comparison with HER2-negative tissue, the nanoshells do appear to penetrate the tissue throughout a similar depth, but labeling is reduced due to the decrease in HER2 receptor expression. Upon further analysis performed using Image J imaging software, which was used to calculate the area of tissue labeled with nanoshells at each focal plane, the percentage of nanoshells varied from approximately 42% to 0% in HER2-positive tissue from the surface up to 25 microns of penetration depth. For

HER2-negative tissue, this range varied from only about 1.5% to 0%. Thus, the nanoshell labeling on the surface of intact *ex vivo* tissue specimens was approximately 28 times greater for HER2-positive tissue over HER2-negative tissue. However, at a depth beyond 10 microns, this substantial difference in labeling is not qualitatively or quantitatively perceivable.

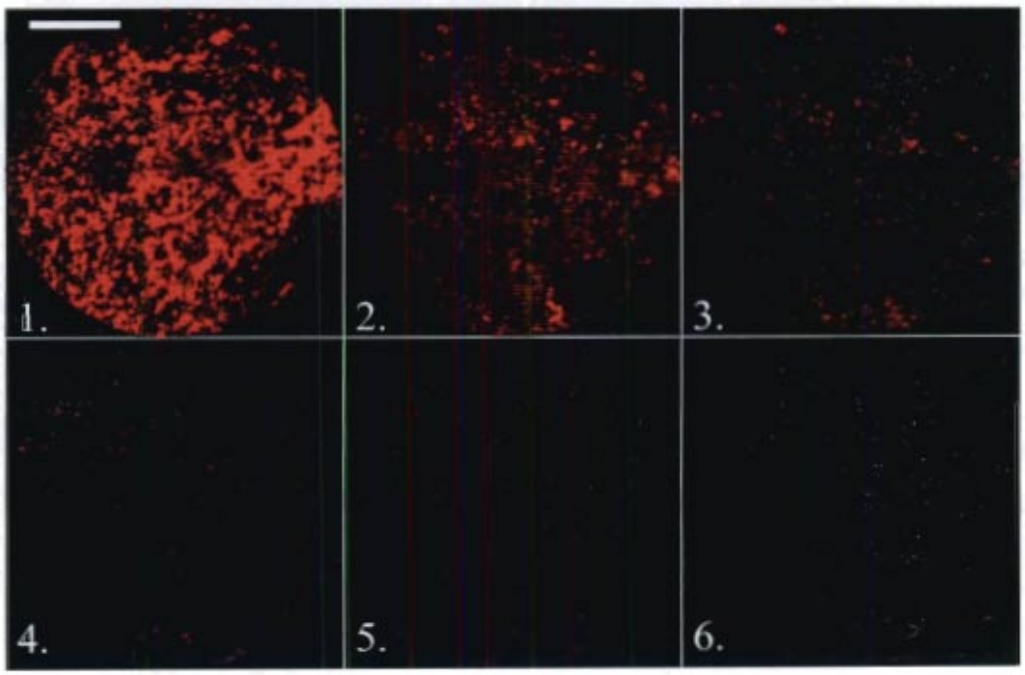

Figure 9.2. Z-stack two-photon luminescence images of HER2-positive tissue incubated with HER2-targeted nanoshells for 5 minutes at 37°C. Each progressive image represents an increase in depth penetration of 5 μm. Magnification = 20x. Scale bar = 50 μm.

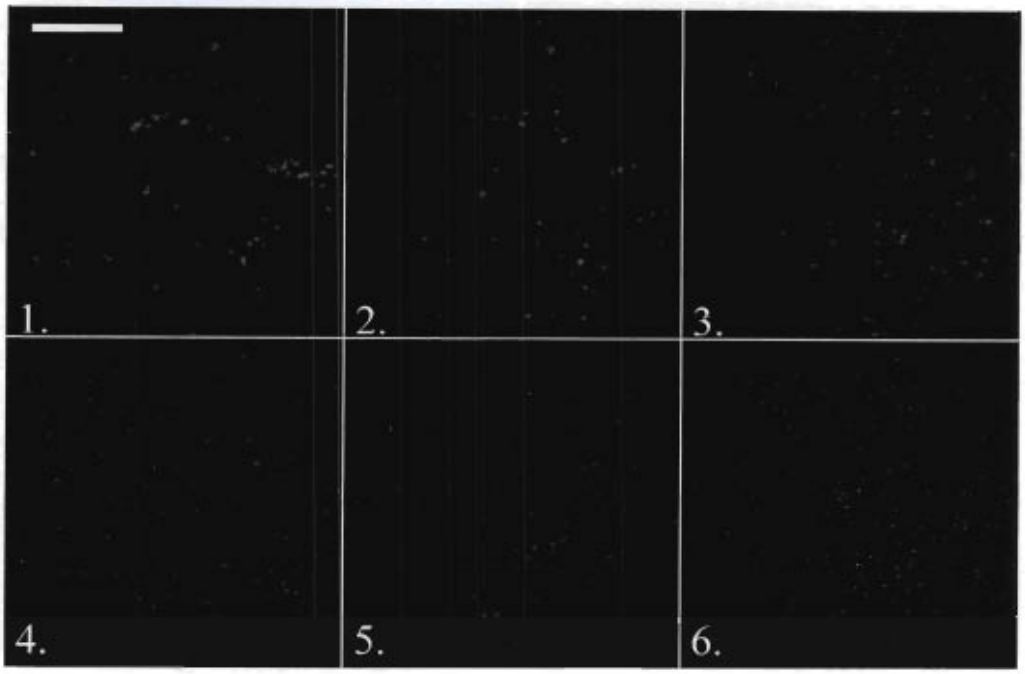

Figure 9.3. Z-stack two-photon luminescence images of HER2-negative tissue incubated with HER2-targeted nanoshells for 5 minutes at 37°C. Each progressive image represents an increase in depth penetration of 5 μm. Magnification = 20x. Scale bar = 50 μm.

9.3.2 Enhanced Optical Imaging of Intact Ex Vivo Human Breast Cancer Tissue Using Gold Nanoshells

Based on the two photon results demonstrating the superior labeling of HER2-targeted nanoshells on the surface of intact *ex vivo* HER2-positive tissue specimens, we assessed the potential of using a standard stereomicroscope to visualize this enhanced contrast. For this component of the study, human breast tissue specimens that over-expressed HER2 receptors at the time of patient diagnosis were evaluated and compared to normal (nonneoplastic) tissue. Due to the ultimate goal of utilizing gold nanoshells to rapidly label tumor margins intraoperatively, we examined tissue from patients who had not undergone previous therapy before surgery as well as tissue from patients who had undergone neoadjuvant chemotherapy. All tissue samples were incubated with either

antibody diluent buffer or the anti-HER2-targeted nanoshells for 5 minutes at 37°C. As shown in Figure 9.4, which represents raw images taken with a stereomicroscope, intact tissue specimens incubated with antibody diluent alone showed no markings or features characteristic of nanoshells. However, tissue specimens incubated with the anti-HER2-targeted nanoshells demonstrate numerous particles on the surfaces (and slightly beyond the surfaces) of the tissues. Qualitatively, the HER2-positive tissue from the patient who did not undergo previous chemotherapy shows the greatest labeling with the targeted nanoshells. The HER2-positive tissue from the patient who did undergo neoadjuvant chemotherapy does demonstrate enhanced nanoshell labeling, though not to the same extent as the patient without previous chemotherapy. In contrast, the nonneoplastic tissue shows the least amount of nanoshell labeling and only a few areas of nanoshells can be visually perceived.

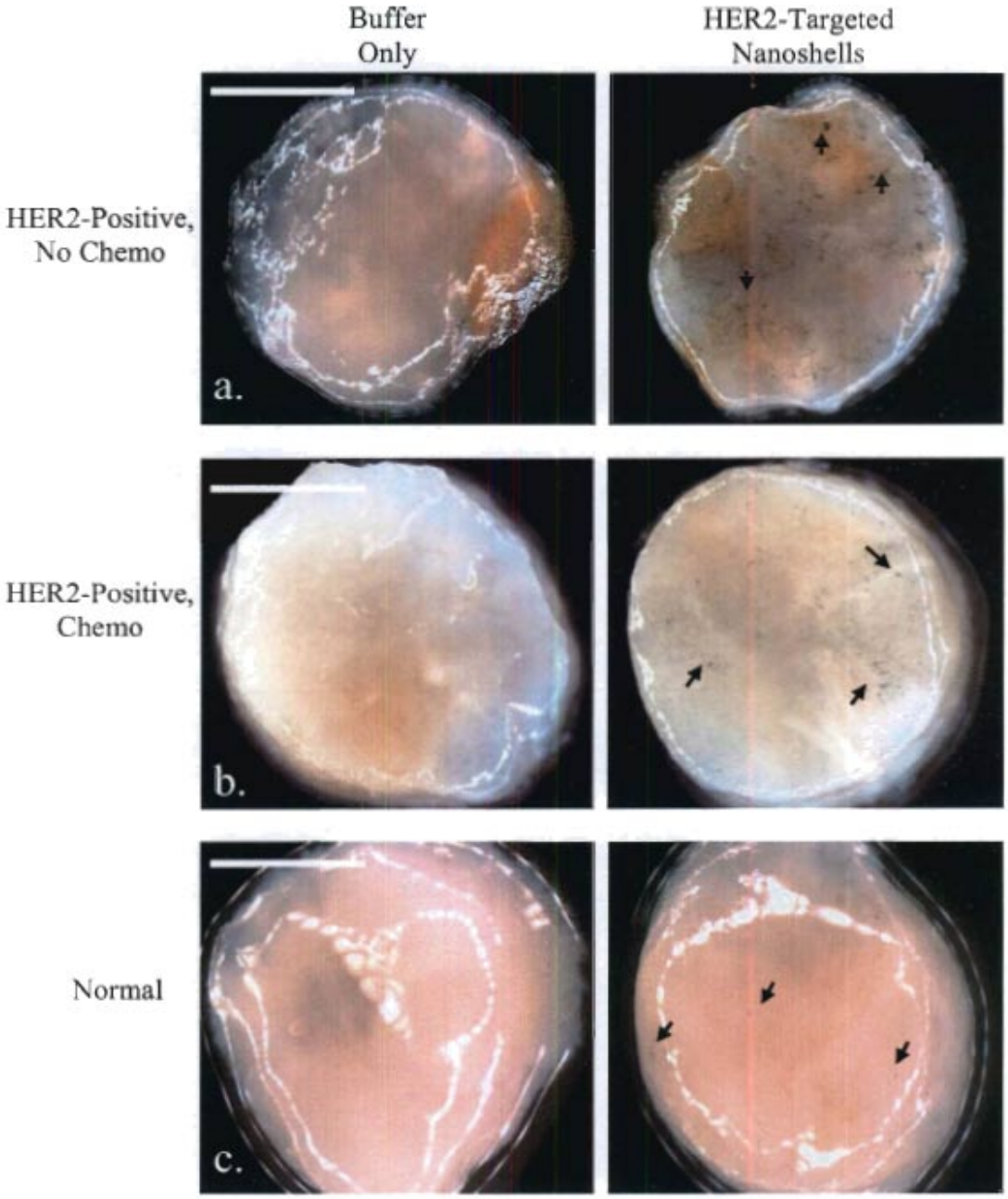

Figure 9.4. Raw stereomicroscope images of (a.,b.) HER2-overexpressing cancerous and (c.) nonneoplastic tissue incubated with either buffer or HER2-targeted nanoshells for 5 minutes at 37°C. Cancerous tissue taken from a patient (a.) without chemotherapy and (b.) following neoadjuvant chemotherapy. Arrows represent nanoshells. Images taken at 2x. Scale bars = 2.5 mm.

While the degree of nanoshell labeling can be visualized without image adjustments under a standard stereomicroscope, the superior extent of this labeling can be seen more clearly after simple contrast enhancement through imaging software (Image J). As seen in Figure 9.5 (a.), the nanoshells are even more discernable against the tissue background regardless of inherent tissue constituents. Furthermore, in order to validate the enhanced nanoshell labeling seen by widefield imaging, the surfaces of the same tissue samples were also imaged using reflectance confocal microscopy (Figure 9.5 (b.)). Concurring with the stereomicroscopic images, we see dramatic nanoshell surface-labeling when using targeted nanoshells with previously untreated HER2-positive tissue. For the HER2-positive sample which had formerly undergone chemotherapy, we also see enhanced nanoshell labeling, though to a lesser degree than the untreated sample as suggested by the stereomicroscopy results. The normal, nonneoplastic tissue displays the least amount of surface labeling with only minimal nanoshells evident with either imaging system. Reflectance intensity measurements (data not shown) demonstrated that the HER2-positive tissue samples were ~2.5 to 3 times greater for the treated and untreated samples, respectively, than the normal sample. Subsequent histological analysis shown in Figure 9.5 (c.) reveals that the distribution of HER2 receptors seen with nanoshell-enabled contrast corresponds to that seen with IHC against HER2. The HER2 expression seen by IHC is greater for the previously untreated HER2-positive tissue sample than for the sample which had undergone neoadjuvant chemotherapy. This is believed to be due to the effects of chemotherapy and resulting tissue necrosis. However, both tissues which were previously identified as overexpressing HER2 during patient

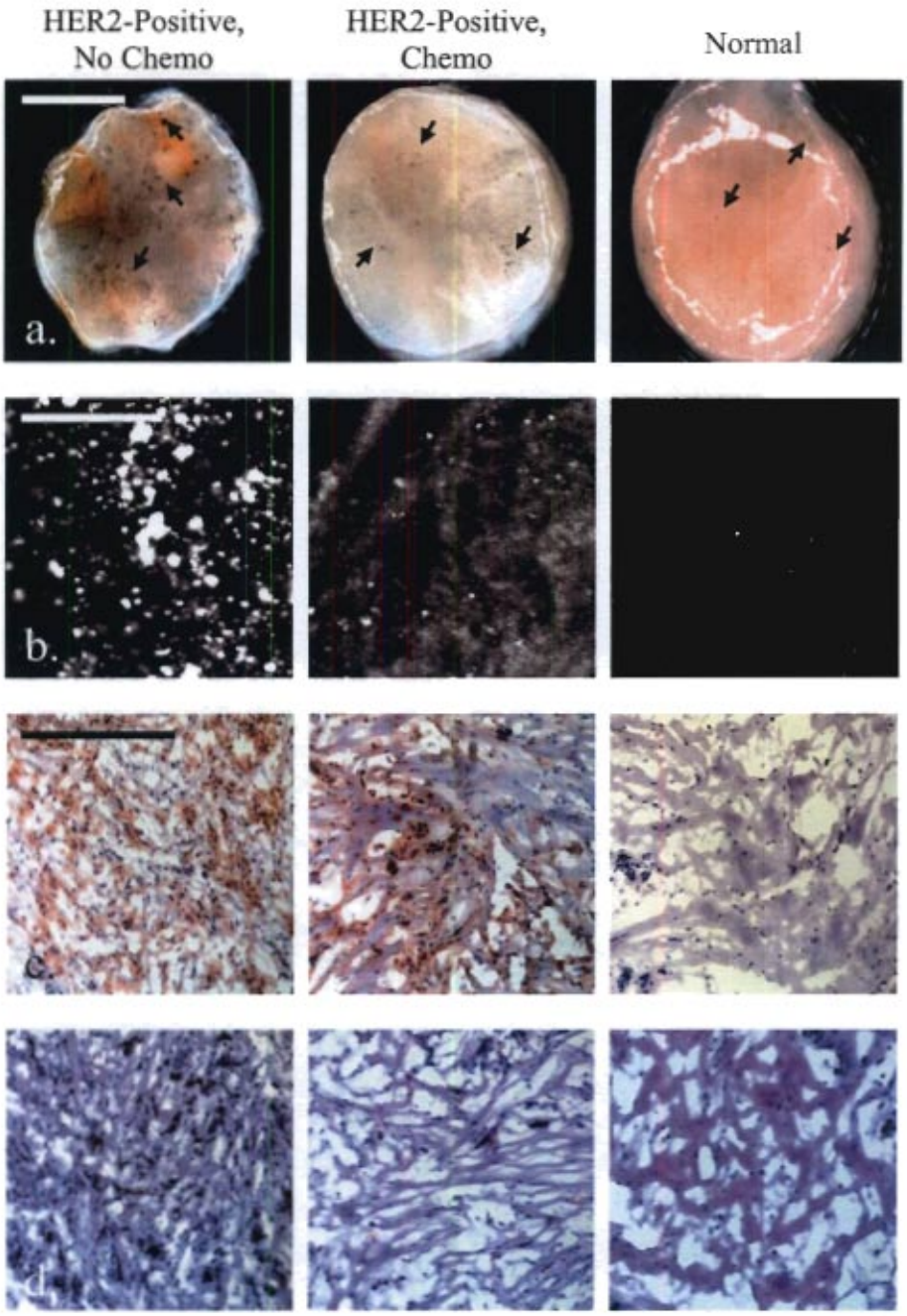

Figure 9.5. (a.) Stereomicroscopic images of HER2-overexpressing breast tissue (with and without neoadjuvant chemotherapy) and normal breast tissue incubated with HER2-targeted nanoshells for 5 minutes at 37°C after contrast enhancement. Magnification at 2x; scale bar = 2.5 mm. Arrows represent nanoshells. (b.) Respective reflectance confocal microscopy images of tissue samples from (a.). Power = 0.4 mW and scale bar = 75 μm. Respective (c.) HER2/neu immunohistochemistry and (d.) H&E results taken under brightfield microscopy under 20x magnification. Scale bar = 0.35 mm.

diagnosis demonstrate considerably more receptors than the normal, nonneoplastic tissue. Additionally, H&E-stained sections of all tissue samples have been included (Figure 9.5 (d.)) to illustrate the microscopic characteristics and differences associated with neoplastic vs. nonneoplastic conditions.

The macroscopic evaluation of resected tissue is currently the standard of practice for certain patients undergoing breast conservation therapy at tertiary centers, such as MDACC. As mentioned previously, this occurs primarily for non-palpable breast cancers.[1] Furthermore, this extra level of evaluation is not as common in community-based hospitals. Here, we demonstrate the ability to use targeted gold nanoshells to rapidly improve visualization of a specific biomarker associated with disease aggression and progression (HER2) in intact *ex vivo* human breast tissue. By utilizing gold nanoshells designed as rapid diagnostic imaging agents, surgeons and pathologists may be able to realize tumor margin status after both macroscopic and microscopic assessment without the need to transfer the tissue sample out of the operating room.

The ability to enhance contrast of malignancy using topically-applied agents has previously been demonstrated for oral tissue using fluorescently-labeled deoxy-glucose and epidermal growth factor (EGF) conjugates[11,12] as well as cervical tissue using fluorescently-labeled gold nanoparticles targeted to EGF receptors[13]. However, these studies employed incubation times ranging from 30-45 minutes, which exceeds the length of time currently needed to obtain tumor margin status using frozen section histology. Additionally, the aforementioned studies which evaluated malignancy based on EGF expression utilized optical clearing agents, which may be necessary for particles which target intracellular biomarkers.[14,15] Nevertheless, gold nanoshells targeted to extracellular

biomarkers may offer more favorable opportunities for *ex vivo* intraoperative tumor margin detection without the need for lengthy incubation times or the use of optical clearing agents.

9.4 Conclusions

Recently, we verified that silica-based gold nanoshells could be used to enhance contrast of both HER2-overexpressing cells and tissue sections within 5 minutes of incubation time.[3,4] We take these findings one step further and confirm that these particles, when targeted to anti-HER2 receptors, can also be used to distinguish intact HER2-overexpressing *ex vivo* tissue from normal tissue within the same incubation time. Moreover, these results are supported by microscopic imaging with a reflectance confocal microscope as well immunohistochemistry against HER2.

In order to translate these findings more readily to the clinic, we are presently developing a low cost widefield imaging system that can be used to detect the overexpression of HER2 (and other extracellular biomarkers) on account of contrast enhancement provided by gold nanoshells. In addition, we plan to collect data from diverse patient populations and assess results with fresh tissue samples. Our research indicates that *ex vivo* tissue specimens labeled topically with silica-based gold nanoshells can be visualized by both widefield and high resolution imaging systems. By employing widefield imaging intraoperatively, clinicians may be better able to distinguish cancerous and non-cancerous breast tissue prior to further microscopic analysis and subsequent histological processing.

Chapter 9 References

1. Cabioglu N, Hunt K, Aysegul AS, Kuerer HM, Babiera GV, Singletary SE, Whitman GJ, Ross MI, Ames FC, Feig BW, Buchholz TA, and Meric-Bernstam F. "Role for Intraoperative Margin Assessment in Patients Undergoing Breast-Conserving Surgery", Annals of Surgical Oncology 14(4):1458-1471 (2007).

2. Graham RA, Homer MJ, Sigler CJ, Safaii H, Schmid CH, Marchant DJ, and Smith TJ. "The Efficacy of Specimen Radiography in Evaluating the Surgical Margins of Impalpable Breast Carcinoma", American Journal of Roentgenology 162(1):33-36 (1994).

3. Bickford LR, Chang J, Fu K, Sun J, Hu Y, Gobin A, Yu T-K, Drezek RA. "Evaluation of Immunotargeted Gold Nanoshells as Rapid Diagnostic Imaging Agents for HER2-Overexressing Breast Cancer Cells: A Time-Based Analysis", Nanobiotechnol 4(1-4):1-8 (2008).

4. Bickford LR, Agollah G, Drezek R, Yu TK, "Silica-gold nanoshells as potential intraoperative molecular probes for HER2-overexpression in *ex vivo* breast tissue using near-infrared reflectance confocal microscopy"; Breast Cancer Res Treat 120(3), 547 (2010).

5. Loo C, Lin A, Hirsch L, Lee MH, Barton J, Halas N, West J, Drezek R. "Nanoshell-enabled photonics-based imaging and therapy of cancer", Technol Cancer Res Treat 3(1):33-40 (2004).

6. Loo C, Hirsh L, Lee MH, Change E, West J, Halas N, Drezek R. "Gold nanoshell bioconjugates for molecular imaging in living cells", Opt Lett 30(9):1012-1014 (2005).

7. Loo C, Lowery A, Halas N, West J, Drezek R "Immunotargeted nanoshells for integrated cancer imaging and therapy", Nano Lett 5(4):709-711 (2005).

8. Stöber W, Fink A. "Controlled Growth of Monodisperse Silica Spheres in the Micron Size Range", J Colloid Interface Sci 26:62-69 (1968).

9. Duff DG, Baiker A, Edwards PP. "A new hydrosol of gold clusters. 1. Formation and particle size variation", Langmuir 9(9):2301-2309 (1993).

10. Bickford LR, Sun J, Fu K, Lewinski N, Nammalvar V, Chang J, Drezek RA, "Enhanced Multi-Spectral Imaging of Live Breast Cancer Cells Using Immunotargeted Gold Nanoshells and Two-Photon Excitation Microscopy", Nanotechnology 19: 315102 (2008).

11. Nitin N, Carlson AL, Muldoon T, El-Naggar AK, Gillenwater A, Richards-Kortum R. "Molecular imaging of glucose uptake in oral neoplasia following

topical application of fluorescently labeled deoxy-glucose", Int J Cancer 124:2634-2642 (2009).

12. Nitin N, Rosbach KJ, El-Naggar A, Williams M, Gillenwater A, Richards-Kortum R. "Optical Molecular Imaging of Epidermal Growth Factor Receptor Expression to Improve Detection of Oral Neoplasia", Neoplasia 11(6):542-551 (2009).

13. Aaron J, Nitin N, Travis K, et al. "Plasmon resonance coupling of metal nanoparticles for molecular imaging of carcinogenesis in vivo", J Biomed Opt 12(3):034007 (2007).

14. van de Ven A, Adler-Storthz K, Richards-Kortum R. "Delivery of optical contrast agents using Triton-X100, part 1: reversible permeabilization of live cells for intracellular labeling", J Biomed Opt 14(2):021012 (2009).

15. van de Ven A, Adler-Storthz K, Richards-Kortum R. "Delivery of optical contrast agents using Triton-X100, part 2: enhanced mucosal penetration for the detection of cancer biomarkers", J Biomed Opt 14(2):021013 (2009).

CHAPTER 10

CONCLUSIONS AND FUTURE WORK

Silica-based gold nanoshells have formerly demonstrated value in a vast array of biomedical applications and are expected to play a significant role in the future of nanomedicine. Due to their unique design, these nanoparticles can serve as diagnostic or therapeutic agents simply by alterations in their core size and gold shell thickness. More recently, nanoshells have shown their ability to also act as rapid diagnostic imaging agents which may create new venues for their importance in medicine. For instance, by implementing photonics-based tools and nanoparticles, the potential of assisting surgeons to better distinguish cancer vs. non-cancer directly in the operating room may ultimately and effectively reduce the amount of time spent in surgery while providing a means of obtaining rapid diagnostic information.

In this thesis, silica-based gold nanoshells demonstrate their potential to be engineered to function as both macroscopic and microscopic tools for the rapid identification of HER2-overexpression associated with malignancy in breast cancer. This is accomplished through a series of four sequential projects, which translate findings from *in vitro* cell studies to studies of *ex vivo* tissue sections, and ultimately, to *ex vivo* intact tissue specimens.

Undoubtedly, the realistic use of gold nanoshells as rapid diagnostic imaging agents in a clinical setting will require that certain additional objectives be met. While the proof of principle that HER2-targeted gold nanoshells can be used to realize HER2-overexpression in cell and tissue studies has been demonstrated, it is imperative that a

sequence of other experiments be carried out so that adequate adjustments can be made to these procedures for clinical translation.

First, a simplified widefield imaging system should be developed or utilized such that the contrast enhancement provided by the gold nanoshells is visible without the need for large or costly pieces of equipment. Ideally, this instrument would be easy to use and would not occupy much space in the operating suite. Additionally, for those centers interested in using reflectance confocal microscopy, a system with a handheld probe, rather than the tabletop version employed in this thesis, is recommended. This is due largely for maintaining procedural simplicity: a handheld probe would not require additional materials, such as glass slides or spacers, and questionable areas would be easier to interrogate.

In addition to optimizing imaging tools, studies should be executed with fresh tissue specimens, rather than frozen, which may incur the need for different procedures or reagents to acquire rapid labeling. Although 5 minutes was consistently used as the minimum incubation time throughout this work, it is possible that an even lower time may be effective. Thus, exploring opportunities to reduce this time may prove beneficial.

While studying the efficacy of rapid labeling with fresh tissue, it is also necessary to consider true 'tumor margin' tissue to correlate the results of nanoshell labeling with standard procedures of tumor margin detection. This will necessitate the collaboration with a medical center and, specifically, a pathologist who can confirm results. Once the rapid labeling procedure has been optimized for fresh, tumor margin specimens, appropriate statistics should ensue with corresponding specificity and sensitivity data.

Aside from optimization of nanoparticles, equipment, and procedures, the distribution of HER2 receptors throughout HER2-overexpressing tissue should be understood based on diverse patient populations who have either had no previous therapies prior to surgery or who have different neoadjuvant therapies prior to surgery. In this way, the use of gold nanoshells may demonstrate widespread efficacy or be limited only to specific patient subsets.

By optimizing nanoshell design and developing superior, cost efficient imaging tools, a novel guidance system may be designed for assisting surgeons in distinguishing malignancy from benignity. Ultimately, this system could also be used for other diagnostic applications, for other anatomical locations, and for other biomarkers associated with disease. While rapid diagnostic imaging agents may have many potential applications, this research may be implemented in the near future in the area of intraoperative tumor margin delineation. By facilitating fast and accurate tumor margin results intraoperatively and supplementing current diagnostic methods, the incidence of cancer progression and amount of time spent in surgery due to inadequate tissue removal is, correspondingly, expected to be reduced.